UNIVERSITÀ DI PARMA

UNIVERSITÀ DEGLI STUDI DI PARMA

DOTTORATO DI RICERCA IN
"SCIENZE DELLA TERRA"

CICLO XXX

SYNTHESIS, PHASE TRANSITIONS, DEGASSING BEHAVIOUR OF MELANOPHLOGITE (TYPE I CLATHRATE)

Coordinatore:
Prof. Fulvio Celico

Tutore:
Prof. Mario Tribaudino

Co Tutore:
Prof. Mauro Riccò

Co Tutore:
Prof. Daniele Pontiroli

Dottoranda: Daniela D'Alessio

Anni 2014/2018

INDEX

LIST OF ACRONYMS

Following, a list of acronyms, which can be found in this thesis, is reported.

DSC: Differential Scanning Calorimetry

ESRF: European Synchrotron Radiation Facility

FD: Framework Density

FTC: Framework Type Code

HT–XRPD: High Temperature X–Ray Powder Diffraction

ILL: Institut Laue–Langevin

INS: Inelastic Neutron Scattering

IUPAC: International Union of Pure and Applied Chemistry

IZA: International Zeolite Association

MAS: Magic Angle Spinning

MOF: Metal–Organic Framework

NMR: Nuclear Magnetic Resonance

ODP: Ocean Drilling Project

PerBU: Periodic Building Unit

PGAA: Prompt Gamma Activation Analysis

SC–XRD: Single Crystal X–Ray Diffraction

SDA: Structure Directing Agent

TEOS: Tetraethyl orthosilicate

TGA: Thermal Gravimetric Analysis

TMOS: Tetramethyl orthosilicate

XRD: X–Ray Diffraction

XRPD: X–Ray Powder Diffraction

1. INTRODUCTION

Melanophlogite is a member of the clathrasils family, until recently the only one known in nature. It is made up of a framework of [SiO_4] tetrahedra, arranged in a structure with cages where guest molecules can be present. As a mineral, melanophlogite is quite rare, but specific in its findings, so that it could be a good marker for the geochemical conditions at the crystallization. A major interest comes in the possible use for gas storage: respect to zeolites, melanophlogite has a higher capability to hold the gas phases at higher temperature, and could be a candidate to greenhouse gases sequestration, or to stock gases for industrial applications. In spite of the potential interest in this phase, several aspects of its structure and physical properties are still obscure. At high temperature, the structure is cubic, and decreases its symmetry to tetragonal at lower temperature, but the details of this transition and the role of guest molecules in promoting the transition are still unknown. Moreover, no information exists on the lower temperature behaviour, i.e. below room temperature. This would be of interest as at lower temperature the dynamics of the enclathrated guest molecules can be frozen, or become sluggish. Moreover, the degassing at higher temperature, a key feature for any possible industrial application of melanophlogite, has not been described, even at the simplest level of TGA. Last, but not least, the synthesis of melanophlogite is a critical issue for any application, due to rarity of natural samples. This was previously performed (Gies *et al.*, 1982), but the details in the synthesis and characterization of the samples were not given.

The above points have been the focus of this investigation. In detail, in this thesis, the following studies have been developed, to clarify the structural and the thermodynamic behaviour of melanophlogite:

1) a low–high temperature XRPD study was carried out, exploiting both X–Ray conventional and unconventional (that is synchrotron radiation) sources, to enlighten the phase transitions occurring in melanophlogite, and link them to their thermodynamic behaviour via DSC and the analysis of the spontaneous strain;

2) TGA, together with DSC, were done to detail the degassing behaviour with temperature, in natural and synthesized samples;

3) the synthesis of melanophlogite with methylamine as templating agent was carried out, and the behaviour of synthesized melanophlogite was compared to the one of natural samples.

This thesis is therefore made up of the following chapters. In the first chapter, after a preliminary introduction on clathrasils, and their differences in respect to the broader family of zeolites, the known literature on melanophlogite and its properties is presented. In the

second chapter, materials and methods are reported. In the third chapter, the results of experimental investigations, carried out on the natural melanophlogite samples, which come from three different Italian localities, and on synthesized melanophlogite, are reported. In this chapter, the synthesis of melanophlogite is addressed, and the synthesized samples are characterized. In the fourth chapter, a discussion on the experimental results, to detail the phase transition and degassing behaviour, is reported. In the conclusive chapter, the results are summarized and interpreted in view of possible applications to the geological investigation. In an appendix, additional information about the materials exposed in the introductory chapter are provided.

1.1. ZEOLITES, CLATHRASILS AND MELANOPHLOGITE

Melanophlogite belongs to the family of porous tectosilicates, in the clathrasils group. Porous silicates are subdivided in two classes, depending on the dimensions of the void "windows" (Higgins, 1994; Liebau *et al.*, 1986):

1) zeosils and zeolites have channel–like voids with "windows" large enough for guest species to pass through;

2) clathrasils and clathralites have cage–like voids with small windows, typically six–membered or smaller rings, into which void–filling guest species cannot pass through.

Before the description of the structure and the physical properties characteristic of melanophlogite, a brief discussion on the general properties of these two groups is here presented.

1.1.1. ZEOLITES AND ZEOLITE–LIKE MATERIALS

Zeolites and zeolite–like materials are a quite difficult to define large family of crystalline solids (Baerlocher *et al.*, 2007): historically, a zeolite is an aluminosilicate with an open framework, which allows for ion exchange and reversible dehydration (Smith, 1984). This definition includes the crystalline substances, which can be also non–aluminosilicates, which have a structure made up of a framework of linked tetrahedra, each of them consisting of four atoms of oxygen surrounding a cation (Coombs *et al.*, 1997). In the definition of zeolite, the framework contains open cavities in the form of channels and cages, which are usually

occupied by H_2O molecules and extra–framework cations, commonly exchangeable. A simple criterion to distinguish zeolites and zeolite–like materials from denser tectosilicates is based on the framework density (FD), that is the number of tetrahedrally–coordinated atoms per 1 nm^{-3} (Bnmner & Meier, 1989). For all the framework topologies with FD < 21, a framework type code (FTC), consisting of three capital letters (marked in boldface type), is assigned by the Structure Commission of the International Zeolite Association (IZA). As of July 2013, 213 unique topologies are listed in the IZA database: The Atlas of Zeolite Framework Types (Baerlocher *et al.*, 2001; Baerlocher *et al.*, 2007). Among these, we can find **MEP** for melanophlogite, the mineral studied in this research project. Other FTCs for silica porous minerals are reported in Appendix (Chapter "**6.1**", Table 6.1).

1.2. CLATHRATES

A clathrate is a chemical substance with a characteristic structure in which cages are present, and can host guest species. The word "clathrate" is derived from the Latin word "*clatratus*", with the meaning of "with bars or lattice".

According to IUPAC definition, the clathrates are inclusion compounds in which the guest molecule is in a cage formed by the host molecule or by a lattice of host molecules (McNaught & Wilkinson, 1997).

As a matter of fact, the crystalline clathrates we are dealing off form cages by a lattice of host molecules.

The clathrates are also defined as a particular species of inclusion compounds. An inclusion compound is a complex in which one component (the host) forms a cavity or, in the case of a crystal, a crystal lattice containing spaces in the shape of long tunnels or channels, in which molecular entities of a second chemical species (the guest) are located. There is no covalent bonding between guest and host, and the attraction is generally due to van der Waals forces (McNaught & Wilkinson, 1997).

According to the chemistry of the molecules forming the host framework, among the clathrates can be included clathrasils (silica clathrate compounds) and methane hydrates (or methane clathrates), with a pure silica framework and an ice–like structure made up of water cages surrounding guest hydrocarbon molecules, respectively.

1.2.1. CLATHRASILS

Silica clathrate compounds (or clathrasils) are zeolite–like materials constructed of pure silica framework structures that possess small cage–like cavities. Clathrasils have been discovered for the first time in the 19th Century, in the form of the natural mineral melanophlogite, studied in this thesis (Von Lasaulx, 1876), although melanophlogite crystal structure has not been clarified until 1965 (Kamb, 1965). High–silica zeolites have been synthesized for the first time in the early 1960s, and this result has been the starting point for an intensively research on clathrasils, since, after the work concerning the synthesis of the high–silica clathrate compound ZSM–39 (Schlenker *et al.*, 1981), clathrasils have been constantly studied and synthesized (Gerke & Gies, 1984; Gies *et al.*, 1982; Gies, 1983; Gies, 1984 (a); Gies, 1984 (b); Gies, 1986; Marler *et al.*, 1986; Gunawardane *et al.*, 1987).

The properties of clathrasils, analogously to what is for the larger zeolite family, are closely linked to their framework structures and chemical compositions. The electrostatically neutral frameworks characteristic of the clathrasils are highly hydrophobic, consequently can preserve their structural stability even after the degassing, at high temperature, of the guest molecules present inside the structural voids (Liu *et al.*, 1997; Nakagawa *et al.*, 2005). An improved structural stability at high temperature and an optimized catalytic capacity are two esteemed features, above all thinking about the potential technological applications, which encourage the development of clathrasils, as well as, in general, zeolites, with higher Si/Al ratios, since such density values have been associated to higher catalytic levels (Higgins, 1994).

Clathrasils have attracted interest as analogue materials of other classes of clathrate compounds, for instance the clathrate hydrates, which are probably the best–known example among all the clathrate compounds. Clathrate hydrates are clathrate compounds in which the host molecule is water and the guest molecule is typically a gas or a liquid: without the support of the entrapped molecules, the structure of hydrate clathrates would collapse into conventional ice crystal structure or liquid water. Three structural types of clathrate hydrates are found in nature (Sassen & MacDonald, 1994): Structure I (McMullan & Jeffrey, 1965), Structure II (Mak & McMullan, 1965), and Structure H (Ripmeester *et al.*, 1987). All of the three isotypic materials are synthesized in the clathrasil families (Kamb, 1965; Schlenker *et al.*, 1981; Gerke & Gies, 1984).

Clathrate hydrates are potential candidates for hydrogen and geological CO_2 storage (House *et al.*, 2006; van den Berg & Areán, 2008). Clathrasils could be employed as materials for

permanent CO_2 storage, and consequently their thermochemistry is of special interest in this field (Navrotsky *et al.*, 2003). Further details on clathrasils structure, thermodynamic properties and potential applications, are reported in Appendix, Chapter "**6.2**".

1.2.1.1. STRUCTURAL TOPOLOGY

1.2.1.1.1. MELANOPHLOGITE

The name "melanophlogite" derives from the Greek words "*melanos*" and "*flogos*", with the meaning of "black" and "fire" respectively, indicating the tendency of the mineral to change its colour, blackening, if subjected to thermal treatment, which promotes the decomposition of the organic compounds, present as guest species in the structural cavities or included organic material.

Melanophlogite (**MEP**) is a tectosilicate belonging to SiO_2 type I clathrate compounds, zeolite–like materials with microporous framework of corner sharing [SiO_4] tetrahedra. It is a low–density polymorph of silica, with an average value of the specific gravity of 2.04 and characterized by a FD of 17.9 (Momma, 2014).

In melanophlogite, there are two types of structural isolated cages: pentagondodecahedral [5^{12}] and tetrakaidecahedral [$5^{12}6^2$].

The superscripts 12 and 2, above 5 and 6 respectively, are the number of pentagonal and hexagonal faces of each kind of cavities inside the silica framework: pentagondodecahedral [5^{12}] voids are formed by twelve pentagonal faces, and twenty vertices, and tetrakaidecahedral [$5^{12}6^2$] voids are made up of twelve pentagonal faces and two hexagonal faces, with twenty–four vertices.

In Fig. 1.1, the cubic structure of melanophlogite, viewed along [100], is reported, with the unit cell shown in the square, Si and O atoms highlighted as blue and red dots respectively, and guest molecules inside [5^{12}] and [$5^{12}6^2$] cages as yellow dots (from Tribaudino *et al.*, 2008).

In Fig. 1.2, the polyhedral drawing of melanophlogite structure, together with characteristic structural topologies of all the other clathrasils containing [5^{12}] pentagondodecahedral cages, are reported, highlighting the types of cages and the framework structures (Momma, 2014).

The mean Si–O bond lengths of melanophlogite, as well as of other clathrasils, such as **MTN** and **DOH**, are typically shorter than ~ 1.62 Å, that is reported as mean value for the silica frameworks (Liebau, 1985).

Melanophlogite chemical formula, including potential fillers of the cavities, is $46SiO_2 \bullet 2M^{12} \bullet 6M^{14}$, where M stands for the guest molecules inside the voids and M^{12} and M^{14} denote the 12 and 14 coordinated pentagondodecahedral [5^{12}] and tetrakaidecahedral [$5^{12}6^2$] voids, with volume of 97 $Å^3$ and 136 $Å^3$ respectively, present in the unit cell with a ratio of 2:6 (Gies 1983; Kolesov & Geiger, 2003; Nakagawa *et al.*, 2005). In both cage types, weakly bonded guest molecules are present (Gies, 1983; van Koningsveld & Gies, 2004).

CH_4, CO_2, H_2S, N_2 and recently S_2 were reported as guest species in the cages; H_2O has never been found, revealing the mineral hydrophobicity (Tribaudino *et al.*, 2010; Momma, 2014). Guest–free melanophlogite is simply a silica polymorph, but it does not exist in nature: indeed, the formation of melanophlogite requires a templating gas, so that different peculiar guest molecules mixtures are present in the structural cavities, depending on the geological setting of the occurrence sites. For instance, melanophlogite from Fortullino (near Livorno, Tuscany, Italy) contains almost uniquely CO_2 (Grassellini Troysi & Orlandi, 1972), whereas melanophlogite from Varano Marchesi (near Parma, Emilia Romagna, Italy) contains only CH_4 (Tribaudino *et al.*, 2008; Tribaudino *et al.*, 2010; Gatta *et al.*, 2014). In other cases, a mixture of different guest molecules can be present, like in melanophlogite from Racalmuto (near Agrigento, Sicily, Italy), with H_2S and, to a minor extent, CH_4, and melanophlogite from Mt. Hamilton (in Santa Clara County, California, USA), with CH_4, CO_2 and N_2 (Skinner & Appleman, 1963; Nakagawa *et al.*, 2001; Kolesov & Geiger, 2003; Nakagawa *et al.*, 2005; Lazzeri *et al.*, 2017; Likhacheva *et al.*, 2018).

Melanophlogite is found only in few localities all around the world. Sicilian melanophlogite, found in Racalmuto and Lercara–Friddi (near Palermo), has been described for the first time by Von Lasaulx (1876). The second find has been reported from Chvaletice, a small town in the Pardubice Region of the Czech Republic, in a metamorphosed pyrite and rhodochrosite sedimentary deposit (Žák, 1967; Žák, 1972). In 1972, two additional localities have been reported: Fortullino and near Mt. Hamilton, in a serpentinite breccia at the contact with magnesite lodes (Grassellini Troysi & Orlandi, 1972) and in a serpentinite included in sandstones and Jurassic clayed schists (Cooper & Dunning, 1972), respectively. The fifth find has been reported from Tsekur–Koyash (in Crimean Peninsula), in a sulphur deposit (Kopatsheva & Makarov, 1975). Moreover, there has been the discovery of melanophlogite–containing pebble in the Pacific Ocean, off the coast of Oregon (Kohler *et al.*, 1999): the specimen has been dredged from a depth of about 700 m by the research boat called *Sonne*, near ODP (Ocean Drilling Project) Point 892, at a seafloor with vents expelling fluids rich in methane in Cascadia accretionary prism (Lazzeri *et al.*, 2017). The sixth worldwide

melanophlogite discovery has been reported in a quarry located near Parma, associated with other silica polymorphs (Adorni *et al.*, 2004).

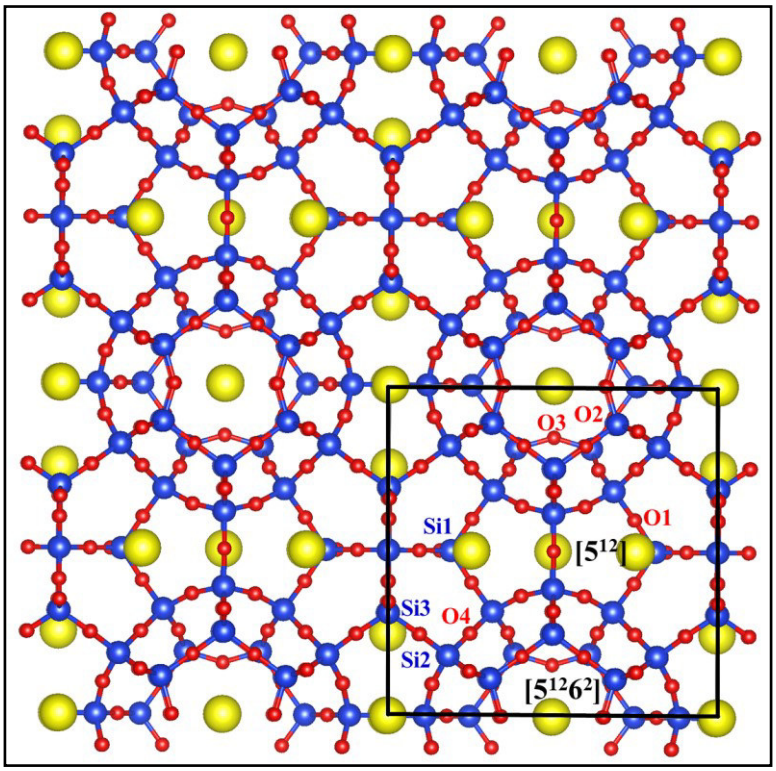

Figure 1.1. The cubic structure of melanophlogite viewed along [100]. The unit cell is shown in the square. Si and O atoms are shown as blue and red dots respectively, guest molecules inside [5^{12}] and [$5^{12}6^2$] cages as yellow dots (from Tribaudino *et al.*, 2008).

In nature, melanophlogite is related to low temperature hydrothermal processes in connection with gas venting (Tribaudino *et al.*, 2008), so that a critical issue is melanophlogite synthesis. The formation enthalpy of melanophlogite is very similar to that of amorphous silica (Navrotsky *et al.*, 2003) and its crystallization process is likely due to the templating action of guest phases, which enables the mineral nucleation process (Gunawardane *et al.*, 1987; Kolesov & Geiger, 2003; Navrotsky *et al.*, 2003).

Zeolites and clathrasils are generally synthesized hydrothermally with water as the solvent in a sealed autoclave at temperatures typically between 150 and 250 °C. The crystallization of zeolites and the resultant crystal structures are sensitive to the precursor composition, the use of a structure directing agent (SDA), also called “template”, the specific route of precursor preparation, and the synthesis temperature and duration. Crystal size are controlled by the rates of nucleation and crystal growth, which are strongly dependent on the supersaturation of the solution (Momma, 2014).

For crystallization of clathrasils, guest species seem to play an indispensable role. The cage–like framework structures cannot be constructed without guest molecules (Momma, 2014). For more details about the synthesis procedures of clathrasils, and in particular of melanophlogite, see the Chapter "**3.2**".

Recently, in a paper on the isotope content characteristic of enclathrated molecules (Lazzeri *et al.*, 2017), the potential of melanophlogite as a proxy for fluids circulation in sedimentary rocks has been enlighted. The apparent rarity of melanophlogite is currently disputed (Beard *et al.*, 2013). Melanophlogite is the most common clathrate silicate phase and one of the few minerals providing information on degassing in sedimentary assemblages: even though classified as a rare mineral for a long time, recent findings as an alteration product of volcanic ashes may indicate that it is likely overlooked, mostly when occurs as a quartz pseudomorphosis (Beard *et al.*, 2013).

Since the first description by Von Lasaulx (1876), it has been clear that the loss of guest molecules could happen maintaining the mineral crystal structure (Liu *et al.*, 1997; Navrotsky *et al.*, 2003), which makes melanophlogite also interesting for gas storage, with potential environmental application in greenhouse molecules sequestration. For this purpose, the determination of sorption and desorption conditions and kinetics are major problems, but very few data are at present available to describe the desorption process of guest molecules with temperature.

Degassing to a guest–free melanophlogite has been obtained in several studies, as preliminary to further investigation (Žák, 1972; Liu *et al.*, 1997; Xu *et al.*, 1997; Navrotsky *et al.*, 2003), and at temperatures higher than 1000 °C, after several hours heating; however, thermogravimetric analysis was never done to detail the guest molecules release. For instance, it is not clear whether degassing occurs with a steady rate, from which temperature and to which extent, or whether there are some differences due to the kind of enclathrated species. Moreover, thermodynamic and crystallographic details of the degassing process were not clarified.

Melanophlogite is energetically metastable with respect to α–quartz by 9.5 ± 0.5 kJ mol^{-1} (Navrotsky *et al.*, 2003). The entropy and Gibbs free energy for guest–free melanophlogite relative to quartz at 298 K are ΔS_{trans} = 6.7 J mol^{-1} K^{-1} and ΔG_{trans} = 7.5 kJ mol^{-1}, respectively (Geiger *et al.*, 2008).

The heat capacities and entropies of guest–containing melanophlogite are larger than those of guest–free one, reflecting the presence of enclathrated molecules, such as CH_4, CO_2 and N_2. Some difficulties remain in determining the heat capacity and entropy at 25 °C, accompanied

by the enclathration of molecules, since concentrations and distributions of various molecules in the natural melanophlogite samples are not quantitatively known. By using cage occupancies based on previous studies, in addition to thermodynamic properties for ideal CH_4, CO_2 and N_2, Geiger *et al.* (2008) have obtained preliminary values of 80.1 J mol^{-1} K^{-1} and –642.2 J mol^{-1} K^{-1} for heat capacity and entropy, respectively, for a melanophlogite sample from Mt. Hamilton, at 25 °C and 1 bar, and 202.2 J mol^{-1} K^{-1} and –802.2 J mol^{-1} K^{-1} for heat capacity and entropy, respectively, for a melanophlogite sample from Racalmuto, at 25 °C and 1 bar. The formation enthalpies for the guest–containing samples remain unknown, and therefore their Gibbs free energies cannot be determined.

A calorimetric investigation was done by Kolesov & Geiger (2003) and Navrotsky *et al.* (2003), but only below room temperature, whereas previous high temperature crystallographic investigations were basically aimed to clarify the transition behaviour below 200 °C (Liu *et al.*, 1997; Nakagawa *et al.*, 2005), with little interest on the higher temperature evolution.

Melanophlogite has been the only known natural SiO_2 clathrate, until the discovery of two new silica clathrate minerals, chibaite (**MTN**) and the **DOH**–type mineral, which are isostructural with Structure II and Structure H clathrate hydrates and contain hydrocarbon gases originated from geothermal activities at convergent plate boundary. This finding is similar to that of thermogenic gas hydrates in terms of the origin of hydrocarbons and tectonic setting of the occurrence (Momma *et al.*, 2011). Silica clathrate minerals store hydrocarbons, which have vanished from sedimentary rocks, and therefore, they provide new evidence about geological carbon cycle at convergent plate boundaries (Momma *et al.*, 2011).

1.2.1.1.2. MELANOPHLOGITE AND NATURAL CLATHRASILS

Three types of clathrasils occur in nature: melanophlogite (**MEP**), chibaite (**MTN**), and the **DOH**–type mineral. These clathrasils crystallize from low–temperature hydrothermal solutions occurring in the diagenesis process of sedimentary rocks (Momma *et al.*, 2011). Based on the association with other silica minerals and their relation in the diagenesis process, the formation temperatures of natural clathrasils are estimated to be much lower than synthesis conditions of laboratory, i.e. 160–200 °C (Gunawardane *et al.*, 1987). Melanophlogite often occurs with amorphous silica (opal–A), cristobalite (opal–CT) and chalcedony (Cooper & Dunning, 1972; Žák, 1972; Tribaudino *et al.*, 2008). Chibaite and the **DOH**–type mineral are closely associated with opal–A and are rarely in contact with quartz (Momma *et al.*, 2011).

The euhedral crystals of chibaite are often found in small cavities located in veins. Chibaite and **DOH**–type mineral are epitaxially intergrown with each other: the <001> axis of **DOH**–type mineral is parallel to the <111> axis of chibaite. Chibaite has a cubic symmetry, with a refractive index of 1.470(1) and a Mohs hardness of 6.5–7. The **DOH**–type mineral is optically uniaxial and has higher refractive indices than the chibaite, the crystals of which often contain domains of low symmetry with anisotropic optical properties (Momma *et al.*, 2011).

The gas hydrates have recently come under much investigation because of their possible use in CO_2 sequestration, natural gas storage, and as potential energy resource. Members of the corresponding SiO_2 group are of interest because of their unusual physical properties, including the ability to enclathrate different types of guest molecules (Kolesov & Geiger, 2003).

The growth process of natural clathrasil minerals and their alteration process during diagenesis are of special interest (Navrotsky *et al.*, 2003; Momma *et al.*, 2011). CO_2–containing clathrasil minerals can store greenhouse gases in geological settings without the requirement of metal ions, which are necessary when trapping CO_2 as carbonates. Compared with CO_2 hydrates, clathrasils are more resistant to high temperatures and high pressures in geological settings. However, because of higher solubility of clathrasils with respect to quartz, initially occurring clathrasil crystals are often dissolved and recrystallized to quartz during subsequent diagenesis (Skinner & Appleman, 1963; Momma *et al.*, 2011). At temperatures well below 100 °C, these dissolution and recrystallization processes occur simultaneously and very slowly at the micrometer or submicrometer scale while preserving the original clathrasil crystal shape. These quartz "crystals" that possess clathrasil shapes are referred as "pseudomorphs" after clathrasils.

1.2.1.1.3. OTHER CLATHRASILS CONTAINING [5^{12}] CAGES

In Fig. 1.2, types of cages and framework structures of clathrasils with pentagondodecahedral [5^{12}] cages are shown (Momma, 2014).

MEP is the framework topology characteristic of melanophlogite, which is historically recognized as the first clathrasil (Kamb, 1965).

With an exception of **MEP**, the framework topologies of all the other clathrasils with [5^{12}] cages are based on the "dodecasil layer", comprising a polytypic series of dodecasils and deca–dodecasils.

Dodecasil–1H (**DOH**) (Gerke & Gies, 1984) is the simplest member of the dodecasil series, formed by hexagonal layers of face–sharing [5^{12}] pentagonal dodecahedra cages, and with additional [$4^3 5^6 6^3$] and [$5^{12}6^8$] cages. [$4^3 5^6 6^3$] voids are made up of three squared faces, six pentagonal faces, and three hexagonal faces; [$5^{12}6^8$] voids are made up of twelve pentagonal faces and eight hexagonal faces. The framework topology of **DOH** is identical of that of the hexagonal Structure H of clathrate hydrates (Ripmeester *et al.*, 1987).

Dodecasil–3C (**MTN**) (Gies, 1984 (a); Könnecke & Fuess, 1995; Knorr & Depmeier, 1997), also known as ZSM–39 (Schlenker *et al.*, 1981), holdstite (Smith & Blackwell, 1983) or CF–4 (Long *et al.*, 1987), is another member of the dodecasil series. Dodecasil–3C, isotypic with the cubic Structure II of clathrate hydrates (Schlenker *et al.*, 1981), has a framework consisting of face–sharing [5^{12}] and additional [$5^{12}6^4$] cages. [$5^{12}6^4$] voids are made up of twelve pentagonal faces and four hexagonal faces. At high temperature, the space group of dodecasil–3C is the highest possible symmetry of the topology *Fd*–3*m* (Könnecke *et al.*, 1992), but its actual symmetry depends on the temperature and guest species. For instance, the reported symmetries of the room temperature phases are: *Fd*3 for spherical guest species (Kr, Xe, CH_4, and $N(CH_3)_3$) (Gies, 1984 (a)); $I4_1/a$ for tetrahydrofuran (Knorr & Depmeier, 1997) and *t*–butylamine (Könnecke & Fuess, 1995); *I*–42*d* for pyridine (Chae *et al.*, 1991); *F*222 or *F*2*dd* for pyrrolidine (Könnecke & Fuess, 1995).

The deca–dodecasil framework comprises a dodecasil layer interconnected through additional six–membered rings (T6 rings). Deca–dodecasil–3R **DDR** (Gies, 1986) is the only confirmed member of this polytypic series. Another polytype, deca–dodecasil–3H (DD3H), has been synthesized only in minor amounts (Gies & Czank, 1986; van Koningsveld & Gies, 2004). In the **DDR** structure, the 19–hedra [$4^3 5^{12} 6^1 8^3$] are interconnected through eight–membered rings, forming a two–dimensional pore system between the dodecasil layers. [$4^3 5^{12} 6^1 8^3$] voids are made up of three squared faces, twelve pentagonal faces, one hexagonal face, and three octagonal faces, and this polytypic series has no current counterpart in the clathrate hydrates chemistry (van Koningsveld & Gies, 2004).

MEP, **DOH**, **MTN**, **DDR** and DD3H are the only topologies known for clathrasils with [5^{12}] cages. Disordered structures have not been found till now, although oriented intergrowth between **DOH** and **DDR** (Gunawardane *et al.*, 1987) and between **DOH** and **MTN** (Momma *et al.*, 2011) has been observed. A complex clathrate hydrate of choline hydroxide tetra–n–propylammonium fluoride ($C_{16}H_{99.66}FN_2O_{32.33}$), having an extremely long *c*–dimension (~ 9 nm), has been found (Udachin & Ripmeester, 1999), with large super–cages formed by four [5^{12}] and/or [$4^3 5^6 6^3$] cages, in which large molecules can be present.

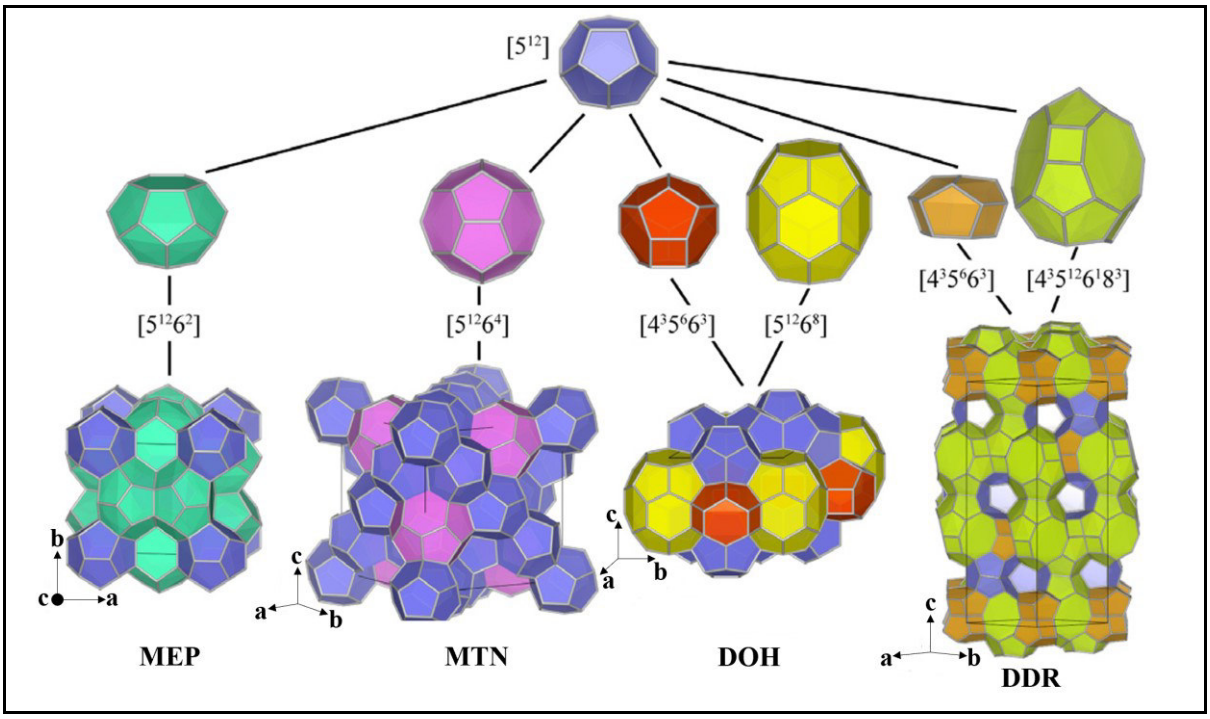

Figure 1.2. The types of cages and the framework structures of clathrasils containing pentagondodecahedral [5^{12}] cages (Momma, 2014).

1.2.1.2. PHYSICAL PROPERTIES

1.2.1.2.1. BEHAVIOUR UNDER HIGH TEMPERATURE AND HIGH PRESSURE OF MELANOPHLOGITE AND OTHER CLATHRASILS

Clathrasils and zeosils show more structural stability, in respect to aluminosilicate zeolites, at high temperature. The framework structures of aluminosilicate zeolites generally collapse on heating for temperature lower than 625 °C, accompanied by loss of molecular water or the reactions between the framework atoms and the extra–framework cations (Momma, 2014). The framework structures of clathrasils and zeosils remain stable at temperature higher than 625 °C. Pure SiO_2 frameworks requires no extra–framework atoms for stabilizing framework structures. These frameworks are electrostatically neutral and highly hydrophobic, having only weak van der Waals interactions between their guest species. Upon heating, small guest molecules can be removed and guest–free materials can be obtained. For instance, CH_4, CO_2, and N_2 molecules can be removed after heating at 650 °C for seven hours (Yagi *et al.*, 2007), and guest–free melanophlogite can be obtained after heating at 950 °C for six hours (Navrotsky *et al.*, 2003). However, the complete removal of larger guest molecules is difficult, if not impossible, because of the relatively small windows of the cages and lack of

channels. Tetramethylammonium in dodecasil–3C has not been completely removed after heating at 1200 °C in air for nine hours (Daqing *et al.*, 1990). A pyridine guest has not been removed after rapidly heating dodecasil–3C to 700 °C (Chae *et al.*, 1991). During the heat treatment of clathrasils, the organic molecules often decompose and remain in the structure, changing the crystals colour to black (Momma, 2014).

Low density zeolites collapse to the rigid amorphous state by temperature and pressure at temperatures that are well below the melting points of crystals of the same composition, but of conventional density (Greaves *et al.*, 2003).

Xu *et al.* (2007) have discussed a pressure–induced amorphization for guest–free melanophlogite at ~ 8 GPa. The sample has been directly compressed using a diamond anvil cell, without a pressure medium. The pressure–induced amorphous phase is an intermediate, metastable state. When the amorphous phase at 8.03 GPa has been heated up to 1200 °C, diffraction peaks characteristic of coesite, which is the thermodynamically stable phase at these pressure conditions, have started to appear at 600 °C. Yagi *et al.* (2007) have reported similar but more complicated amorphization behaviours of melanophlogite at high pressure. Natural guest–bearing melanophlogite samples, containing CO_2 as a main guest molecule, and preheated guest–free melanophlogite samples have been compressed up to 25 GPa, using various pressure media at room temperature. When methane or an alcohol–water mixture have been used as pressure–transmitting media, unheated melanophlogite has shown an irreversibly amorphization at approximately 17 GPa, in which the volume has been decreased to approximately 70 % of its original volume. No structural phase transition has been detected up to that pressure. Preheated melanophlogite, however, has been much more compressible, amorphizing only at approximately 3 GPa, with volume decreased to 80 %. This behaviour changes completely with helium used as the pressure–transmitting medium. The unheated sample has been much less compressible and neither a phase transition nor amorphization has been observed up to approximately 25 GPa. Preheated samples have exhibited the same compression curve up to approximately 17 GPa of that observed for unheated samples using a helium pressure medium. However, with pressure exceeding approximately 17 GPa, isostructural transition has occurred with a sudden increase in unit cell volume by 10 %. The two isostructural phases with different volumes are coexisting in a narrow pressure range of less than 1 GPa, and above 18 GPa, the high pressure phase has been compressed in a normal manner up to 24 GPa. This sudden increase in volume is a reversible process with a large hysteresis of approximately 6 GPa. In the pressure–decreasing cycle, a sudden decrease of the unit cell volume to its original compression curve has been observed. This anomalous volume

increase by compression can be attributed to the intrusion of additional helium into the cage. Various other experimental and computational studies have demonstrated that intrusion of guest species into zeolite frameworks increases their bulk modulus, and prevents amorphization from occurring up to higher pressures (Huang & Havenga, 2001; Isambert *et al.*, 2008; Haines *et al.*, 2010; Coasne *et al.*, 2011). A high–pressure cubic–to–tetragonal phase transition of the cubic phase of melanophlogite has been reported by Tribaudino *et al.* (2010). The sample contains only methane as a guest molecule and shows cubic symmetry at room temperature. A methanol:ethanol:water (16:3:1, MEW) mixture and silicone–oil (Si–oil) have been employed as the pressure media. The phase transition from cubic to tetragonal has been observed at 1.14 GPa in both MEW and Si–oil runs. The tetragonal phase is stable up to the highest pressure (6 GPa) in the run with MEW, but it has switched back to cubic symmetry at 3.12 GPa in Si–oil. This difference is probably due to the non–hydrostatic character of Si–oil at pressures higher than 0.9 GPa. The high–pressure transition has been found to be very similar to the thermally induced cubic–to–tetragonal transition observed by Nakagawa *et al.* (2005).

In a study by Gatta *et al.* (2014), the evolution with pressure of the CH_4 vibrational modes related to C–H stretching has been followed by *in–situ* Raman spectroscopy on a single crystal of cubic melanophlogite, coming from the Italian location of Varano Marchesi and containing only CH_4 in the structural voids. The sample has been compressed hydrostatically in a diamond anvil cell up to 6.5 GPa, using a non–penetrating pressure–transmitting medium. Two Raman modes at 2900 and 2910 cm^{-1}, corresponding to C–H stretching of CH_4 entrapped in the $[5^{12}6^2]$ and $[5^{12}]$ cages respectively, have been followed in response to the applied pressure. A change in the slope of the frequency in dependence of pressure linear trend of the sharper peak at 2900 cm^{-1}, observed between 1 and 1.5 GPa, has been interpreted as an evidence of the pressure–induced cubic–to–tetragonal transition, previously observed by XRD at pressure higher than 1.2 GPa. At pressure below the transition, the shift with pressure of the CH_4 modes is comparable to that observed in methane ice hydrate, which however becomes hexagonal at pressure higher than 1.2 GPa. The ratio of the integration areas of the two C–H stretching Raman peaks does not change significantly with pressure across the phase transition. At pressure higher than 5.1 GPa, a shoulder appears, close to peak at 2900 cm^{-1}, along with a slight change in the slope of the peak shift and the peak broadening. The shoulder is maintained in decompression down to pressure of 4.4 GPa, with a slight hysteresis. At the same pressure, however, XRD does not show any evidence of phase transition, suggesting that a rearrangement of CH_4 configuration could occur, without any

effect on the tetrahedral framework (Gatta *et al.*, 2014). A breaking of the isotropic character of CH_4 at higher pressures seems to take place, as previously observed in free methane (Wu *et al.*, 1995; Chen *et al.*, 2011).

A pressure–induced amorphization of clathrasils has been reported for the first time by Tse *et al.* (1994) and Tse & Klug (1995) in dodecasil–3C (**MTN**) and deca–dodecasil–3R (**DDR**). NaCl has been employed as a pressure–transmitting medium, compressing both guest–containing and guest–free samples. Dodecasil–3C has been transformed to an amorphous material at ~ 6 GPa, and the transition can be reversible, with a guest tetrahydrofuran inside the cages, or irreversible, with empty cages. Transformation of deca–dodecasil–3R to a (probably) disordered phase has been observed with infrared spectra changes at ~ 4 GPa for the guest–free sample and at ~ 7 GPa for the guest (aminoadamantane)–containing sample. Through experimental tests and theorical molecular dynamics calculations, the presence of underformable units, such as guests, has been determined to be essential for the reversible process (Tse *et al.*, 1994; Tse & Klug, 1995).

1.2.2. METHANE HYDRATES

Among clathrate hydrates, methane clathrates (also called methane hydrates) are noteworthy. When various low molecular weight gases (e.g. methane, ethane, carbon dioxide, hydrogen sulphide) combine with water at pressures and temperatures common in the sediments of continental margins and permafrost regions, the resulting compound is gas hydrates, an ice–like substance consisting of water cages surrounding guest molecules in a clathrate structure.

Melanophlogite is isostructural with ice hydrates, with the ice molecules substituted by $[SiO_4]$ tetrahedra (Gatta *et al.*, 2014). As melanophlogite, Structure I clathrates, the most widespread type, have cubic symmetry (space group: $Pm3n$; lattice parameter: ~ 12 Å) with forty–six water molecules and eight potential guest sites, which are two smaller pentagondodecahedral and six larger tetrakaidekahedral cavities, with an average radius of 3.95 and 4.33 Å respectively (Sloan, 2003). If guest molecules fill all the cages, as they rarely do in nature, Structure I clathrate can concentrate methane by ~ 160 times compared to gas at standard pressure and temperature.

Methane hydrate deposits and the often–proximal gas–charged sediments constitute a potentially large, but currently untapped, hydrocarbon reserve within porous sediments (Ruppel, 2007). Further details on the methane hydrates properties and potential applications are reported in Appendix, Chapter "**6.3**".

1.3. OPEN PROBLEMS AND GOALS OF THIS STUDY

The aim of this thesis is the crystallographic and mineralogical characterization of one of the silica clathrate compounds: melanophlogite.

The characteristic structure consisting of a three–dimensional network in which the four vertices of the tetrahedra [SiO_4] are shared to arrange a framework hosting polyhedral cages, populated by guest molecules, could make melanophlogite interesting for the gas storage, with potential environmental application in greenhouse gases sequestration. For this purpose, the determination of sorption and desorption conditions and kinetics are the major problems, but at present very few information are available to describe the release of guest molecules with increasing temperature. From a practical point of view, gas storage presents two crucial problems concerning energy and technological aspects: 1) clarifying the conditions in which absorption and desorption phenomena take place; 2) defining the methods to store/extract molecules in/from absorbing materials, respectively.

A particularly interesting aspect concerns the possibility of synthesizing melanophlogite, trying to reproduce the same conditions of natural genesis in laboratory. To be able to carry out the most complete possible characterization of the synthesized material, it is necessary to have an adequate quantity to conduct the required experimental analyses and, consequently, it is fundamental to define synthesis procedures, which allow to obtain material as pure as possible and in appropriate quantities, that is hundreds of milligrams. This goal seems to have never been achieved before, as there are no references in the literature.

Samples of natural and synthesized melanophlogite have been studied, using a multi–analytical approach. The choice of the experimental analyses to be used has been strongly influenced by the characteristics of natural and synthesized melanophlogite samples to be investigated. On account of this, it has been not possible to carry out the same experimental analyses on all the natural and synthesized samples of melanophlogite, steered towards this study.

XRD analyses, using conventional and unconventional X–Ray sources, on powders and single crystals, at room and varying temperature, have been carried out in order to define: 1) how pure and crystalline the natural and synthesized samples are, in terms of possible presence of accessory mineralogical phases and of the amorphous fraction, respectively; 2) the structure characterizing the natural and synthesized samples, with the thermal ranges of stability and

the possible phase transitions, specifying the temperatures at which they take place and the symmetries involved.

Raman spectroscopy analyses have been carried out to ascertain the presence of characteristic guest molecules on samples of natural melanophlogite from different localities and to identify the guest molecules within the structural cavities on synthesized melanophlogite.

TGA has been done to define the behaviour of natural and synthesized melanophlogite samples as function of increasing temperature, in terms of release of guest molecules and consequent mass variation. Till now, TGA has been never done to detail the guest molecules release process: for instance, it is not clear if degassing takes place with a steady rate or if it is different with varying temperature or if there are some differences in degassing due to the kind of guest molecules enclathrated in the structural cavities.

DSC has been carried out on natural and synthesized melanophlogite in order to identify possible phase transitions, specifying the temperature at which they occur and the type of these, for instance, if they are reversible or not reversible processes.

An INS study is currently in progress on synthesized melanophlogite in order to clarify the interactions between the guest molecules into the structural voids and the silicate framework, which host them, in particular in order to gain a deeper insight into the dynamical properties of the host framework, as well as onto the diffusion mechanism of the guest molecules.

2. MATERIALS AND METHODS

The natural samples studied in this thesis come from collectors gifts, namely by Prof. E. Acerbi, for Fortullino, Prof. D. Bersani, for Varano Marchesi, and Dott. M.E. Ciriotti, for Racalmuto melanophlogite. Fortullino and Varano Marchesi melanophlogite are on open surface of veins, whereas for Racalmuto only some crystals are available. Sample descriptions will be given in the experimental section, as well as a description of the analytical conditions at each sample.

In the following, a general outline of the instrumental facilities used in this study is shown, and the goals meant for their use. Detailed analytical conditions will be instead reported with each experiment.

DSC

All DSC experiments have been carried out at the Chemistry Department of University of Pavia, employing a Sensys calorimeter by Setaram (France). The setting is in differential scanning calorimetry, i.e. no direct information on unit heat is given (Milanese pers. comm.).

The powdered sample is heated or cooled, at 2 or 5 °C/min, always under an atmosphere of Ar, and using open alumina crucibles as sample–holders.

The purpose of this investigation is to find the onset of heat exchange during phase transitions and degassing.

RAMAN SPECTROSCOPY

All Raman spectroscopy investigations have been carried out employing a portable Enspectr RaPort–Raman Handheld Analyser, equipped with a green laser (λ_{green} = 532 nm), and at a maximum output power of 30 mW. Raman spectra have been collected in the wavenumber range 100–4000 cm^{-1}, and with a spectral resolution of 8 cm^{-1}.

The portable instrument pays a lower spectral resolution, but has the advantage to sample a larger area than the laboratory Raman, and can probe all the frequency range in one single collection. This aspect is quite useful for melanophlogite, whose characteristic silicate pattern is the same in all the samples of melanophlogite (natural and synthesized ones), and the well identified spectral features of guest molecules, placed between 1000 and 3500 cm^{-1}, are the sole difference between natural and synthesized samples. For the natural samples, the guest molecules spectral features are the only one difference between their localities of findings.

Moreover, the portable instrument can be brought directly in the outcrop, allowing to check immediately the presence of pseudomorphic quartz. The instruments pays a lower spatial resolution, but in this case, where a relatively large sample is available, the point is not critical.

SC–XRD

SC–XRD measurements have been carried out at the Department of Chemistry, Life Sciences and Environmental Sustainability of University of Parma, using a Bruker AXS Smart single–crystal diffractometer, equipped with an APEX II CCD, and operating with MoKα radiation (MoKα: λ = 0.71073 Å).

The purpose of this investigation was to determine the crystal structure of the melanophlogite at the different experimental conditions. This was not achieved, as suitable single crystals were never found, being extensively mosaicized and/or twinned.

TGA

All TG analyses have been carried out at the Chemistry Department of University of Pavia, taking advantage of a Q5000 thermogravimetric analyser by TA Instrument (USA).

A powdered sample is undergone to a heating, from a temperature close to room temperature, up to high temperatures, at a rate of 5 °C/min, in accordance with the characteristics of each sample, always under nitrogen flow, and with pans of platinum as sample–holders.

XRPD WITH CONVENTIONAL SOURCE

In the presence of highly twinned crystals powder diffraction proved to be an effective alternative to single crystal diffraction. In this thesis, different powder diffractometers were used. For preliminary characterization of the synthesized samples, a Bruker D2 Phaser powder diffractometer, hosted at Department of Chemistry, Life Sciences and Environmental Sustainability of University of Parma, equipped with a copper anode (CuKα: λ = 1.5460 Å), and operating in the Bragg–Brentano θ–θ geometry, and at 30 kV and 10 mA was used.

Linxeye position–sensitive detector and zero–background sample–holder are employed.

The advantage of this diffractometer is to obtain well resolved diffraction patterns, thanks to the solid state detector, in times of few minutes, and to have an immediate feedback on the experimental results. However, to obtain a good diffraction pattern with reduced power, the detector is closer to the sample, which reduces the actual resolution, making it very sensitive

to sample position, i.e. to the thickness of the powdered sample, which, if too high, can distort the positions of peaks, displacing them.

For higher resolution, i.e. for the unit cell determination at room temperature, a Thermo Arl X'TRA powder diffractometer, at Department of Chemistry, Life Sciences and Environmental Sustainability of University of Parma, equipped with a Thermo Electron solid state detector, operating in the Bragg–Brentano θ–θ geometry, and with CuKα radiation (CuKα: λ = 1.5460 Å) has been used. As in the Bruker D2 Phaser analyses, the powdered samples are prepared on a quartz zero–background sample–holder. The diffractometer is in conventional setting, with larger goniometer than the Bruker D2 Phaser.

High temperature powder diffraction was done with the Bruker D8 Discover diffractometer, at Department of Mathematical, Physical and Computer Sciences of University of Parma, equipped with HISTAR area detector and GADDS software, operating at 40 kV and 40 mA, and in a Debye–Scherrer geometry, with a copper anode (CuKα: λ = 1.5460 Å).

The peculiar geometry, and the presence of the area detector, allow to collect reasonably good statistics data, even with a small amount of powdered samples (that is few milligrams), sealed in a glass capillary, which rotates during the data acquisition to average possible preferential orientations.

Diffraction patterns are obtained by merging different frames, with the detector placed at 20 cm apart from the sample.

The sample temperature can be changed between 30 and 400 °C by means of a specifically designed furnace, made up of two heating prongs, placed close to the capillary, and allowing the X−Ray beam to pass through the sample, and reach the detector. The hot region around the sample is protected by a thin Kapton cap.

A background strongly structured has to be connected to instrumental specifications, such as: 1) the presence of the capillary, which causes an increase of the signal around the angular position of 20 °2θ; 2) the fact of using a 2D detector, and the resulting increased sensitivity of diffuse scattering measurement.

The sample is placed in a glass capillary, due to peculiar geometry. The advantage of having a two dimensional pattern, however, was not exploited in this work, due to the lack of preferential orientation. A drawback was in the poor sample to detector positioning, which potentially leads to systematic over or underestimation of unit cell values. Moreover, a rather large background is present. Therefore, unit cell values have been recalibrated against those obtained at room temperature by the Thermo Arl X'TRA powder diffractometer.

XRPD WITH UNCONVENTIONAL SOURCE

XRPD, using a non–conventional source (synchrotron radiation), has been carried out at ID22 beamline of ESRF of Grenoble (France), employing a high resolution powder diffractometer, equipped with a sample changing robot, and an Oxford Cryosystems 700–series nitrogen cryostat. The cryostream allows to change the temperature, through a nitrogen flow. Powder diffraction measurements of high resolution, in terms of minimum instrumental contribution to the widths of the diffraction lines, were carried out at a wavelength of 0.354205(6) Å. The powdered sample (~ 10 mg) was loaded in a 1 mm Ø quartz capillary. Because data collection times for each whole pattern at a given temperature were less than 2 minutes, the samples were spun at high speed to ensure reasonable powder averaging. The sample scan lasted less than 12 hours total.

3. EXPERIMENTAL INVESTIGATIONS ON MELANOPHLOGITE

3.1. NATURAL SAMPLES

The natural melanophlogite samples are from Italian localities, namely: Fortullino (Livorno, Tuscany), Racalmuto (Agrigento, Sicily), and Varano Marchesi (Parma, Emilia Romagna). In this thesis, they will be named from their own locality of finding as “melanophlogite from Fortullino”, “melanophlogite from Racalmuto” and “melanophlogite from Varano Marchesi”. The three melanophlogite from the three localities host clearly defined guest molecules within the microporous framework of melanophlogite, made up of corner sharing [SiO_4] tetrahedra and isolated cages between them, whose chemical composition is strongly related to geological setting.

3.1.1. GEOLOGICAL SETTING

The information on the geological settings are taken from the literature, with the exception of the field observations in melanophlogite pseudomorphosis from the outcrop of Varano Marchesi, which are discussed within the general geological description.
All the other investigations were made specifically for this thesis.

FORTULLINO

Fortullino is a locality between Castiglioncello and Quercianella, near Livorno. It takes its peculiar name from the small *botro* (a deep and steep ditch, with flowing or stagnant waters), locally named as “*Fortulla*”.
The outcrop is located in the formation of the "ophiolithic scaled clays" emerges, which, in the area between Castiglioncello and Gabbro (two fractions of the Municipality of Rosignano Marittimo, near Livorno), contains numerous masses of green rocks, mainly serpentineous. The serpentines are sometimes crossed by a series of large faults with Apennine direction: these faults have been affected by a mineralization mainly made up of magnesite with minor amounts of chalcedony and, sometimes, of iron sulfides (Marinelli, 1955).
Upon contact with these veins of magnesite, the encasing serpentine takes on the appearance of a chaotic breccia, cemented by a paste of magnesite and crossed by a thick network of

veins, which are mainly of dolomite: here melanophlogite has been found, sometimes also in considerable quantities. The highest concentration of melanophlogite has been discovered in the northernmost part of the main vein of magnesite, on the left side of the *Fortulla* Valley, about 4 km far from the sea. Sporadic occurences have been found further south, near Castiglioncello (Grassellini Troysi & Orlandi, 1972).

Melanophlogite usually occurs in the form of spheroidal aggregates with a diameter between 1 and 3 mm, sometimes in aggregated cubes and only rarely in isolated cubes, with edge of 1 mm (Grassellini Troysi & Orlandi, 1972). Melanophlogite spherules are normally limpid, and the opacity of some of them is due to a rough surface caused by the aggregation of tiny crystal cubes on the surface of the spherules. Sometimes, both the globular clusters and the cubic crystals are constituted by actual pseudomorphosis of cryptocrystalline or microcrystalline quartz.

Melanophlogite samples have been discovered also along the road which connects the town of Nibbiaia to the sea, where, in the midst of the palombini limestone, serpentineous rocks emerge, crossed by some predominantly dolomite veins: here, small crystalline aggregates containing rhombohedral dolomite, quartz and melanophlogite, have been collected. Microcrystalline cinnabar has been rarely found. In this area, melanophlogite has been always found well crystallized, in the form of cubic crystals aggregated to each other, with dimensions reaching 3–4 mm of edge (Grassellini Troysi & Orlandi, 1972).

The research of melanophlogite has been extended to the veins of magnesite in other areas of Tuscany, among which Gabbro, Montefuroli, and Elba Island, without success (Grassellini Troysi & Orlandi, 1972).

In the samples available for this study, melanophlogite appears in the form of translucent or transparent spheroid aggregates, scattered like dewdrops on the surface of ophiolite rocks. Even though the typical aggregation is spheroidal, the small globules, if observed by an electron microscope or by a strong optical microscope, are formed by a set of cubic microcrystals, aggregated so to form tiny balls. Individual cubic crystals have not been found in the samples examined till now.

Carbonate alteration processes of ophiolitic rocks (serpentinites) led to Mg–rich carbonate rocks formation and SiO_2–rich phases separation in the form of melanophlogite and opal (Bracci & Orlandi, 1985), according to the formation processes shown below:

$$Mg_6[(OH)_8Si_4O_{10}] \text{ (serpentine group mineral)} + (n–4)H_2O + 6CO_2 \rightarrow$$

$$6MgCO_3 \text{ (magnesite)} + 4SiO_2 \bullet nH_2O \text{ (opal)}$$

and

$$Mg_6[(OH)_8Si_4O_{10}] \text{ (serpentine group mineral)} + (n–10)H_2O + 6Ca(HCO_3)_2 \rightarrow$$
$$6CaMg(CO_3)_2 \text{ (dolomite)} + 4SiO_2 \bullet nH_2O \text{ (opal)}$$

The above–related carbonate alteration processes of serpentinites promoted the formation of Mg–rich carbonate rocks, typical of the area around Livorno, which underwent an intensive magnesite mining during the first half of the last century (Nannoni & Sammartino, 1975; Barsotti, 1999).

Melanophlogite from Fortullino crystallized in an environment rich in CO_2, as the hydrothermal solution which has led to the deposition of the veins of magnesite (Grassellini Troysi & Orlandi, 1972).

The CO_2–rich environment promoted melanophlogite crystallization: the transformation of opal into melanophlogite requires a template (in this case, CO_2).

RACALMUTO

Melanophlogite from Racalmuto was found as regular cubes with a maximum size of 2 mm, encrusting sulphur, calcite, and celestine crystals (Von Lasaulx, 1876). Melanophlogite has been sometimes, but not invariably, separated from the sulphur and calcite crystals by a thin film of opaline silica. In many instances, melanophlogite has grown on a nucleus of quartz or opal.

Crystals of melanophlogite can be found, on rare occasions, as single, undistorted individual cubes. More commonly, however, they occur as complex intergrown, rounded aggregates, which may coalesce to form a continuous crust over the sulphur crystals. The unaltered melanophlogite cubes range from colourless through pale yellow to a deep red–brown, and are finely zoned.

It appears that the sulphur and calcite crystals have been the earliest minerals, and all evidences have shown that the opaline silica ceased deposing before melanophlogite. The sulphur crystals did not stop growing after the melanophlogite began to crystallize, since some minor overgrowths of melanophlogite have been discovered close to sulphur. It seems that melanophlogite did not grow as oriented overgrowths on sulphur or calcite (Skinner & Appleman, 1963).

According to Friedel (1890; 1891; 1892), several crystals assumed to be of melanophlogite were actually pseudomorphic quartz, and unaltered crystals of melanophlogite were scarcely found. Samples of altered melanophlogite can be easily distinguished from unaltered ones by

their characteristic opacity, showing a turbid–white colour and lacking in the sparkle and luster typical of the unaltered ones (Skinner & Appleman, 1963).

The organic matter and sulphur can be related to film of sulphur–bearing organic pigment, trapped on the faces of the crystal, during their growth. The incorporation of organic matter indicates that melanophlogite possibly precipitated from an organic medium, although the method of precipitation, whether by breakdown of organo–silica compounds, by direct precipitation of SiO_2 from solution or even by aggregation of colloidal silica, is not known (Skinner & Appleman, 1963).

In spite of the well–shaped cubic appearance of the melanophlogite, apparent anisotropic optical behaviour was observed and interpreted as an effect of the organic matter, making a film within the crystal, rather than by a property of bulk melanophlogite. The inorganic film is not crystalline and shows birefringence due to an orientation imposed on the organic molecules incorporated in the film. Melanophlogite is isotropic, and it can be verified by destroying the birefringence of the organic film by heating (Skinner & Appleman, 1963).

Dessau *et al.* (1962) studied the geology of the Sicilian sulphur deposits, pointing out that sulphur is almost certainly of biogenic origin, rather than of volcanic one. Thus, it appears that melanophlogite may be crystallized as an end–product of the syngenetic–diagenetic processes, which gave rise to the sulphur deposits and to their enclosed bituminous fluids (Skinner & Appleman, 1963).

VARANO MARCHESI

The investigated samples have been found in a marl quarry used for pozzolanic concrete, at Case Montanini, near the locality of Varano Marchesi (Parma). The quarry occurs within the Contignaco Formation, which is formed by the Early Miocene hemipelagic siliceous marls and silty marls, with few Tripoli (siliceous limestone) beds and volcaniclastic layers of rhyolitic composition. The geological setting of this area is quite complex: the quarry is on the northern limb of an upright faulted syncline, which belongs to a series of NNE–vergent folds affecting the Middle Eocene to late Miocene epi–Ligurian succession (Ricci Lucchi, 1986). The latter lies on the top of the allochthonous Ligurian units, i.e., the remnants of Mesozoic oceanic and forearc deposits derived from the closure of the Ligurian–Piedmont Ocean and its continental margins (Boccaletti *et al.*, 1971; Marroni *et al.*, 2002). The quarry is located about 2 km south of the Salsomaggiore tectonic window, defined by the allochthonous Ligurian and the epi–Ligurian units overthrusting the Langhian to Serravallian turbiditic foredeep deposits

cropping out in the Salsomaggiore anticline. The Salsomaggiore anticline has been exhumed during the Messinian and then covered by Late Messinian–Early Pliocene continental to marine deposits. The latter have been folded by Early Pliocene and Pleistocene tectonic events. During this multiphase and complex geological evolution of the Salsomaggiore area, seepage of CH_4 and other hydrocarbons has occurred, as testified by a Late Serravallian methane–related faunal assemblage and deposits (Conti *et al.*, 2007) and present–day fluids rising in localized spots around the Salsomaggiore anticline (Artoni *et al.*, 2004).

Melanophlogite has been found in pocket and veins, only in the more siliceous and compact levels of the Contignaco Formation, i.e., those with apparently lower porosity, always in association with opal. Melanophlogite is present as euhedral cubes, from 0.1 to 1 mm in size, and found in veins, which are never completely filled: on the contrary, in filled veins only opal is present. A thin crust of opal, with thicknesses lower than 1 mm, has been always found between melanophlogite and the host rock (Tribaudino *et al.*, 2008).

The outcrop observations provided some constrains on the genesis of melanophlogite from Varano Marchesi, which has been found in open veins, always grown on opal, and never been in direct contact with the host rock. These features suggest a formation at very mild hydrothermal conditions. A possible source of silica for the hydrothermal fluid could be the dissolution of biogenic silica from the diatom shells in the surrounding siliceous shales. At high temperature, the formation of the thermodynamically stable quartz is promoted, as testified by melanophlogite cubic pseudomorphic quartz.

Melanophlogite was found in a fracture system related to one of the Middle Miocene to present–day tectonics events, in pockets or open veins, where crystals could grow unstrained, without interfering each other. This aspect suggests that this shear stress would cause the leakage of guest molecules and, consequently, the structural collapse of melanophlogite.

As reported in Fig. 3.1, the presence of opal within melanophlogite with corroded rims could indicate that melanophlogite has grown, at least in part, at expenses of opal. A similar observation has been made for melanophlogite from Racalmuto by Skinner & Appleman (1963).

This may be related to a secondary incursion of CH_4–rich fluids, which could have dissolved opal, and promoted melanophlogite crystallization.

The host veins have been found within layers more compact and with carbonate cement between the grains; in most of the outcrop, melanophlogite and opal have not occurred. It seems that fractures present within the harder cemented layers could provide a trap for

incoming CH_4–rich fluids, which have been diffusing within the more porous marls (Tribaudino *et al.*, 2008).

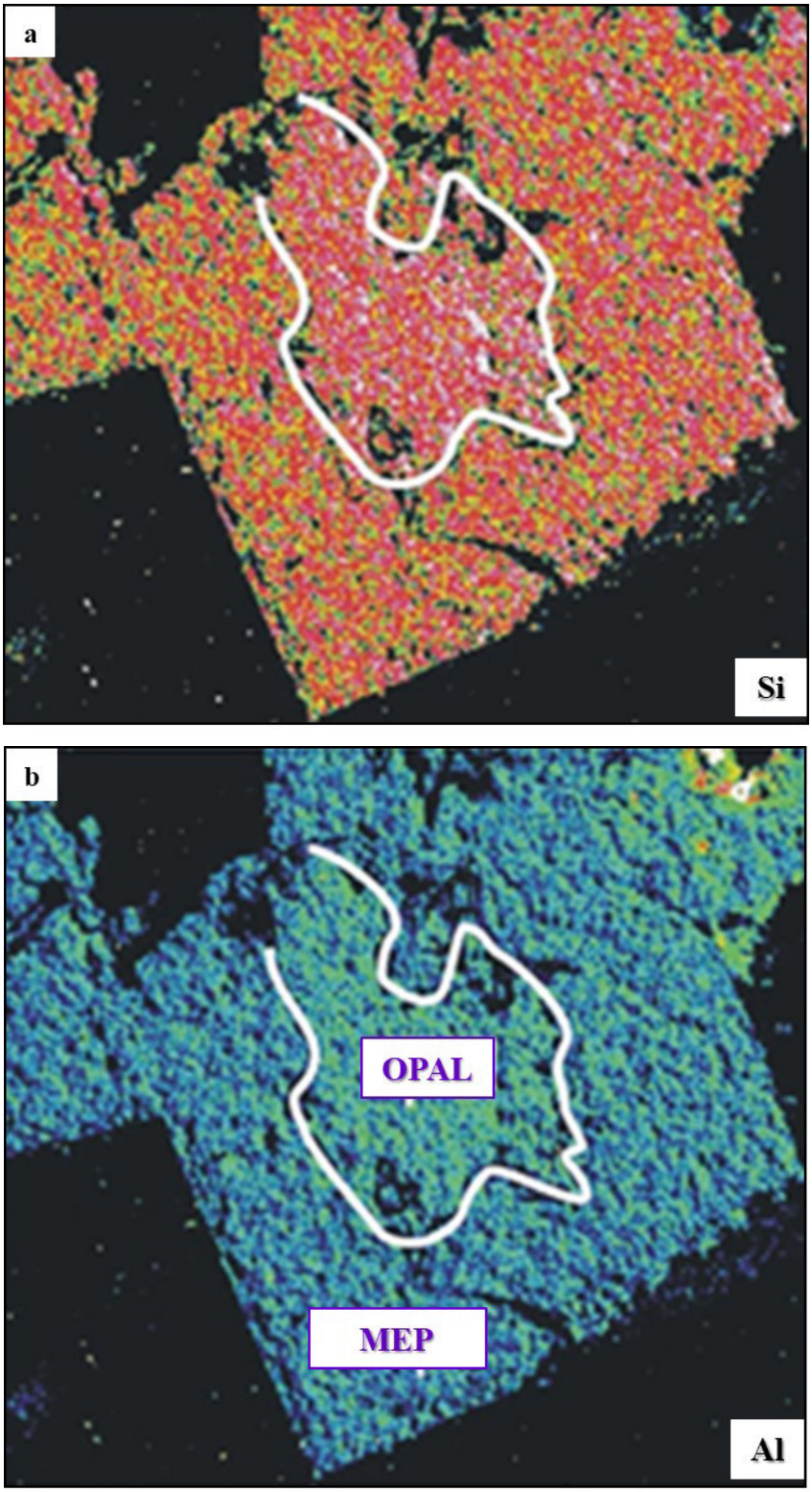

Figure 3.1. SEM–EDS qualitative X–Ray map of Si (a) and Al (b), in a melanophlogite crystal enclosing opal. The different colour of opal with respect to melanophlogite indicate a slightly higher Si and Al content (from Tribaudino *et al.*, 2008).

3.1.2. RAMAN SPECTROSCOPY

Raman spectroscopy was performed to identify the guest molecules in melanophlogite structural cavities, and to estimate whether they are present in [5^{12}] and [$5^{12}6^2$] cages.

Moreover, Raman spectroscopy allows to detect cubic shaped crystals of melanophlogite transformed in pseudomorphic quartz, thanks to the presence of characteristic quartz peak.

Raman spectroscopy measurements have been carried out employing the portable Enspectr RaPort–Raman Handheld Analyser, and Raman spectra have been taken in the wavenumber range 200–3500 cm^{-1}.

The positions of the Raman modes of the guest molecules in the Raman spectra, for samples of melanophlogite from Fortullino, Racalmuto, and Varano Marchesi, have been calculated by fitting the experimental spectra, employing a Gauss–Lorentzian function.

As a first result, Raman spectroscopy enabled to detect the transformation of melanophlogite in pseudomorphic quartz, by the peaks of quartz, and the absence of those of the guest molecules in the melanophlogite from Varano Marchesi (Fig. 3.2).

This was found in cubic shaped melanophlogite crystals collected during a sampling in the same quarry where melanophlogite was found. A change in quarry outcrop, within the same geological formation, corresponding to a change in the stratigraphic position, could be related to the transformation to pseudomorphic quartz.

Raman spectra for the samples of melanophlogite from the Italian localities considered in this study are reported in Fig. 3.3. Fig. 3.4, and Fig. 3.5.

Guest species were identified by their peak positions in encaged melanophlogite, as reported in Tribaudino *et al.* (2008). As a rule, the positions in encaged melanophlogite are lower in frequency than the free gas; moreover, they are split, whereas in free gas the peaks are single. For instance, a strong free methane is at 2917 cm^{-1}, whereas the same peak of CH_4 in Varano Marchesi becomes a doublet of a stronger peak at lower frequency and a smaller one at higher, namely at 2900 and 2907 cm^{-1}.

The Raman spectra showed as expected the peaks of the guest molecules characteristic of the considered Italian localities (CO_2 for Fortullino, H_2S and CH_4 for Racalmuto, CH_4 for Varano Marchesi); however, in the Raman spectra taken for melanophlogite from Fortullino and from Racalmuto, other compounds have been identified in smaller quantities, i.e. CH_4 and CO_2, respectively for Fortullino and Racalmuto.

In the Raman spectrum collected for the sample from Fortullino (Fig. 3.3), no evidence was found of the hydrocarbons at low atomic weight, reported in literature by mass spectroscopy

investigation by Grassellini Troysi & Orlandi (1972). The CO_2 peaks are unsplit; they show the characteristic Fermi doublet, but without the same peak splitting as in CH_4 for Varano Marchesi.

In the Raman spectrum for the sample from Racalmuto (Fig. 3.4), H_2S and CH_4, which are the major guest molecules for this occurrence localities, and, in a small amount, CO_2, have been identified. The H_2S and CH_4 peaks are split, and CO_2 peaks are unsplit (Tribaudino *et al.*, 2008).

Moreover, a faint peak, broad and unsplit, was observed at 2947 cm^{-1}, which could be ascribed to a small C_2H_6 ethane content, the position of ethane in liquid is 2954 cm^{-1}, and the small decrease is within the expectation for encaged molecules (Frezzotti *et al.*, 2012).

In the Raman spectrum for the sample from Varano Marchesi (Fig. 3.5), only CH_4 has been identified, and its peak is split (Gatta *et al.*, 2014). Other peaks were not identified, besides a small peak in one spectrum at 3054 cm^{-1}, possibly ascribed to N–H vibrations (Frezzotti *et al.*, 2012).

Most important, no evidence between 3600 and 3700 cm^{-1} was found in any sample of the peaks for OH vibrations, which should be present in the event of an exchange of some oxygen with the hydroxyl, as postulated by Grassellini Troysi & Orlandi (1972), to cope with some chemical inconsistency in their data.

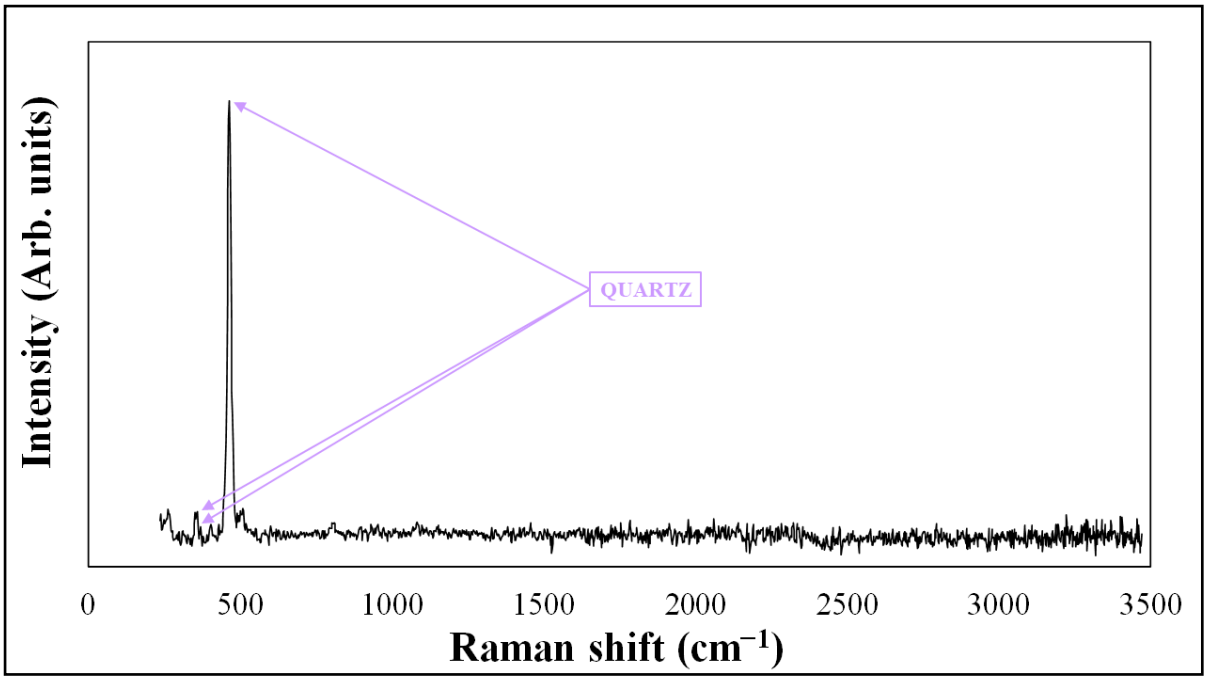

Figure 3.2. Raman modes of quartz in a rock sample from the quarries near Varano Marchesi, testifying the transformation of melanophlogite in pseudomorphic quartz.

Moreover, some information on the crystallographic position of the guest molecules could be obtained.

If the Raman peak is not split, the guest molecules occupy only one type of cage, among [5^{12}] and [$5^{12}6^2$] (Kolesov & Geiger, 2003); if split, the higher frequency peak was ascribed to the smaller [5^{12}] cage, and the lower frequency one to the [$5^{12}6^2$].

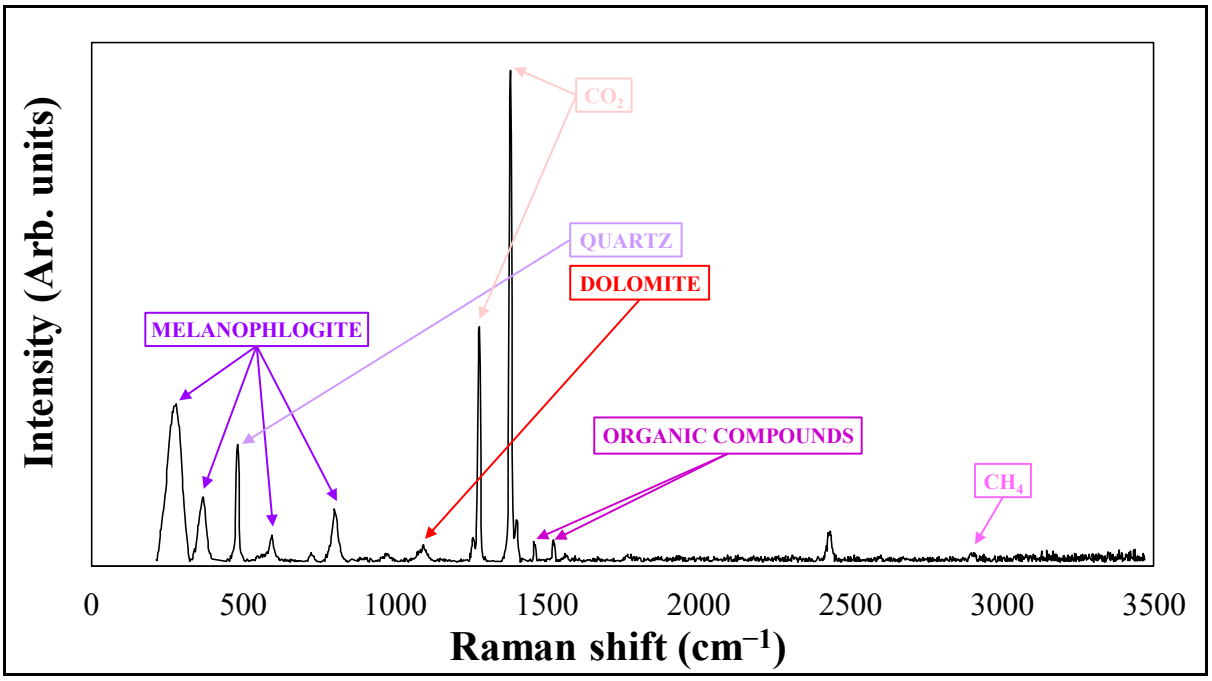

Figure 3.3. Raman modes in a sample of melanophlogite from Fortullino.

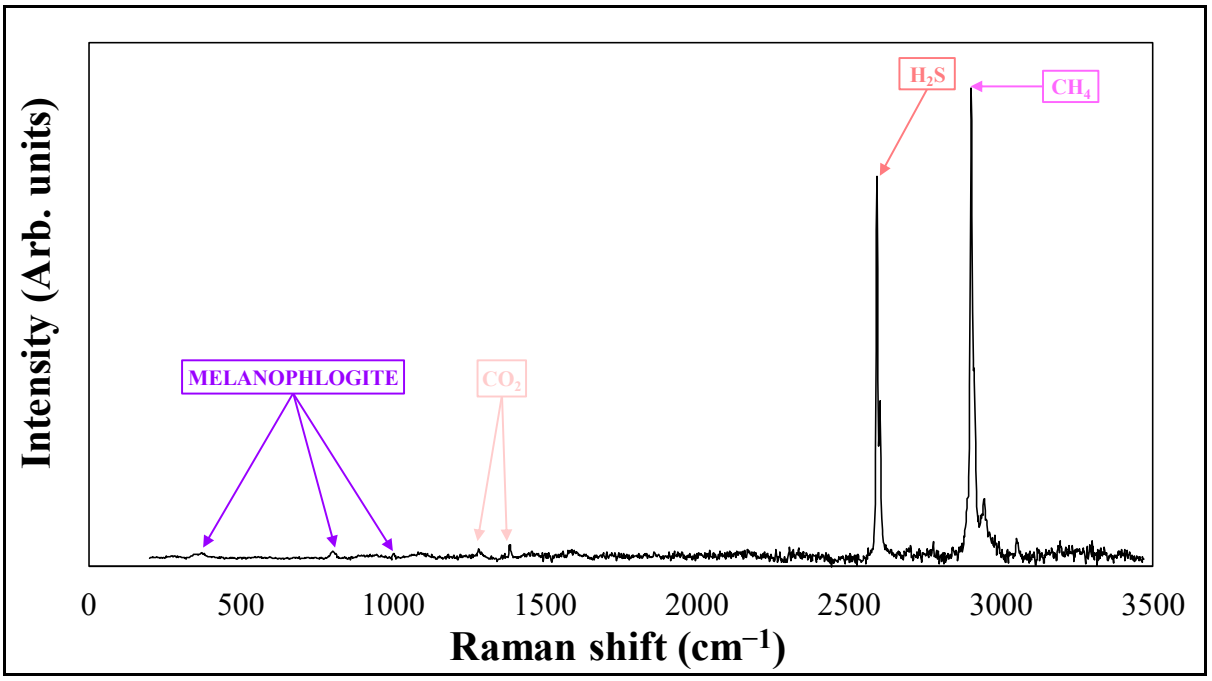

Figure 3.4. Raman modes in a sample of melanophlogite from Racalmuto.

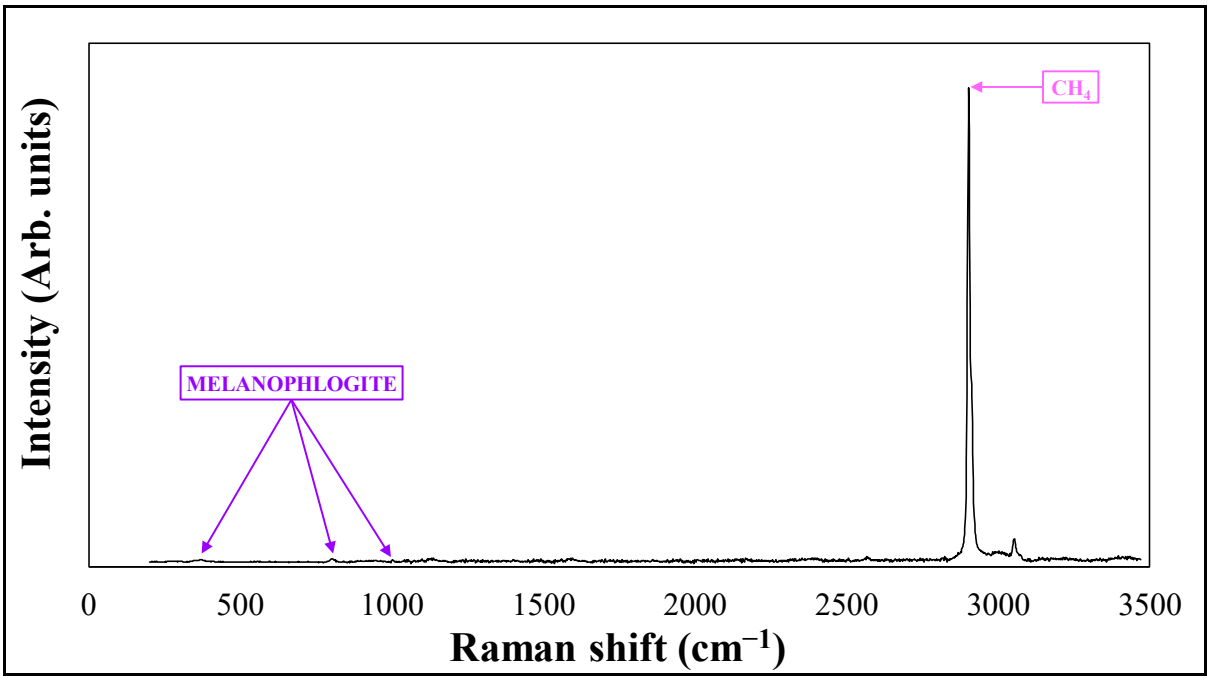

Figure 3.5. Raman modes in a sample of melanophlogite from Varano Marchesi.

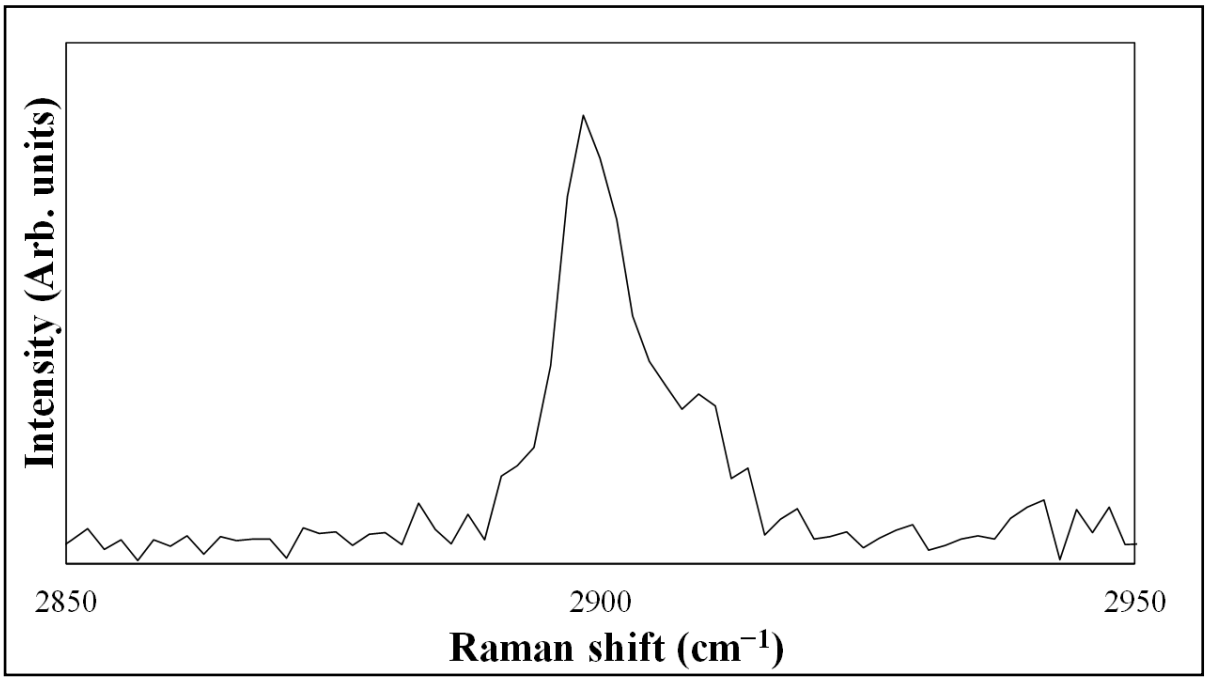

Figure 3.6. Raman modes in a sample of melanophlogite from Varano Marchesi, between 2850 and 2950 cm^{-1}: focus on CH_4 peaks.

In previous studies, it was found that the lower frequency peak of the split guest species peaks has an intensity which is generally three times higher than higher frequency one, in agreement with the higher site occupancy (Kolesov & Geiger, 2003).

To note, enclathrated species show lower frequencies than free gases (Kolesov & Geiger, 2003; Tribaudino *et al.*, 2008).

Consequently, the position and intensity of the Raman peaks can provide information about the distribution of the various guest species in the two types of structural cages characteristic of melanophlogite.

	CO_2	
Melanophlogite from Fortullino	1279 cm^{-1} and 1381 cm^{-1}	
Free state	1285.5 cm^{-1} and 1388.3 cm^{-1}	
	H_2S	CH_4
Melanophlogite from Racalmuto	2593 cm^{-1} and 2603 cm^{-1}	2901 and 2911 cm^{-1}
Free state	2611 cm^{-1}	2917 cm^{-1}
	CH_4	
Melanophlogite from Varano Marchesi	2901 and 2911 cm^{-1}	
Free state	2917 cm^{-1}	

Table 3.1. Wavenumber of Raman peaks for CO_2, H_2S and CH_4, and CH_4, the main guest molecules characteristic of melanophlogite from Fortullino, Racalmuto and Varano Marchesi, respectively, and the same ones in the free state, at room temperature. Raman peaks of CO_2 in their free state have been calculated by Herzberg (1989; 1991); Raman peaks of CH_4 in their free state have been reported by Tribaudino *et al.* (2008); Raman peaks of H_2S in the free state has been calculated by Schrötter & Klöckner (1979).

In Table 3.1, the wavenumber of Raman modes for CO_2, H_2S and CH_4, and CH_4, guest species of melanophlogite from Fortullino, Racalmuto and Varano Marchesi, respectively, and the same ones measured in the free state, at room temperature, are reported.

The difference between the position of Raman peaks for guest molecules entrapped in the samples of melanophlogite from different localities and in their free states could probably be connected to the interaction between the guest molecules and the wall of melanophlogite silica framework (Chazallon *et al.*, 2007).

The mode wavenumbers for the enclathrated molecules exhibit only small differences from those in the free state, due to very weak dispersion (van der Waals) interactions with the silica framework (Kolesov & Geiger, 2003).

To note, the unsplit nature of CO_2 was related to the presence of CO_2 only in the $[5^{12}6^2]$ cage, which, being larger, is supposed to host the CO_2 molecule. In the sample from Fortullino, a very broad CH_4 peak is present, between 2900 and 2910 cm^{-1}, without a stronger peak at 2900 cm^{-1}, i.e. without a concentration on the $[5^{12}6^2]$ cage. Such feature could be interpreted as related to a concentration of small amount of methane in the $[5^{12}]$ cage, being CO_2 confined in the larger cage.

3.1.3. XRPD AT ROOM TEMPERATURE

XRPD analyses at room temperature have been carried out on melanophlogite from Fortullino and from Racalmuto, to confirm the identification of melanophlogite and identify and quantify the accessory mineralogical phases.

The diffraction patterns have been collected with the Bruker D2 Phaser diffractometer. The patterns have been taken over the 3–60 °2θ range, with a counting time of 1 sec/step and 0.018 ° as 2θ step.

Rietveld full–profile fit has been performed with the GSAS suite and the EXPGUI interface (Larson & Von Dreele, 1997; Toby, 2001).

For melanophlogite, the structural model has the cubic symmetry *Pm*3*n* (Gies, 1983). At first, zero–shift on theta, unit cell parameters and background have been refined, and the background curve has been fitted with a Chebyshev polynomial, with 24 coefficients. The pseudo–Voigt profile function has been used (Thomson *et al.*, 1987), refining GW Gaussian and LX Lorentian profile components. Atomic positions and isotropic displacement parameters were fixed to the values reported in Gies (1983) and were not further refined.

In the samples from Fortullino and Racalmuto, the carbonate phases are present to some extent. Their contribution was modelled, starting from the trigonal symmetries *R*−3 and *R*−3*c*, as structural models for dolomite (Steinfink & Sans, 1959) and calcite (Althoff, 1977), for the samples from Fortullino and Racalmuto respectively, for which the refined carbonate phases are (11.11 ± 0.80) wt.% and (12.28 ± 0.46) wt.%. Preferential orientation was tested by March–Dollase formalism, but without any actual advantage in the refinement.

Despite the quite high values of χ^2 achieved at the end of the refining procedures, especially for the sample from Fortullino ($\chi^2 = 23.08$), the structural models used for melanophlogite and the carbonate phases (calcite and dolomite, for Racalmuto and Fortullino, respectively) fit adequately the experimental profile, at room temperature, for each sample (Fig. 3.7: a and b).

No peak splitting nor superstructural reflections were shown in these diffraction patterns. However, significant residuals in diffraction peaks are present and the final values of χ^2 are relatively high, indicating that the structural model is not fully adequate. This was found to be a limitation of the resolution of laboratory equipment: as already found by Fyfe & Gies (1990) and Likhacheva *et al.* (2018), in the analysis of powder patterns collected with the laboratory equipment, tetragonal melanophlogite failed to show peak splitting, which could help to distinguish the tetragonal melanophlogite from the cubic one.

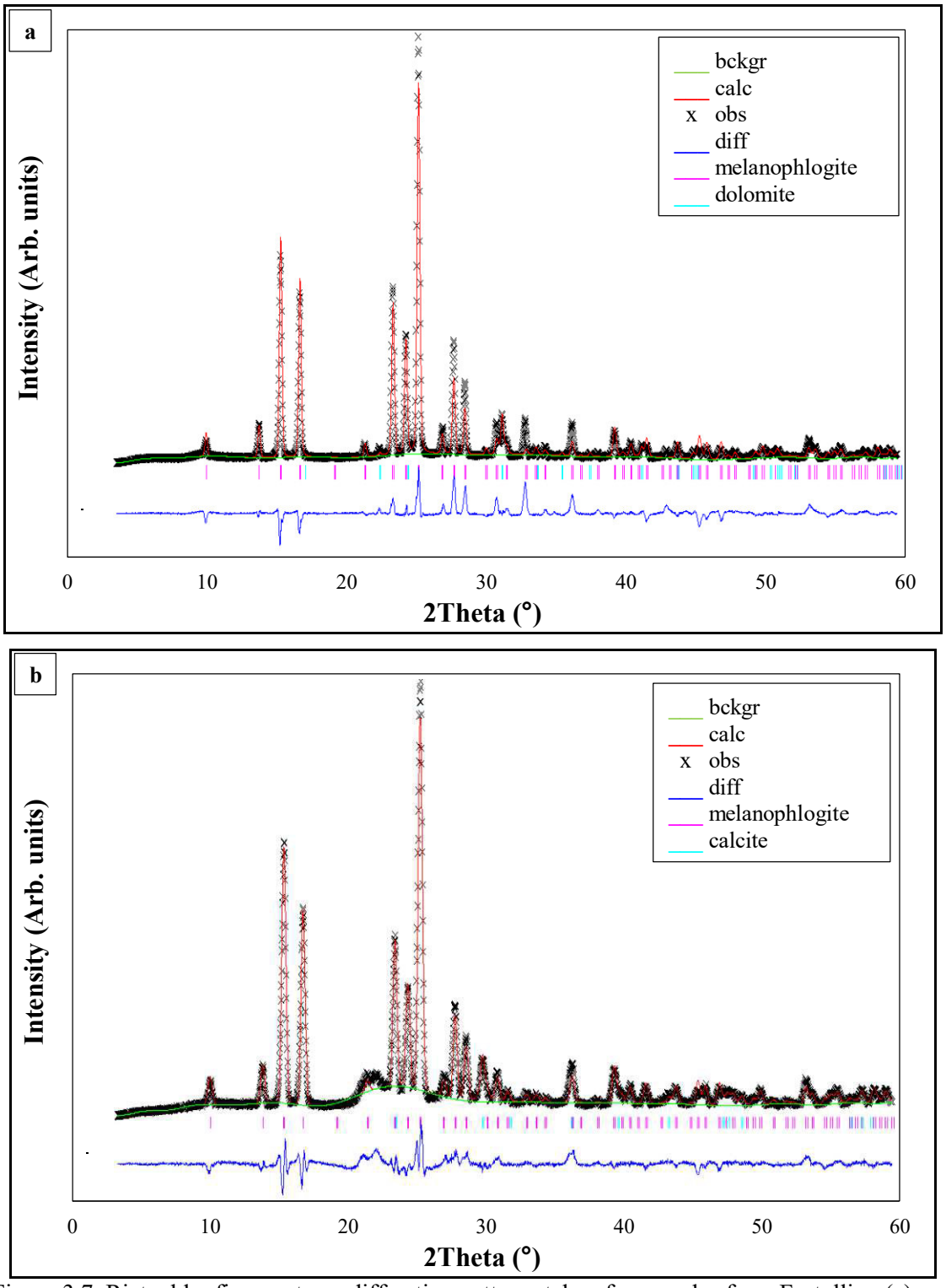

Figure 3.7. Rietveld refinements on diffraction patterns taken for samples from Fortullino (a) and Racalmuto (b), at room temperature in the cubic symmetry, in a spectrum taken with conventional source. The difference between calculated and observed patterns (in red and marked with crosses, respectively) is in blue and the background in green. Melanophlogite and carbonate phases (dolomite for Fortullino, calcite for Racalmuto) are indicated with pink and light blue bars, respectively.

Moreover, any attempt to refine the powder pattern within the structural model of tetragonal melanophlogite provided by Nakagawa *et al.* (2001; 2005) failed to improve the agreement

between calculated and experimental patterns. The point will be clarified in the following section where high resolution synchrotron data are presented.

In the powder diffraction pattern collected for Racalmuto (Fig. 3.7b), there is a broad peak, at an angular position slightly higher than 22 °2θ, probably characteristic of CT–opal, previously detected in samples from Racalmuto (Skinner & Appleman, 1963) and Varano Marchesi (Tribaudino *et al.*, 2008). Opal constitutes the thin crust, separating melanophlogite from sulphur and calcite crystals, or the nucleus around which melanophlogite has grown.

3.1.4. XRPD WITH VARYING TEMPERATURE

3.1.4.1. CONVENTIONAL X–RAY SOURCE

High temperature XRD has been carried out on the powdered sample of melanophlogite from Fortullino, in order to investigate the variation of unit cell parameters and unit cell volume with increasing temperature, and consequently individuate possible phase transitions.

High temperature XRPD measurements have been done with the Bruker D8 diffractometer, from room temperature up to 400 °C.

The diffraction patterns have been collected from 30 to 55 °C, at steps of 5 °C, and from 75 to 400 °C, at steps of 25−30°C. The explored angular range is between 8 and 45 °2θ, with an acquisition time of 5400 sec for the whole spectrum, between 30 to 55 °C, and of 3600 sec, between 75 and 400 °C. The furnace has been heated at a rate of 10 °C/min, and stabilized at the given temperature before collecting the diffraction pattern.

As shown in Fig. 3.8, a phase transition at a temperature close to 60 °C has been identified by a marked change in the slope of the trend of the unit cell volume with increasing temperature, from a lower symmetry, characteristic of low temperature, to a high temperature cubic one. The low temperature phase was previously reported for melanophlogite from Mt. Hamilton to be tetragonal at room temperature (Nakagawa *et al.*, 2001; Nakagawa *et al.*, 2005).

It is interesting to note that the same trend of the unit cell volume as a function of temperature is noticeable in the samples from Fortullino and Mt. Hamilton, and the phase transition occurs around 60 °C in both occurrence sites, despite the different guest molecules in the structural cages (Fig 3.8).

In Table 3.2, unit cell parameter and unit cell volume values are reported, from 40 up to 400 °C, employing, in the Rietveld refinements, a *Pm*3*n* cubic symmetry (Gies, 1983) as structural

model for melanophlogite, for all the temperatures of the investigated range, also for the ones at which the lower symmetry one is expected (Fig 3.8).

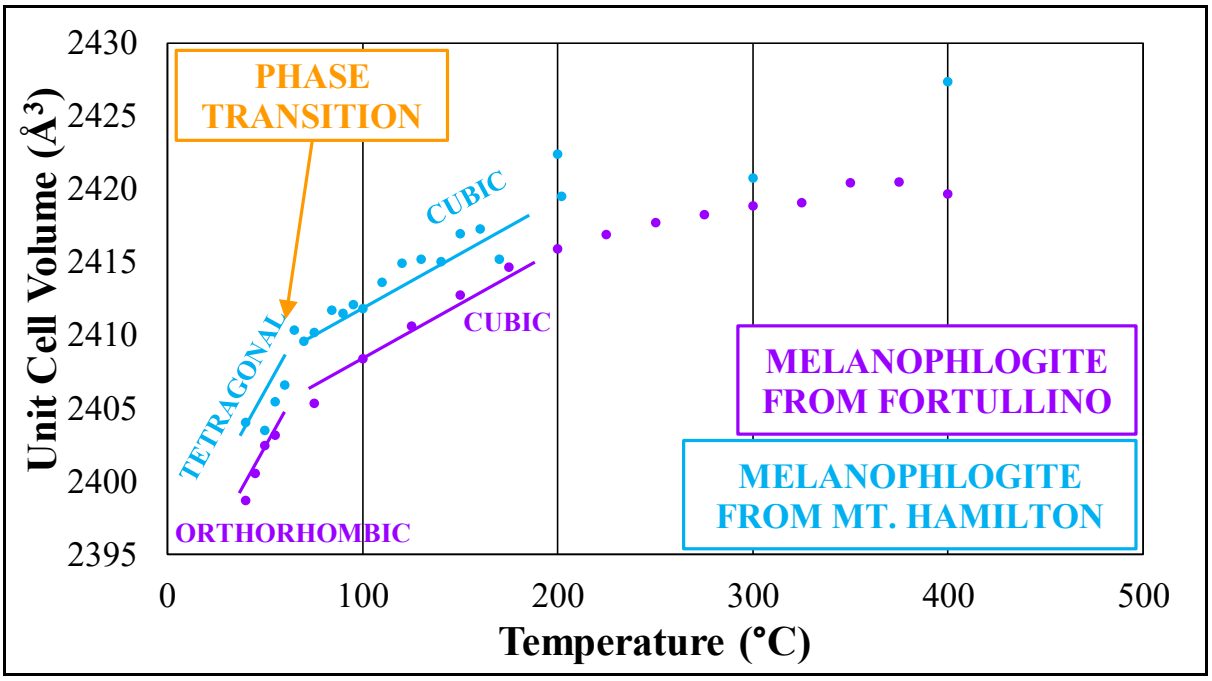

Fig. 3.8. HT–XRPD on melanophlogite from Fortullino, from room temperature up to 400 °C, compared with the results for melanophlogite from Mt. Hamilton (Nakagawa *et al.*, 2005).

T (°C)	UNIT CELL PARAMETER (Å)	UNIT CELL VOLUME (Å^3)
400	13.428(1)	2419.7(5)
375	13.430(1)	2420.5(5)
350	13.430(1)	2420.7(5)
325	13.427(1)	2419.1(5)
300	13.427(1)	2418.9(5)
275	13.426(1)	2418.3(5)
250	13.425(1)	2417.7(6)
225	13.423(1)	2416.9(5)
200	13.421(1)	2415.9(6)
175	13.419(1)	2414.7(6)
150	13.415(1)	2412.8(6)
125	13.412(1)	2410.7(6)
100	13.407(1)	2408.4(5)
75	13.402(1)	2405.4(6)
55	13.398(1)	2403.1(5)
50	13.396(1)	2402.5(5)
45	13.393(1)	2400.6(6)
40	13.389(1)	2398.7(6)

Table. 3.2. Unit cell parameter and unit cell volume variations, from Rietveld refinements on diffraction patterns taken for melanophlogite from Fortullino, from 40 up to 400 °C, considering a cubic symmetry.

The tetragonal model $P4_2/nbc$ of melanophlogite from Mt. Hamilton (Nakagawa *et al.*, 2001; Nakagawa *et al.*, 2005) is not adequate to fit properly to the peaks splitting, which is not observable in the diffraction patterns taken with the Bruker D8 Discover diffractometer, since it has not a resolution high enough.

On the contrary, the peak splitting is well observable in the diffraction patterns collected with an unconventional X–Ray source, that is the synchrotron radiation.

3.1.4.2. UNCONVENTIONAL X–RAY SOURCE

XRPD measurements have been done with the high resolution powder diffractometer at ID22 beamline of ESRF (Grenoble, France), from –173 to 107 °C. Powder spectra were taken every 10 °C between –173 and 27 °C and between 77 and 107 °C, and every 5 °C between 27 and 77 °C, that is, around the temperature at which the phase transition, previously detected through XRPD analysis using a conventional source (Chapter "**3.1.4.1**"), takes place.

Thanks to the high resolution of the diffractometer of ID22 and to the synchrotron radiation, it is possible to observe the splitting of diffraction peaks, testifying the phase transition from a lower symmetry, typical of low temperature, with split peaks, to a high temperature cubic one, with unsplit peaks (Fig. 3.9: a and b).

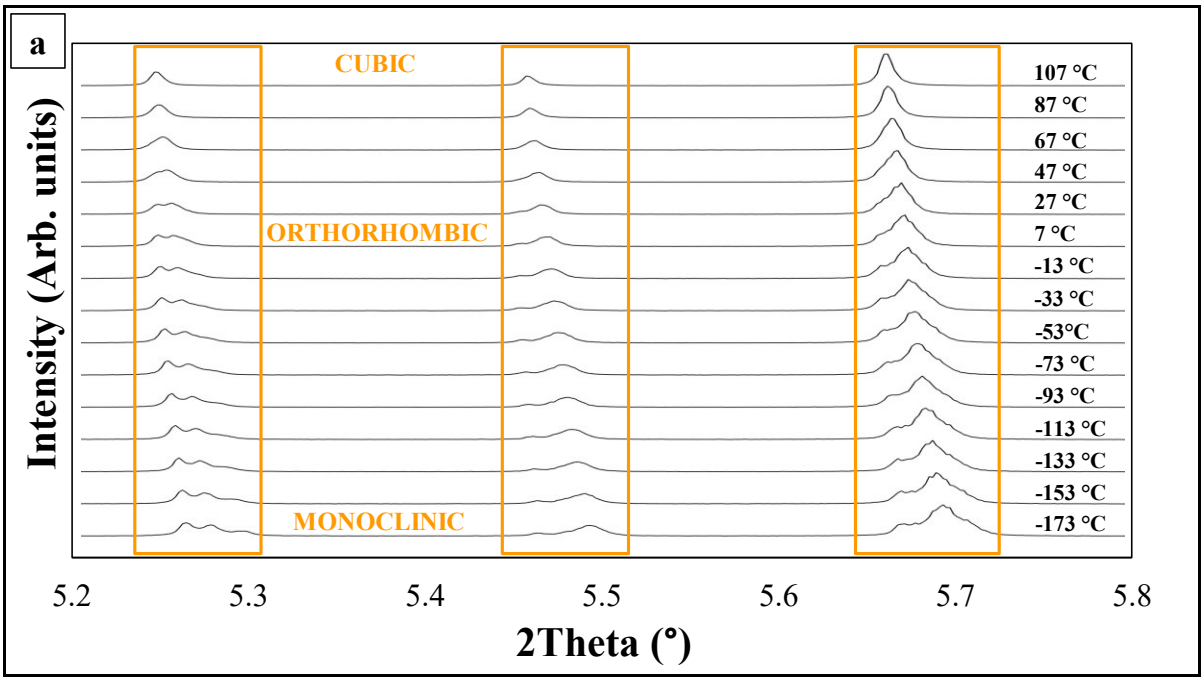

Synchrotron radiation diffraction patterns showed peaks which are split already at room temperature. The splitting is more apparent at lower temperature, and some peaks, showing as

single at the higher temperature, become a triplet with decreasing temperature. Peak splitting is hardly detectable at temperature higher than 50 °C (Fig. 3.9: a and b).

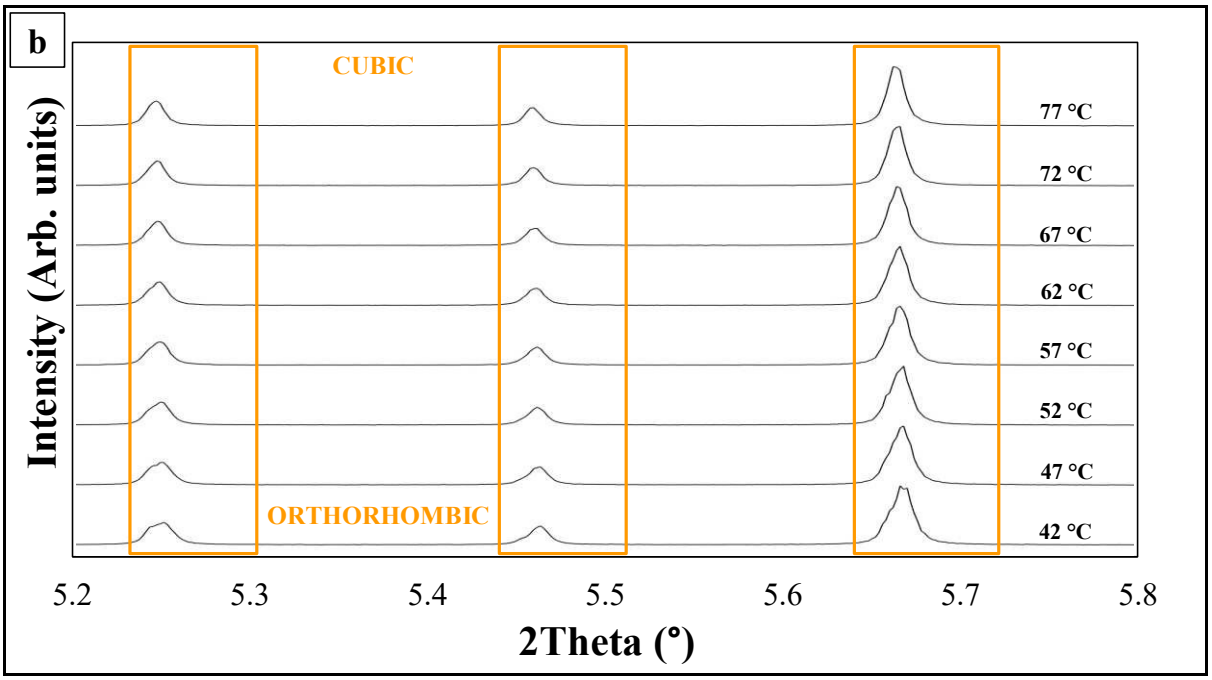

Fig. 3.9. (a) Diffraction patterns taken for melanophlogite from Fortullino, in the whole thermal range investigated with XRPD carried out using synchrotron radiation at ID22 of ESRF (Grenoble, France), and (b) at temperatures close to the phase transition.

Synchrotron radiation diffraction patterns were refined by Le Bail analysis of powder spectra, using Jana2000 Suite (D'Alessio *et al.*, in prep.).

The choice of the lower symmetry model was a rather difficult task, because of the little changes involved in the phase transition, not detectable by a conventional source. Although the tetragonal model fits quite well the room temperature patterns taken by a conventional source, in our synchrotron diffraction data, the tetragonal model fails to fit the observed peak splitting, in spite of repeated attempts. Consequently, it appears that the $P4_2/nbc$ tetragonal symmetry (Nakagawa *et al.*, 2001) is a wrong choice for the low temperature structure of the melanophlogite from Fortullino.

The failure to model the peak splitting in a $P4_2/nbc$ tetragonal lattice is apparent also at room temperature. This may be related to the presence of a symmetry characteristic of Fortullino melanophlogite, different from that one of melanophlogite from other localities. However, it may also come from a wrong symmetry assignment by previous authors.

In fact, the $P4_2/nbc$ is not a subgroup of the $Pm3n$. It was first proposed by Žák (1972), and the structure was refined in $P4_2/nbc$ by Nakagawa *et al.* (2001), for melanophlogite from Mt. Hamilton. NMR investigations by Liu *et al.* (1997) on Fortullino melanophlogite pointed out

that a transformation from *Pm*3*n* to $P4_2/nbc$ would require a route with two other tetragonal intermediate phase transitions. Short–range NMR data from the same authors pointed to a direct transition from the cubic to the lower symmetry phase. In agreement with short–range NMR data, the authors suggested a phase transition from the *Pm*3*n* to the *Pm*3, and then to *Pmmm*, i.e., from a cubic to an orthorhombic symmetry. As it will be shown in the following, our results from the spontaneous strain analysis point to a second–order phase transition, and we assume that group–subgroup relations are respected. Therefore, being the tetragonal model from Nakagawa *et al.* (2001) unsuitable to provide a reasonable fit, an orthorhombic model has been chosen instead.

The orthorhombic model fits quite well the synchrotron radiation diffraction data, from 60 °C down to about –25 °C. Le Bail powder diffraction patterns decomposition suggested that the most suitable structural model to refine the diffraction data is a rotated unit cell, characterized by a and b parameters corresponding to the diagonal along [110] and [–110] of the cubic unit cell with the parameters of 13 Å. A unit cell with a ≠ b and both close to 18 Å , and c ~ 13 Å results (Figure 3.10).

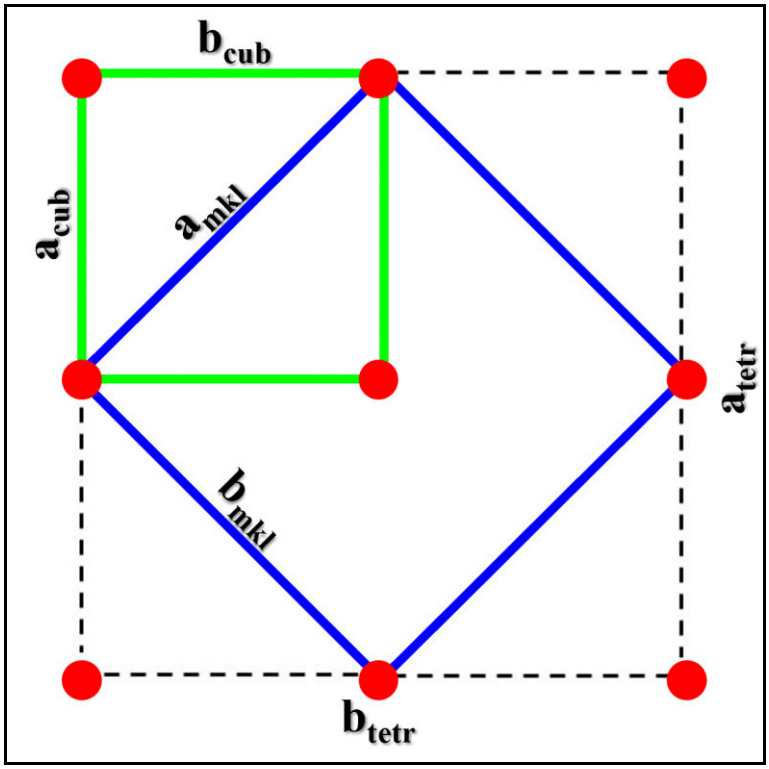

Fig. 3.10. Relative setting of monoclinic 18–18–13 Å (in blue), cubic 13–13–13 Å (in green), and tetragonal 25–25–13 Å (marked with black dashes) unit cells, setting on (001) in a cubic structure. In a cubic structure, $a_{cub} = b_{cub} = c_{cub} = 2^{1/2} * a_{mkl}$, whereas, in the actual monoclinic, the lattice point is offset.

In this unit cell, a *C*222 orthorhombic structure, with a lower symmetry, was proposed for subsequent Rietveld refinement (Mezzadri pers. comm.), which, however, failed in giving sensible results, owing to the very large number of parameters involved.

At –25 °C, we observe a change in the unit cell parameters vs temperature trend. In the diffraction patterns taken throughout the investigated thermal range, it is possible to note that one passes from single peaks of the high temperature *Pm*3*n* cubic symmetry (Gies, 1983), to split peaks of the room temperature *C*222 orthorhombic symmetry, up to triple peaks, at lower temperature, as reported in Fig. 3.11.

Moreover, as shown in the DSC section, there is evidence of a phase transition at –25 °C. The peak splitting at lower temperature can no more be modelled with the orthorhombic lattice, consequently a deviation from this has to be proposed.

A monoclinic structure for the lowest symmetry phase was chosen to obtain a reasonable fit to the observed peak splitting: it is the symmetry predicted by Liang *et al.* (2011), employing quantum mechanical simulations on a guest–free melanophlogite sample, and is coherent with experimental data from preliminary low temperature (T = –115 °C) SC–XRD (Mezzadri pers. comm.).

Le Bail analysis, carried out on the lower temperature diffraction patterns, showed a good fit employing the monoclinic metrics. In this unit cell, a *C*2 monoclinic structure, with a lower symmetry, was proposed (see file.cif deposited), and has the same setting of the orthorhombic unit cell.

The results were transformed to have the ~ 13 Å cell, for comparison with higher temperature, and reported in Table 3.3.

Despite some attempts, the orthorhombic and monoclinic structures could not be refined.

As superstructural reflections indicating a cell doubling were not found in the experimental diffraction patterns, probably due to their weakness, the phase transitions are revealed only by the unit cell distortion, at the phase transition characteristic temperature. The difference between the tetragonal symmetry by Nakagawa *et al.* (2001; 2005) and the orthorhombic and the monoclinic ones is rather subtle, and could be easily neglected in a conventional diffraction pattern, at room temperature. The transition from cubic to monoclinic occurs as the unit cell axes lose their equivalence, and an angle between them changes from 90 ° to a different value. In the monoclinic structure, the a and c axes are very close to each other, and only a slight deviation from 90 ° in the β angle, always found below 0.2 °, is present, and consequently the transition could be overlooked. A lower temperature monoclinic or triclinic

structure is suggested by quantum mechanical calculation in a guest–free melanophlogite sample by Liang *et al.* (2011), but never experimentally verified still now.

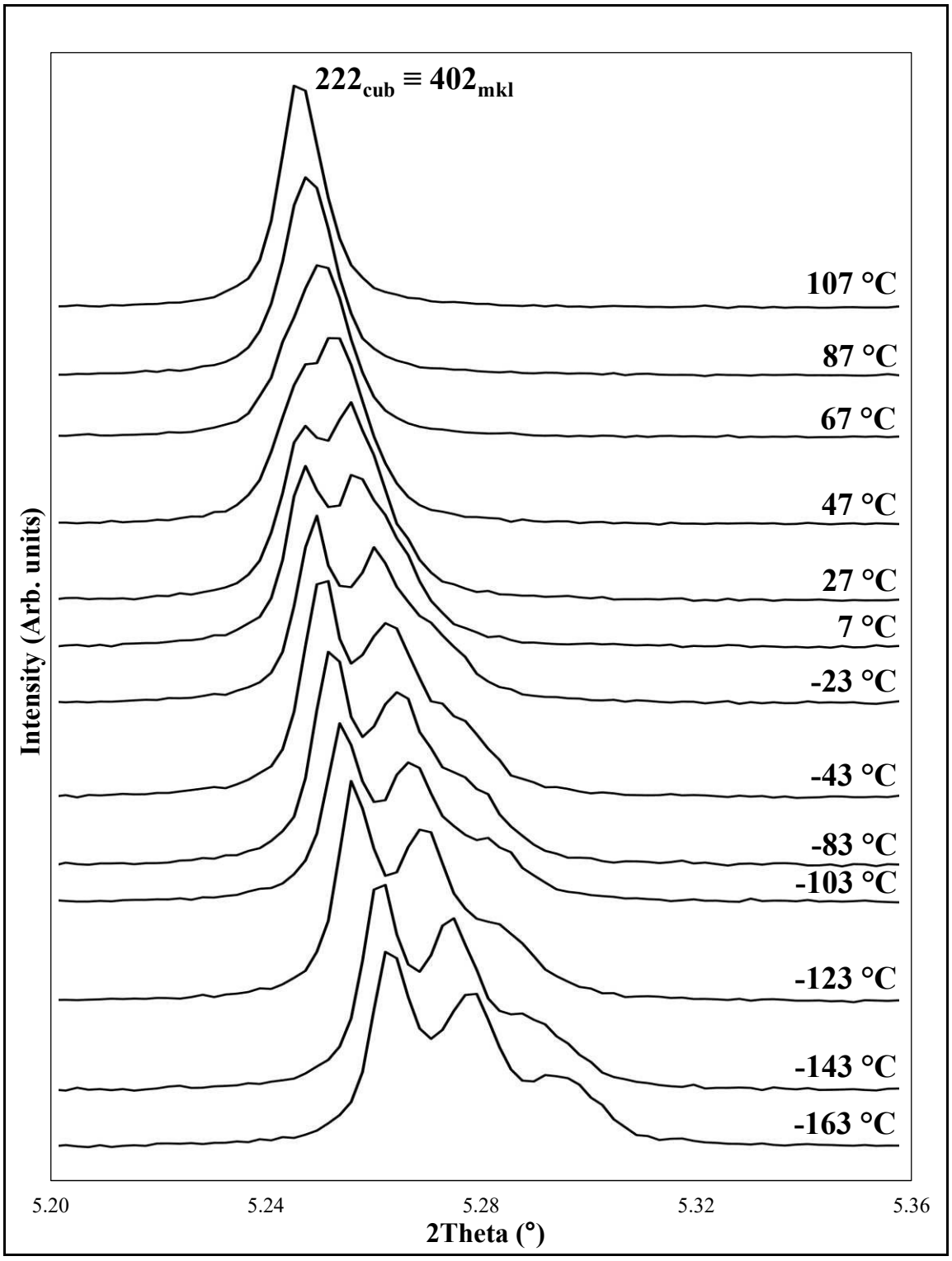

Figure 3.11. Peak splitting in diffraction patterns taken for melanophlogite from Fortullino, in the whole thermal range investigated with XRPD carried out using synchrotron radiation at ID22 of ESRF (Grenoble, France).

	T (°C)	a (Å)	b (Å)	c (Å)	β (°)	V (Å^3)
CUBIC	107	13.4085(1)	13.4085(1)	13.4085(1)	90	2410.67(4)
	97	13.4073(1)	13.4073(1)	13.4073(1)	90	2410.06(4)
	87	13.4054(1)	13.4054(1)	13.4054(1)	90	2409.00(4)
	77	13.4034(1)	13.4034(1)	13.4034(1)	90	2407.92(4)
	72	13.4023(1)	13.4023(1)	13.4023(1)	90	2407.33(4)
	67	13.4012(1)	13.4012(1)	13.4012(1)	90	2406.76(4)
	62	13.4001(1)	13.4001(1)	13.4001(1)	90	2406.14(4)
ORTHORHOMBIC	57	13.4001(5)	13.4001(7)	13.3974(7)	90	2405.17(10)
	52	13.3991(5)	13.3995(7)	13.3949(6)	90	2404.56(10)
	47	13.3978(5)	13.4006(6)	13.3926(6)	90	2404.01(10)
	42	13.3958(5)	13.4003(6)	13.3909(6)	90	2403.28(10)
	37	13.3946(5)	13.4006(6)	13.3885(5)	90	2402.68(10)
	32	13.3927(5)	13.4005(5)	13.3868(5)	90	2404.03(10)
	27	13.3916(6)	13.4009(5)	13.3843(5)	90	2401.45(10)
	17	13.3885(6)	13.4005(5)	13.3804(5)	90	2400.13(11)
	7	13.3849(6)	13.3999(5)	13.3769(5)	90	2398.74(11)
	–13	13.3778(7)	13.3993(5)	13.3696(5)	90	2396.06(12)
	–23	13.3745(7)	13.3987(5)	13.3659(5)	90	2394.70(13)
MONOCLINIC	–33	13.3716(5)	13.4016(4)	13.3595(4)	90.105(2)	2393.55(12)
	–43	13.3682(5)	13.4010(4)	13.3558(4)	90.111(2)	2392.15(12)
	–53	13.3651(5)	13.3988(4)	13.3528(4)	90.115(2)	2390.67(12)
	–63	13.3622(5)	13.3974(4)	13.3492(4)	90.119(2)	2389.27(12)
	–73	13.3596(5)	13.3953(4)	13.3462(4)	90.121(2)	2387.88(12)
	–83	13.3563(5)	13.3930(4)	13.3432(4)	90.124(2)	2386.36(12)
	–93	13.3534(5)	13.3910(4)	13.3396(4)	90.125(2)	2384.82(12)
	–103	13.3507(5)	13.3882(4)	133364(4)	90.128(2)	2383.26(13)
	–113	13.3475(5)	13.3855(4)	13.3331(4)	90.130(2)	2381.62(12)
	–123	13.3441(5)	13.3828(4)	13.3297(4)	90.132(2)	2379.94(13)
	–133	13.3410(5)	13.3819(4)	13.3331(4)	90.137(2)	2378.36(13)
	–143	13.3373(5)	13.3799(4)	13.3249(4)	90.141(2)	2376.55(13)
	–153	13.3328(5)	13.3794(4)	13.3149(4)	90.152(2)	2374.77(13)
	–163	13.3282(5)	13.3789(4)	13.3092(4)	90.160(2)	2372.74(13)

Table. 3.3. Unit cell parameter, β angle and unit cell volume values, from Rietveld refinements on diffraction patterns taken for melanophlogite from Fortullino, with increasing temperature, from XRPD carried out using synchrotron radiation at ID22 of ESRF (Grenoble, France).

Moreover, it is not clear whether the transition from the cubic symmetry occurs to an orthorhombic or already monoclinic one. Attempts to refine the orthorhombic patterns in the monoclinic symmetry gave contrasting results: due to the very small deviations in the β angle for the monoclinic refinements of the orthorhombic patterns (less than 0.1°), the parameters obtained in the orthorhombic and in the monoclinic are very similar to each other.

Clearly, although a quite well fit obtained, our structural assignment awaits a confirmation, possibly by SC–XRD.

In Fig. 3.12 and Fig. 3.13, the unit cell parameters and the unit cell volume variations with increasing temperature are reported, respectively, considering the experimental data collected using both conventional and unconventional X–Ray sources.

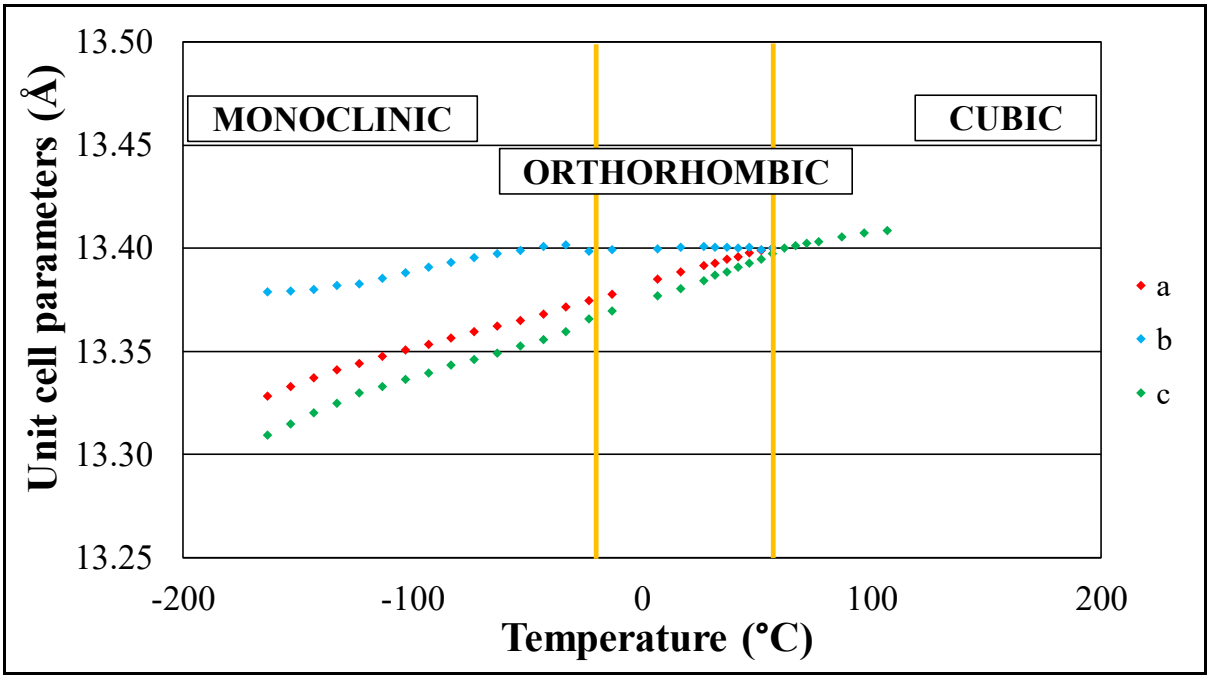

Fig. 3.12. Unit cell parameters variations in melanophlogite from Fortullino, with increasing temperature, from XRPD carried out using synchrotron radiation at ID22 of ESRF (Grenoble, France).

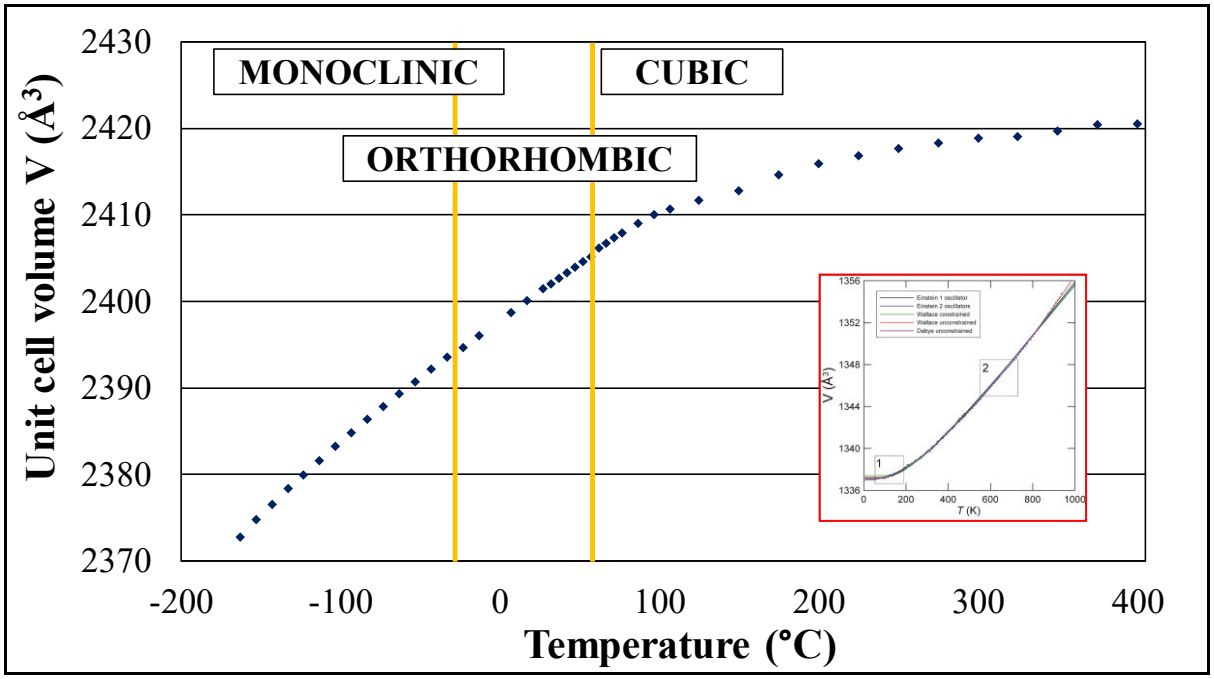

Fig. 3.13. Unit cell volume variation in melanophlogite from Fortullino, from –163 up to 400 °C, considering results from XRPD carried out using synchrotron radiation at ID22 of ESRF (between –163 and 107 °C), and with the Bruker D8 Discover (between 125 and 400 °C). For comparison the behaviour of albite (from Tribaudino *et al.*, 2011) is reported (inset).

To note that the volume shows an anomalous trend as a function of temperature, as shown by comparison with the behaviour of albite, which follows quite closely the physical models for low temperature thermal expansion (Fig. 3.13).

In Fig. 3.14, Rietveld refinement, carried out on diffraction pattern taken for melanophlogite sample from Fortullino, at 97 °C, and employing the cubic *Pm*3*n* symmetry by Gies (1983), is reported.

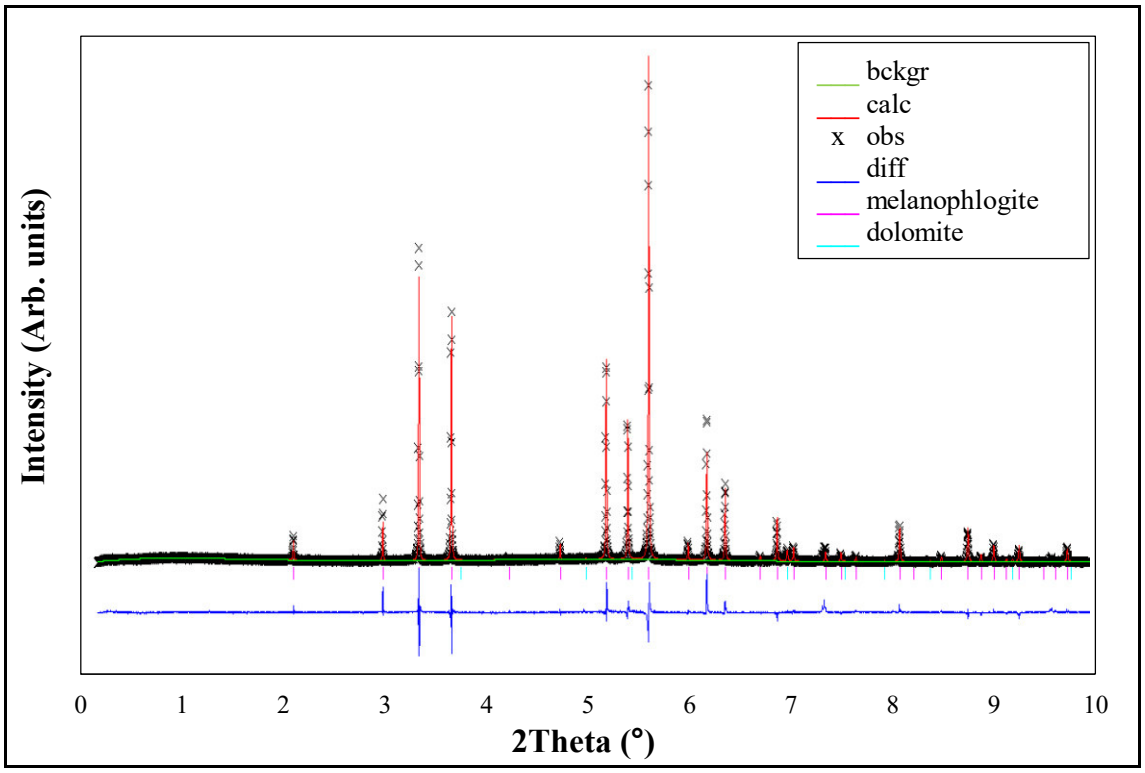

Fig. 3.14. Rietveld refinement on diffraction pattern taken for melanophlogite from Fortullino, at 97 °C. The difference between calculated and observed patterns (in red and marked with crosses, respectively) is in blue and the background in green. Melanophlogite and dolomite are indicated with pink and light blue bars, respectively.

In order to highlight the evolution of the diffraction peaks between cubic, orthorhombic, and monoclinic symmetries, a restricted angular range between 5 and 6 °2θ, which is the same one shown in Fig. 3.9a and in Fig. 3.9b, has been considered, as reported in Fig. 3.15, Fig. 3.16, and Fig. 3.17.

Moreover, the Miller indices characteristic of each diffraction peaks in the above–mentioned angular range are indicated, for cubic, orthorhombic, and monoclinic symmetries (Fig. 3.15, Fig. 3.16, and Fig. 3.17).

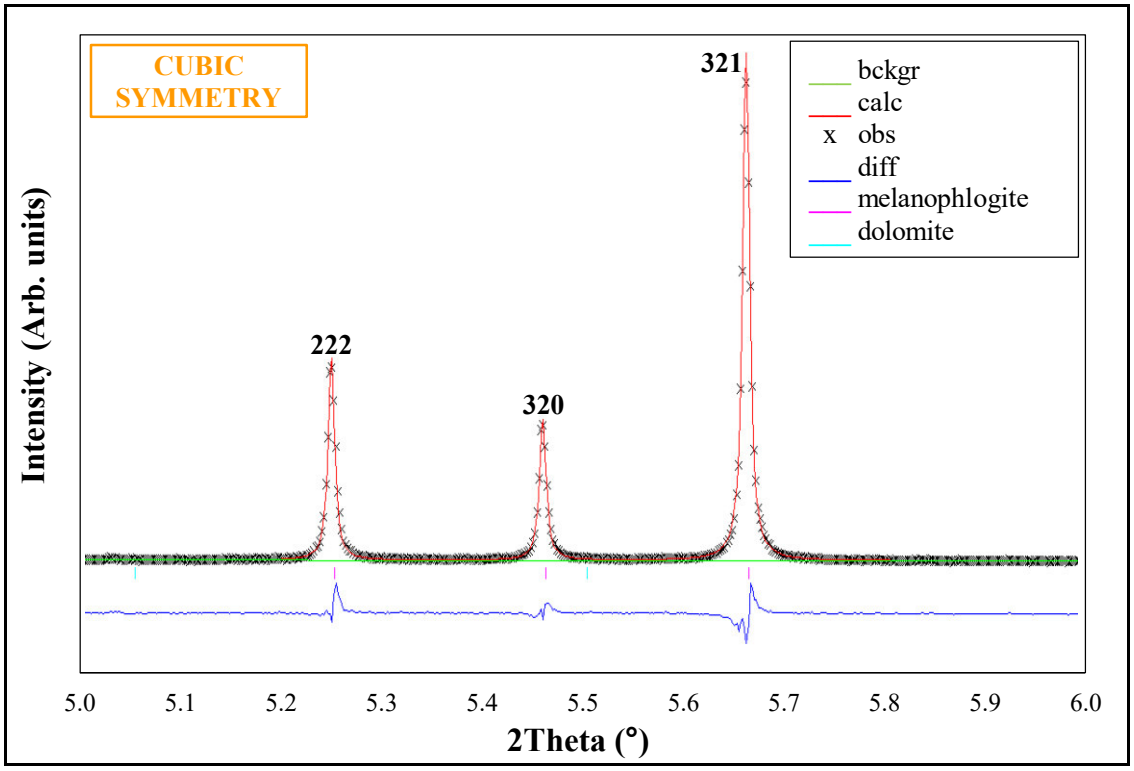

Fig. 3.15. Rietveld refinement on diffraction pattern taken for melanophlogite from Fortullino, at 97 °C, between 5 and 6 °2θ, and with the Miller indices characteristic of peaks.

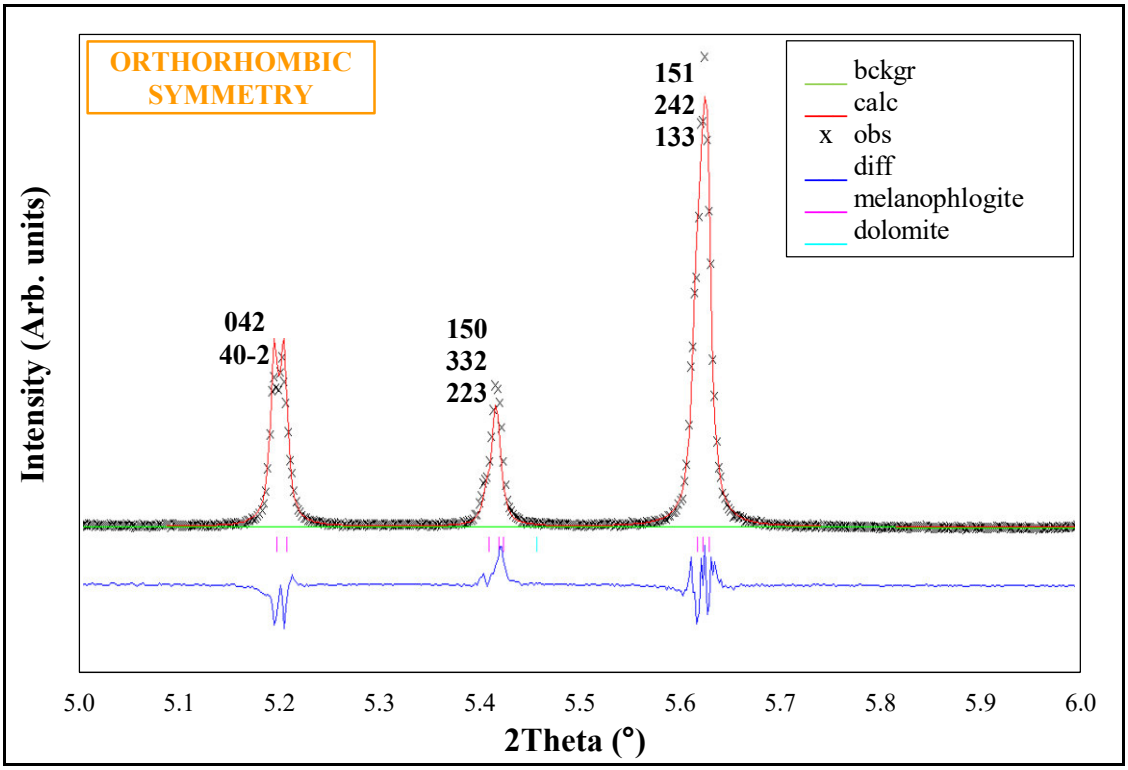

Fig. 3.16. Rietveld refinement on diffraction pattern taken for melanophlogite from Fortullino, at room temperature, between 5 and 6 °2θ.

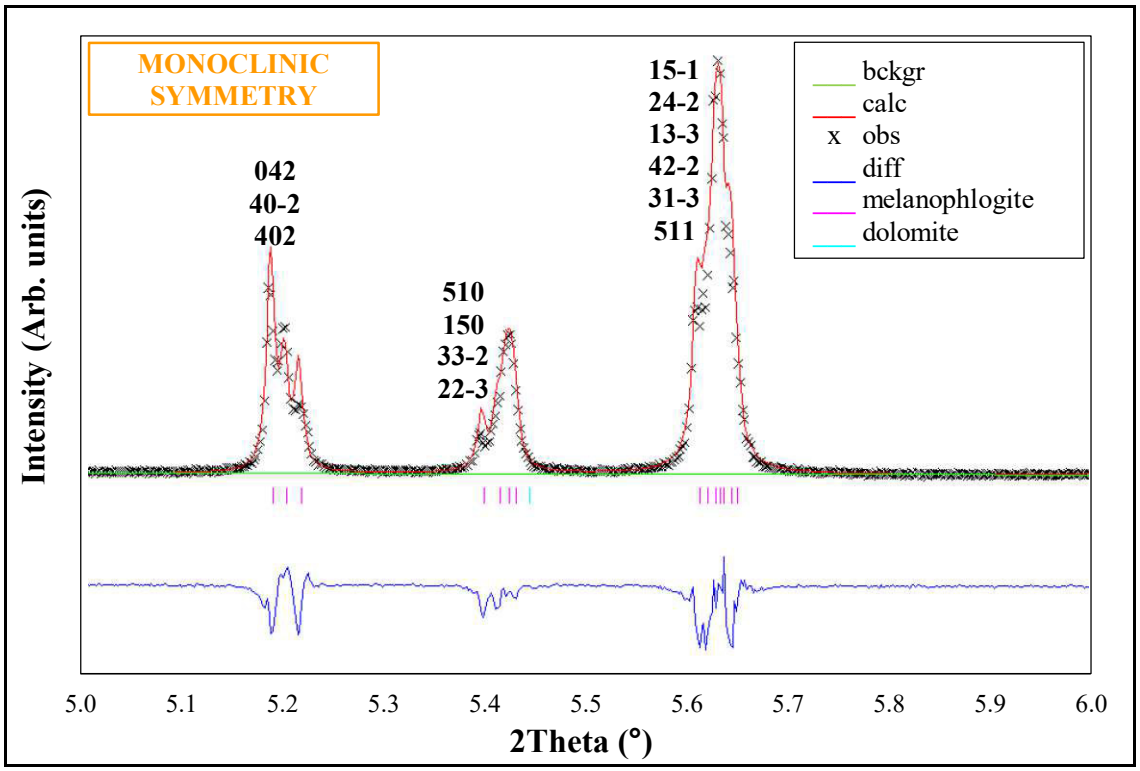

Fig. 3.17. Rietveld refinement on diffraction pattern taken for melanophlogite from Fortullino, at –163 °C, between 5 and 6 °2θ.

3.1.5. TGA

Thermal gravimetric analyses have been done on samples from Fortullino and Racalmuto. Samples with mass between 15 and 20 mg in the runs for Fortullino and between 5 and 10 mg in the runs for Racalmuto (the different amount is due to the availability of each sample) have been heated from room temperature up to 1000 °C and 500 °C, for Fortullino and Racalmuto respectively.

Preliminary analyses on both samples have shown significant peaks related to carbonate phases, i.e. dolomite for Fortullino and calcite for Racalmuto, associated to melanophlogite. Consequently, a purification procedure was necessary to investigate exclusively the behaviour of melanophlogite.

A first attempt to purify melanophlogite from Fortullino from the presence of dolomite has been a chemical attack, done employing HCl acid at 37 % concentration. The melanophlogite spheroidal aggregates, peculiar form of melanophlogite from Fortullino, have been roughly grinded, and immersed in HCl for about 45 days. After that, the material has been accurately cleaned up with chemically purified water, and let dry at room temperature. Once well dry, the material has been finely grinded, and the obtained powdered sample has been analysed with XRPD, to quantify the residual dolomite.

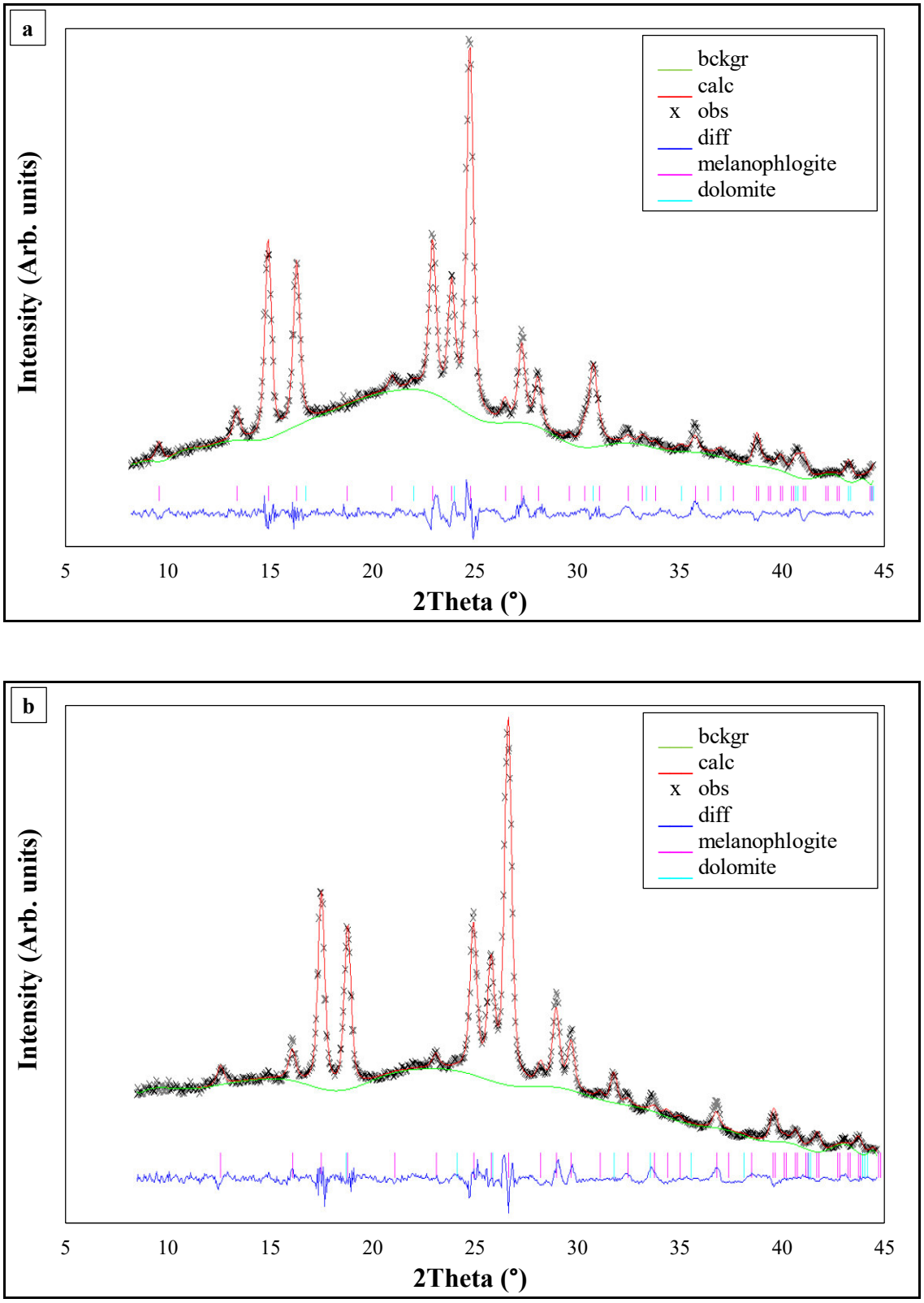

Figure 3.18. Rietveld refinements on diffraction patterns for the samples of melanophlogite from Fortullino, at room temperature, (a) before, and (b) after the chemical attack. The difference between calculated and observed patterns (in red and marked with crosses, respectively) is in blue and the background in green. Melanophlogite and dolomite are indicated with pink and light blue bars, respectively.

The diffraction patterns have been taken for the samples before and after the implementation of the chemical attack, at room temperature, with the Bruker D8 Discover diffractometer, over 8–45 °2θ, and with an acquisition time of the whole spectrum of 180 min (Fig. 3.18a and Fig. 3.18b, respectively before and after the implementation of the chemical attack).

In Table 3.4, the results of quantitative analysis, carried out on diffraction patterns taken for the samples of melanophlogite from Fortullino, before and after the chemical attack with HCl, are shown. After the chemical treatment, thanks to action of HCl, the dolomite almost disappeared.

A possible bias to the attack with HCl could be, as previously suggested (Domenici *et al.*, 2006), a chemical interaction with melanophlogite. The sample from Fortullino was therefore purified also by a manual procedure, done with an optical microscope, by picking away the grains of dolomite, which is easily distinguishable from melanophlogite as not transparent.

After the manual separation of the mineral phases, the sample has been finely grinded, and analysed with XRPD, in order to quantify the dolomite remained after the purification.

The diffraction pattern has been taken with the Thermo Arl X'TRA powder diffractometer, over the 8–70 °2θ range, with a counting time of 2 sec/step and 0.020 ° as 2θ step (Fig. 3.19).

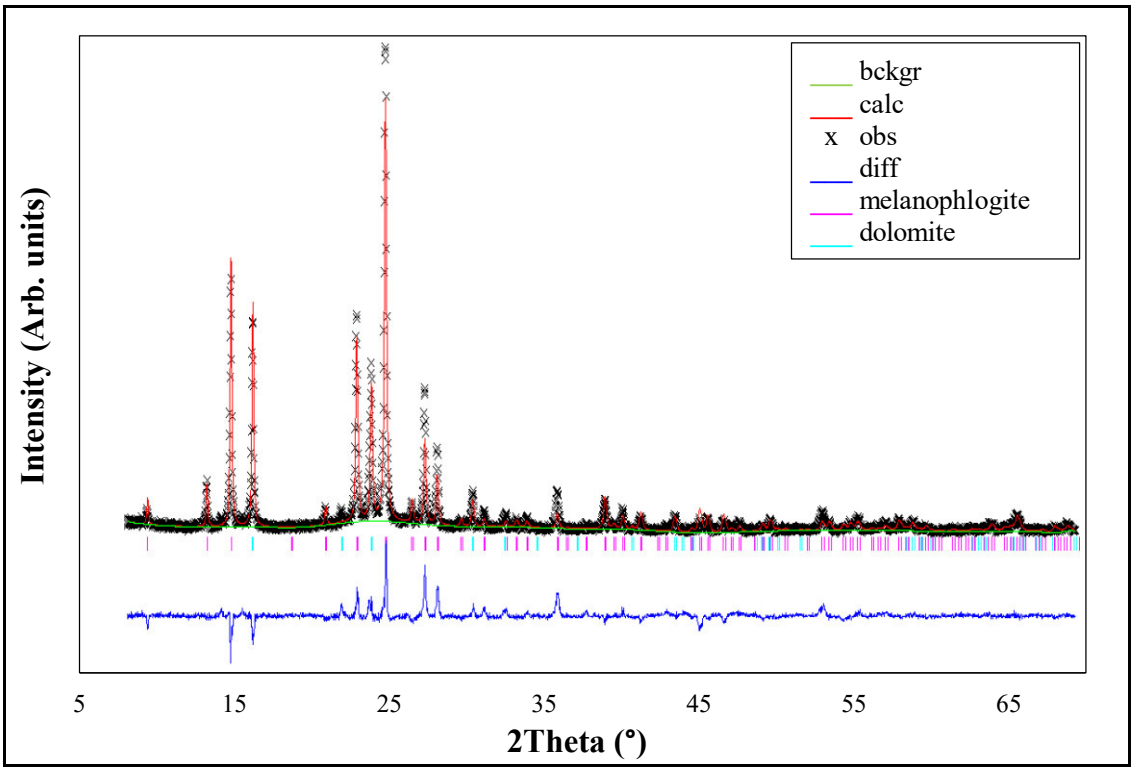

Figure 3.19. Rietveld refinement on diffraction pattern for melanophlogite from Fortullino, at room temperature, after the manual purification from dolomite. The difference between calculated and observed patterns (in red and marked with crosses, respectively) is in blue and the background in green. Melanophlogite and dolomite are indicated with pink and light blue bars, respectively.

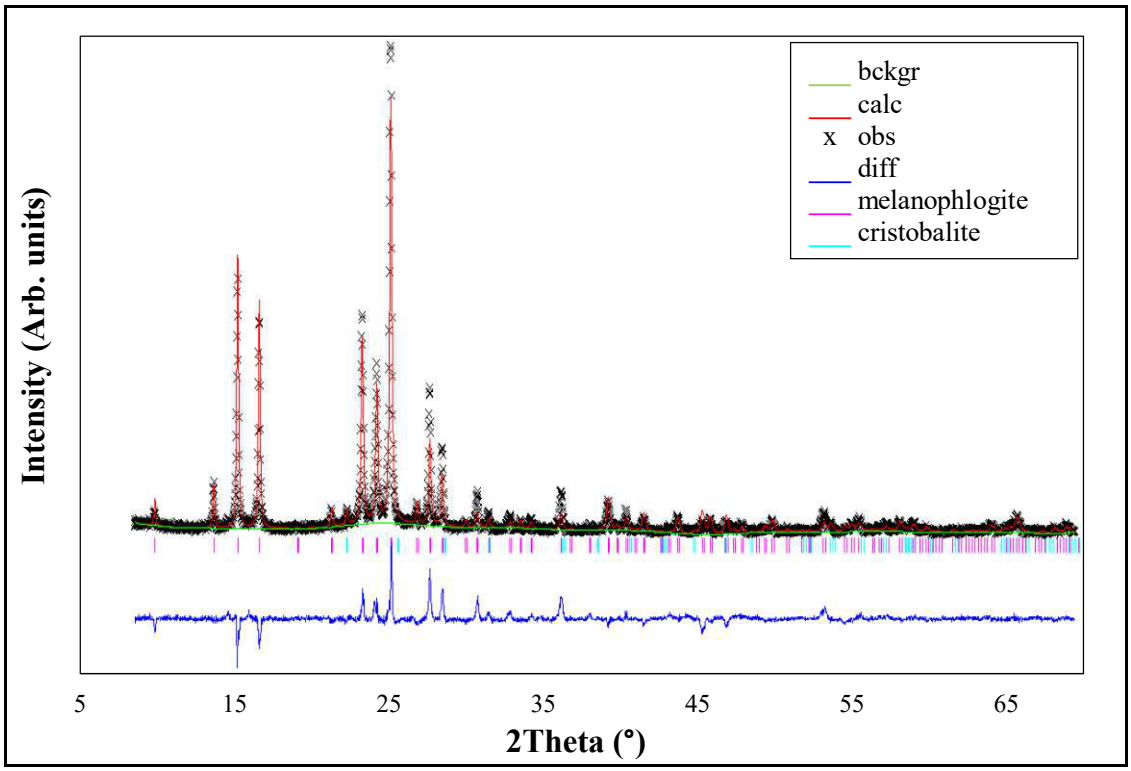

Figure 3.20. Rietveld refinement on diffraction pattern taken, at room temperature, for a manually purified sample from Fortullino. The difference between calculated and observed patterns (in red and marked with crosses, respectively) is in blue and the background in green. Melanophlogite and cristobalite are indicated with pink and light blue bars, respectively.

In the diffraction pattern shown in Fig. 3.19, the peak at 2θ ~ 22 °2θ, found in the preliminary characterization (see the Chapter "**3.1.3**"), was stronger as the chemical attack with HCl got rid of a superimposed peak peculiar of dolomite. The previous identification as cristobalite was confirmed. A Rietveld refinement was performed considering only melanophlogite and cristobalite, to quantify cristobalite (Fig. 3.20), with the tetragonal symmetry $P4_12_12$ (Peacor, 1973), and the result has been a fraction slightly higher than 1.5 wt.%. However attempts to refine residual dolomite and cristobalite together failed.

In the following, results for refinements with melanophlogite and residual dolomite are reported (Table 3.4).

	MINERALOGICAL PHASE (wt.%)	
	MELANOPHLOGITE	DOLOMITE
Before the chemical purification	78.93 ± 0.43	21.97 ± 1.55
After the chemical purification	97.32 ± 0.06	2.68 ± 0.42
After the manual purification	97.66 ± 0.02	2.34 ± 0.25

Table 3.4. Results of quantitative analysis on diffraction patterns taken for melanophlogite from Fortullino, respectively before and after the implementation of the chemical attack with HCl, and after the manual purification.

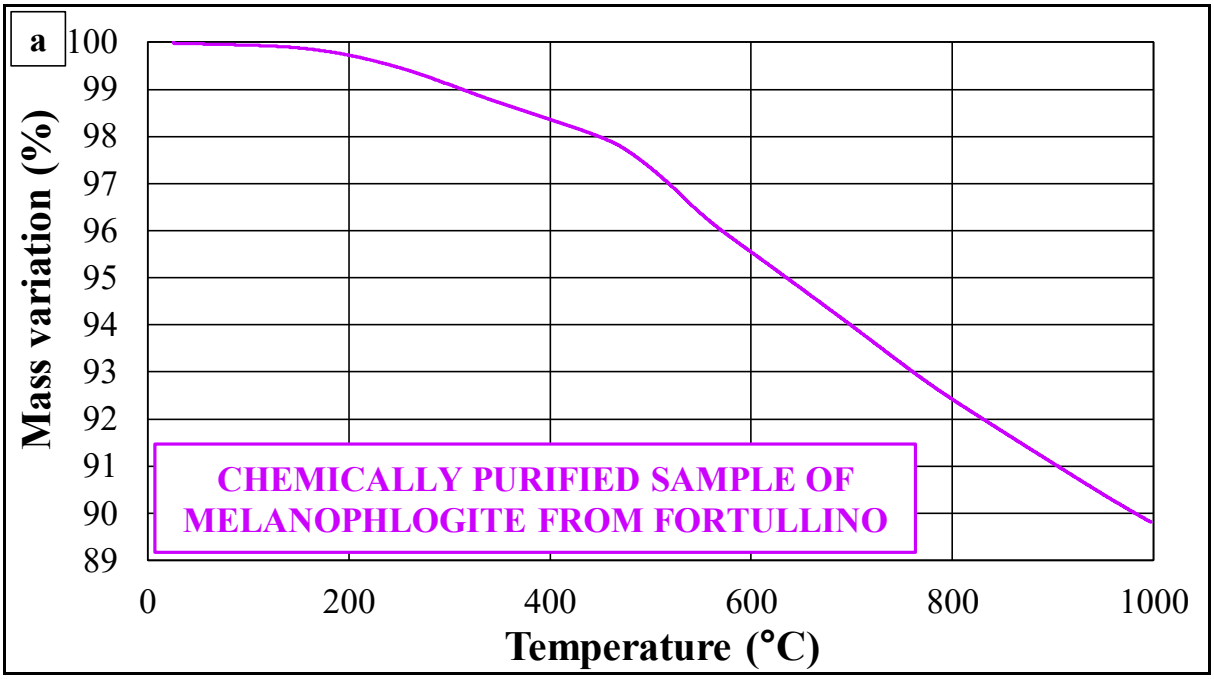

The manually purified melanophlogite sample shows the same thermogravimetric behaviour as the chemically purified one (Fig. 3.21).

It is interesting to note that HCl does not interact with the guest phases, nor causes changes in the structure, contrarily to the observations by Domenici *et al.* (2006).

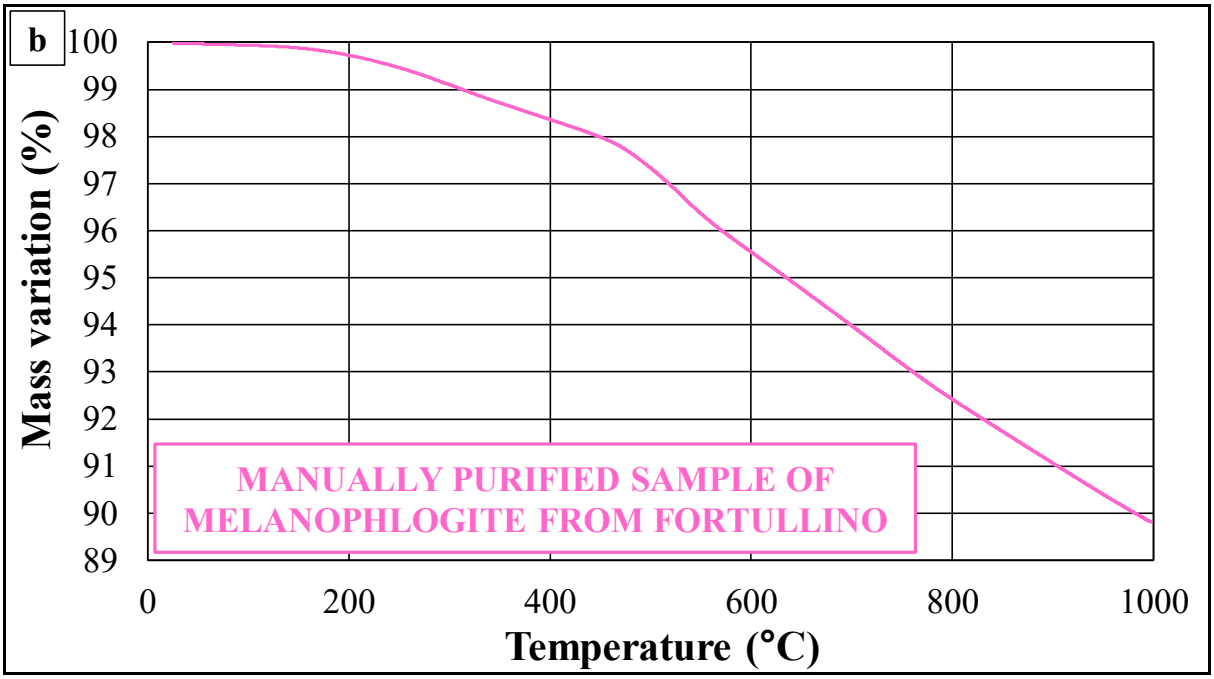

Figure 3.21. TG analyses, up to 1000 °C and with a heating rate of 5 °C/min, on: (a) the chemically purified sample, and (b) the manually purified sample of melanophlogite from Fortullino.

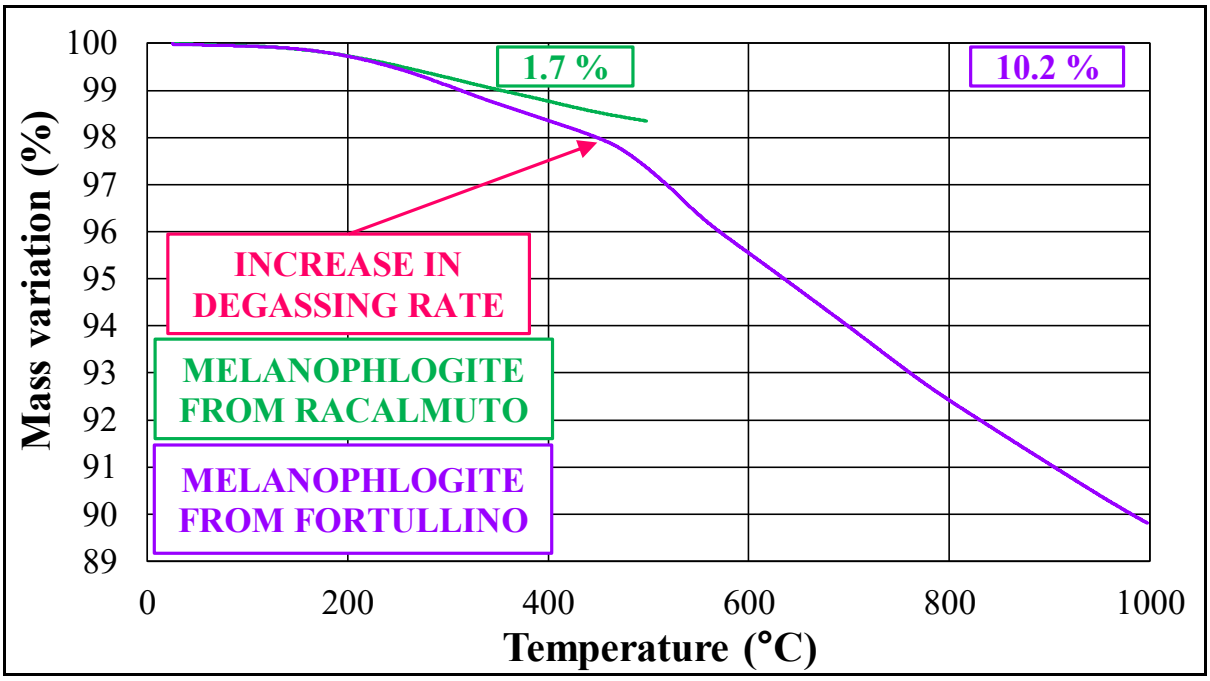

Figure 3.22. TGA carried out on the manually purified sample of melanophlogite from Fortullino and on a not purified sample of melanophlogite from Racalmuto, up to 1000 °C and 500 °C respectively, and with a heating rate of 5 °C/min.

As reported in Fig. 3.22, TGA profiles, for both samples, have shown that the mass variation is not significant up to 180 °C. On the contrary, at higher temperature, the mass variation increases steadily, with a higher rate between 450 and 550 °C. Moreover, between 450 and 550 °C, the slope of the curve of the mass variation is the steepest, indicating, for the sample from Fortullino, a considerable loss of CO_2. This feature was not observed in the sample from Racalmuto, but could possibly occur at temperatures higher than 500 °C. At further higher temperature, the mass variation is continuous up to 1000 °C, at a rate lower than between 450 and 550 °C, but higher than between 200 and 450 °C.

At 1000 °C, there is no evidence of a conclusion of the degassing. This suggests that the release of guest CO_2 was not complete at the end of the thermal treatment, and consequently a second TGA, up to 1000 °C and with a heating rate of 5 °C/min, has been carried out on a small amount (less than 5 mg) of the same sample previously heated (Fig. 3.23). At the end of the first thermal treatment, the mass decreased by 10.2 %; after repeating TGA, a further weight variation of 1.5 % has been observed, mostly at temperatures higher than 500 °C, in correspondence with the major release during the first heating. The sum of the two contributions is 11.7 %, close to the weight loss outlined by Grassellini Troysi & Orlandi (1972) of 11.3 %. The authors reported a "continuous loss between 110 and 1100 °C".

The overall mass variation by 11.7 % is slightly higher than the expected theoretical one of about 11.3 %, assuming full occupancy of the CO_2 in $[5^{12}]$ and $[5^{12}6^2]$ structural cages, i.e. 8

CO_2 molecules *per* 46 SiO_2. The difference may be even higher if, in the absence of a split for the CO_2 Raman peaks, only $[5^{12}6^2]$ cages are occupied.

Site occupancy refinement results on a cubic melanophlogite from synchrotron radiation data (Chapter "**3.1.4.2**") showed that the $[5^{12}6^2]$ cage is fully occupied by an atom isoelectronic with CO_2, and about half in $[5^{12}]$ cage, which might correspond, within error, almost to full occupancy in CH_4. Assuming that as model, we might consider that the expected weight loss is 10.6 %; this would result in a weight loss lower than found here and by Grassellini Troysi & Orlandi (1972) on the same melanophlogite. The reason of this difference is not clear. In part, it may be related to decomposition of the small amount of dolomite residual.

Still, this does not bias the major result: the repeated observation of the same behaviour in chemically and manually purified samples indicates that degassing occurs following a well defined behaviour, starting already at temperature as low as 200 °C, although degassing at a larger extent occurs for temperature in excess of 500 °C. This point falls against previous assumptions that degassing in melanophlogite begins only at higher temperature (i.e. T ~ 700 °C) (Momma, 2014; Likhacheva *et al.*, 2018).

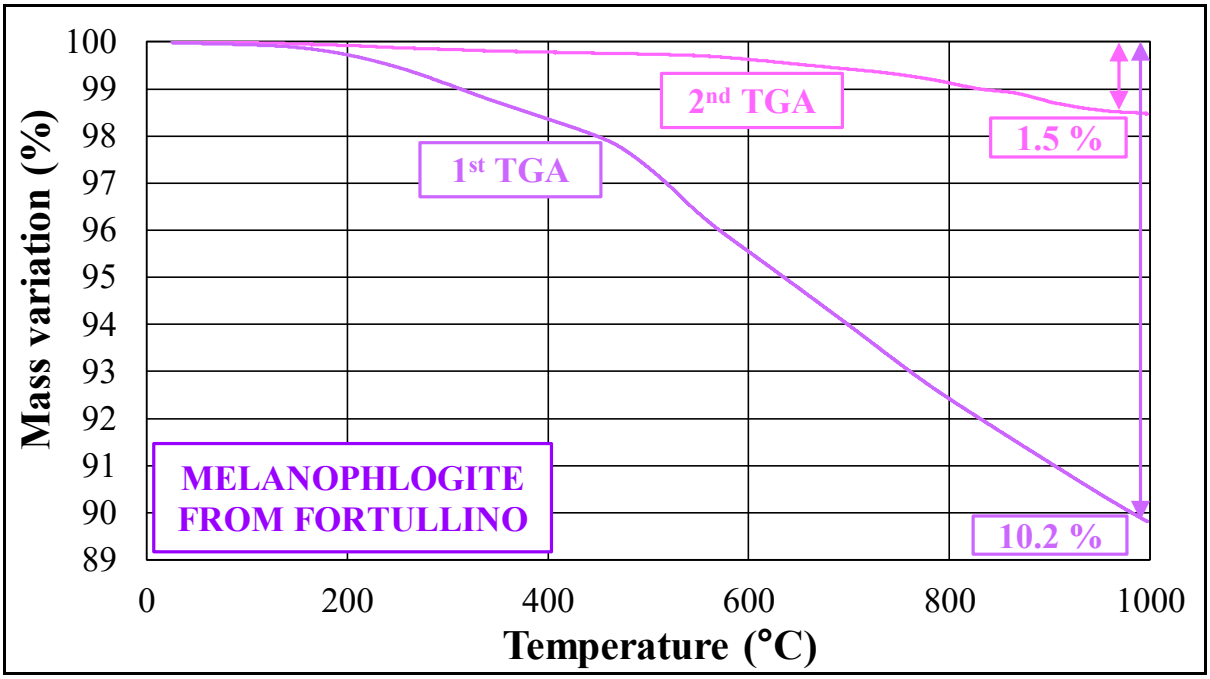

Figure 3.23. Two consecutive TGA, both up to 1000 °C and with a heating rate of 5 °C/min, on the manually purified sample of melanophlogite from Fortullino.

A TGA has been carried out, up to 500 °C and with a heating rate of 5 °C/min, on the sample from Racalmuto (Fig. 3.22), with a calcite fraction of (12.28 ± 0.46) wt.%, as shown by XRPD (Chapter "**3.1.3**").

Since the amount of sample available for this study is very modest, no purification procedure could be done, and the highest temperature was limited to 500 °C, to avoid decomposition of calcite. The total mass variation, up to 500 °C, is 1.7 %. It is reasonable to suppose that the release of the guest molecules, which are H_2S and, in minor amount, CH_4 and CO_2, as revealed by Raman Spectroscopy (Chapter "**3.1.2**"), is not completed at the end of the thermal treatment.

The expected theoretical overall mass variations, considering all the structural cages filled by H_2S or CH_4, are 9 % and 4.4 % respectively. Any mixture of the phases, as found by Raman spectroscopy, would result in an intermediate value (Chapter "**3.1.2**"), in any case weighing more than the observed one.

Unfortunately, the very small amount of sample available for Racalmuto has not allowed a second TGA, after the first one, in order to ascertain a potentially further mass variation.

It has been not possible to perform TGA on melanophlogite from Varano Marchesi, since the available sample was insufficient.

3.1.6. DSC

DSC analyses have been carried out on melanophlogite from Fortullino and Racalmuto.

Powdered samples weighting between 20 and 30 mg have been heated in some separate runs between –90 and 800 °C for Fortullino, and from room temperature to 500 °C for Racalmuto.

As already done for TGA, DSC on melanophlogite from Racalmuto has been done only until 500 °C, that is before calcite decomposition, since the sample was not purified from the associated carbonate phase.

As for TGA, a preliminary test on the sample from Fortullino, up to 800 °C and with a heating rate of 5 °C/min (Fig. 3.24), has shown the strong influence of the carbonate phase, that is dolomite, which shows two well–visible endothermic peaks, related to the decomposition of dolomite between 475 and 575 °C and between 650 and 725 °C (Gunasekaran & Anbalagan, 2007).

Similarly, a preliminary run on the sample of melanophlogite from Racalmuto, carried out up to 800 °C and with a heating rate of 5 °C/min (Fig. 3.25), showed decarbonation of calcite, which is observable in the endothermic peak between 600 and 700 °C. Moreover, another endothermic peak appears to be present at temperatures higher than 725 °C, whose nature is not clearly defined.

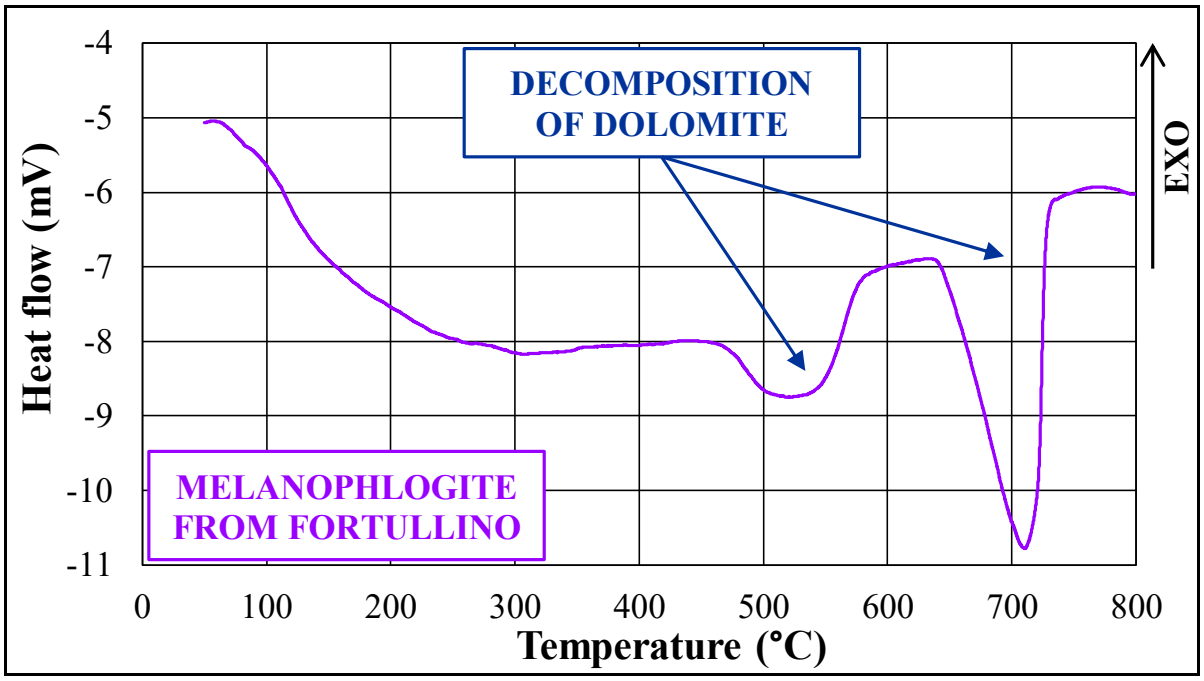

Figure 3.24. A preliminary DSC, up to 800 °C and with a heating rate of 5 °C/min, carried out on a not purified melanophlogite sample from Fortullino, characterized by (11.11 ± 0.80) wt.% of dolomite.

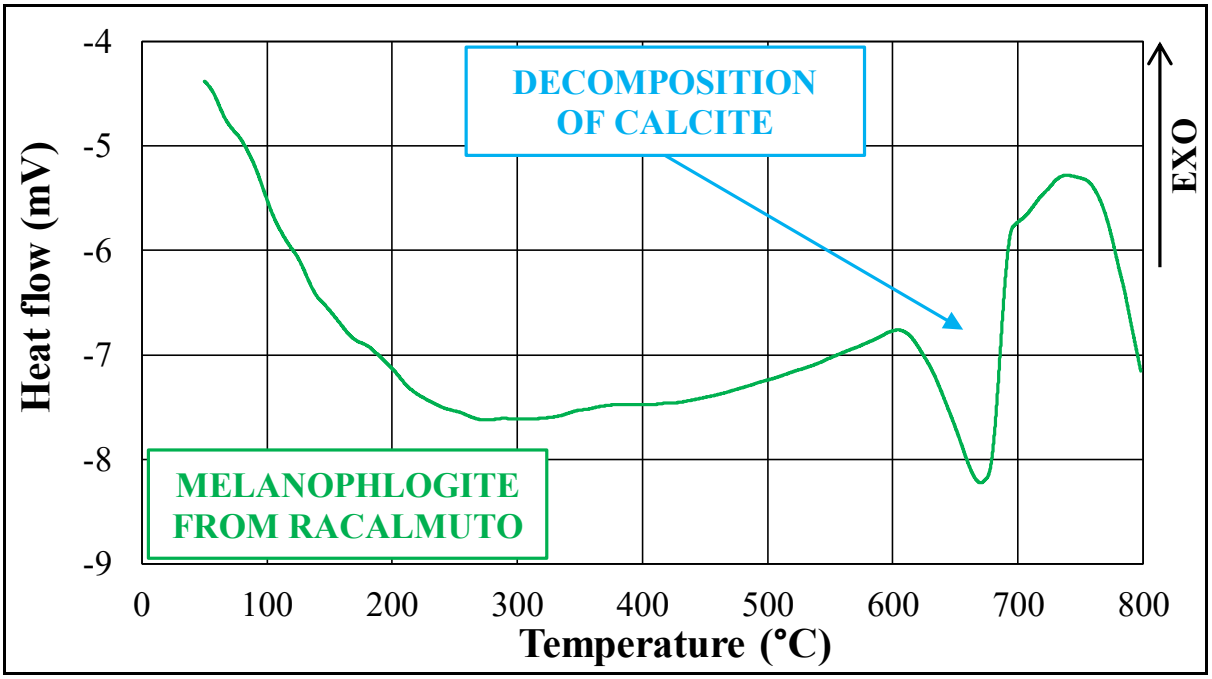

Figure 3.25. A preliminary DSC, up to 800 °C and with a heating rate of 5 °C/min, carried out on a not purified melanophlogite sample from Racalmuto, characterized by (12.28 ± 0.46) wt.% of calcite.

The DSC measurements, on the manually purified sample of melanophlogite from Fortullino and on a not purified one from Racalmuto, have shown similar calorimetric profile, at least at temperature lower than 500 °C (Fig. 3.26). Both calorimetric profiles show an endothermic behaviour, which is detectable in the thermal range up to 200–250 °C, and a slightly exothermic behaviour, which is observable at least up to 500 °C. The onset of the slightly

exothermic behaviour begins in the same thermal range characteristic of the onset of the release of guest molecules found in TG analyses, that is between 180 and 250 °C.

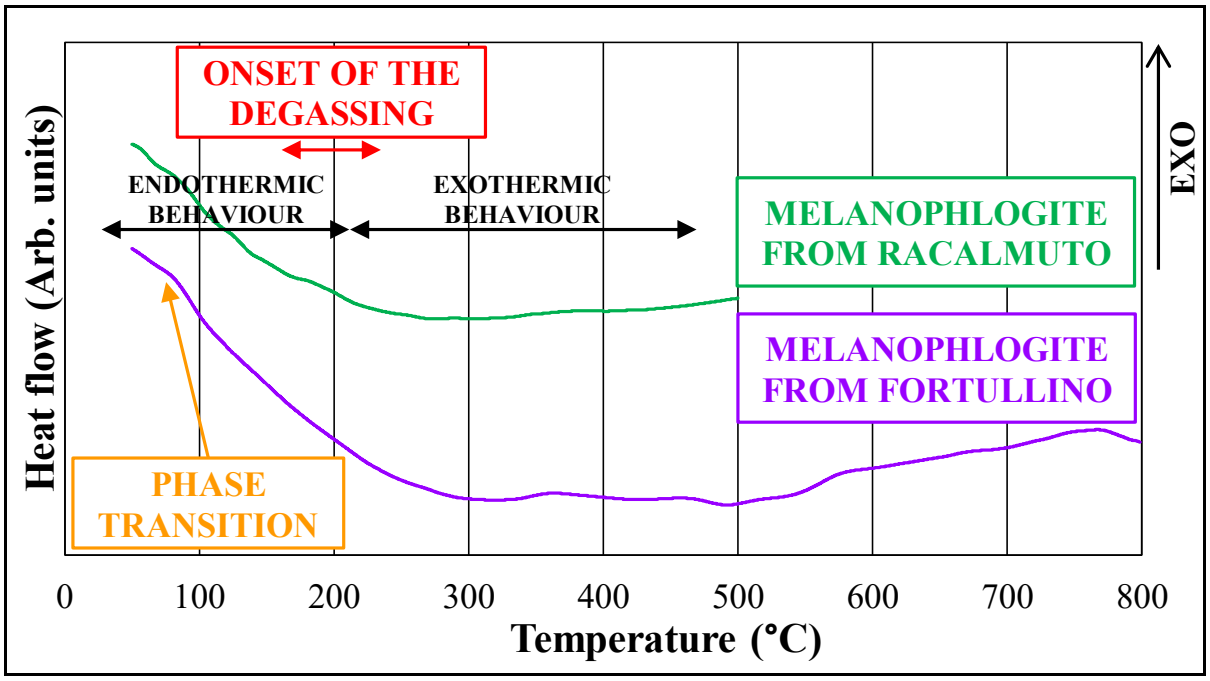

Figure 3.26. DSC on the chemically purified sample of melanophlogite from Fortullino and on a not purified sample of melanophlogite from Racalmuto (marked in electric blue and in green, respectively), up to 800 °C and 500 °C, respectively, and both with a heating rate of 5 °C/min.

Moreover, a slight change in slope in the calorimetric profile has been observed between 60 and 80 °C, in the same thermal range observed by HT–XRPD analysis, testifying a phase transition from low temperature symmetry to that characteristic of high temperature.

At temperatures near 500 °C, the chemically purified sample from Fortullino has shown a slight endothermic behaviour, precisely between 475 and 575 °C. At temperatures higher than 750 °C, the slope of the calorimetric profile changes at a rate very similar to the one found before the onset of degassing.

DSC measurements with varying temperature have been carried out on chemically purified sample of melanophlogite from Fortullino, also at lower temperature. DSC analysis on 19.47 mg of purified melanophlogite was done in three steps on the same sample: 1) heating from –90 to 300 °C, at 2 °C/min (Fig. 3.27); 2) cooling from 300 to –90 °C, at 2 °C/min (Fig. 3.28); 3) heating from –90 to 80 °C at 5 °C/min (Fig. 3.29).

During cooling, a well–shaped peak between –40 and –50 °C was observed, whereas during heating a step at about –30 °C is observed, in both runs at very close temperature. The DSC shape during heating is very similar, irrespective of the different heating rates, and of a partial degassing occurring at temperature in excess of 200 °C. The DSC profiles reveal a phase

transition with a discontinuity in heat capacity. The transition temperature is almost the same as that of the phase transition found by low temperature XRPD by synchrotron radiation.
At higher temperature, a change in the slope of the calorimetric profile can be connected to the evolution of the release of guest molecules, as detail in the Discussion section.

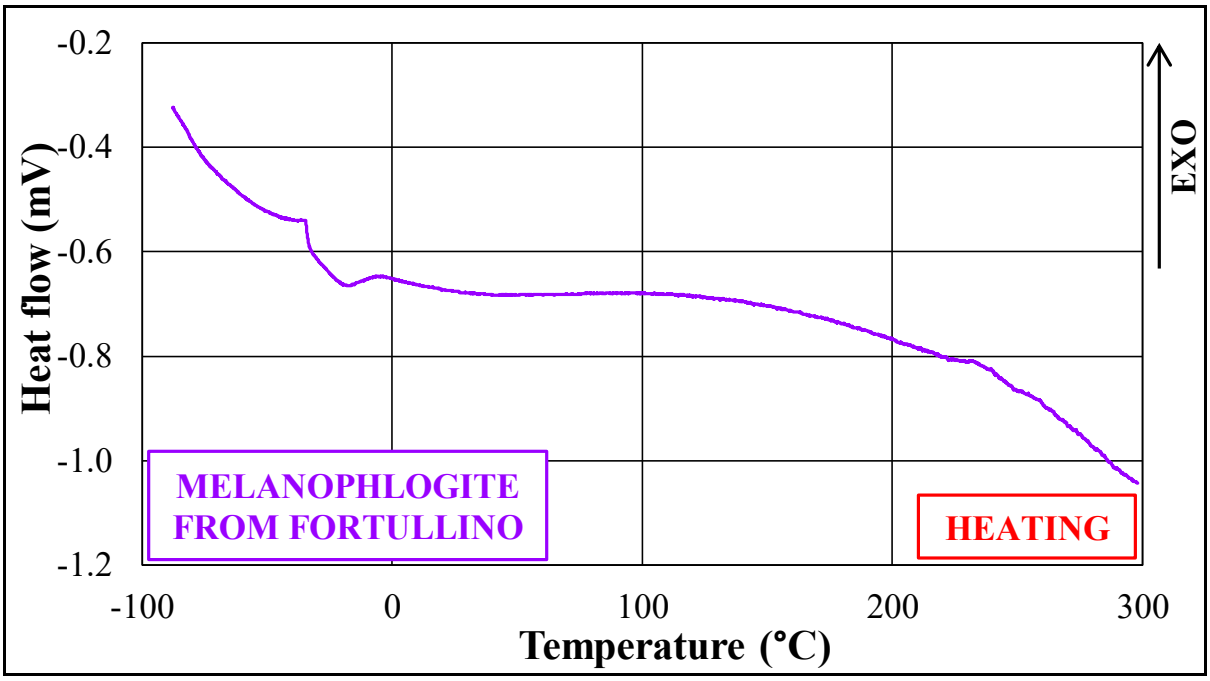

Figure 3.27. DSC at varying temperature on the chemically purified melanophlogite sample from Fortullino: heating from –90 to 300 °C, at 2 °C/min.

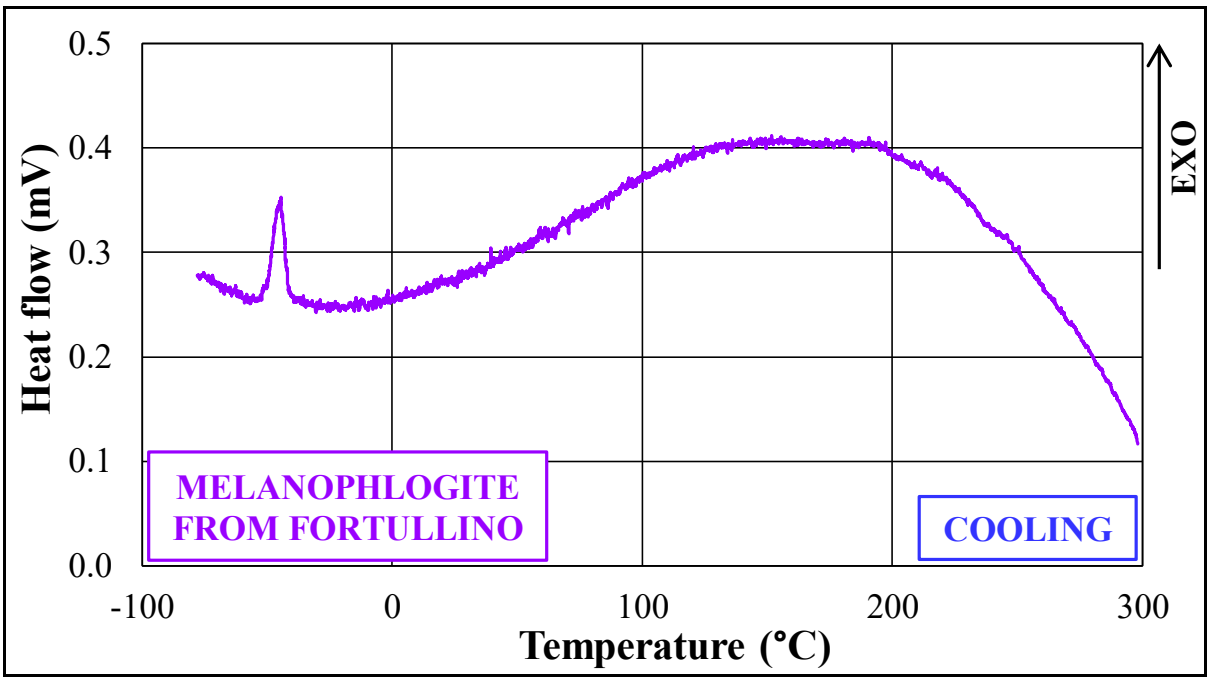

Figure 3.28. DSC at varying temperature on the chemically purified melanophlogite sample from Fortullino: cooling from 300 to –90 °C, at 2 °C/min.

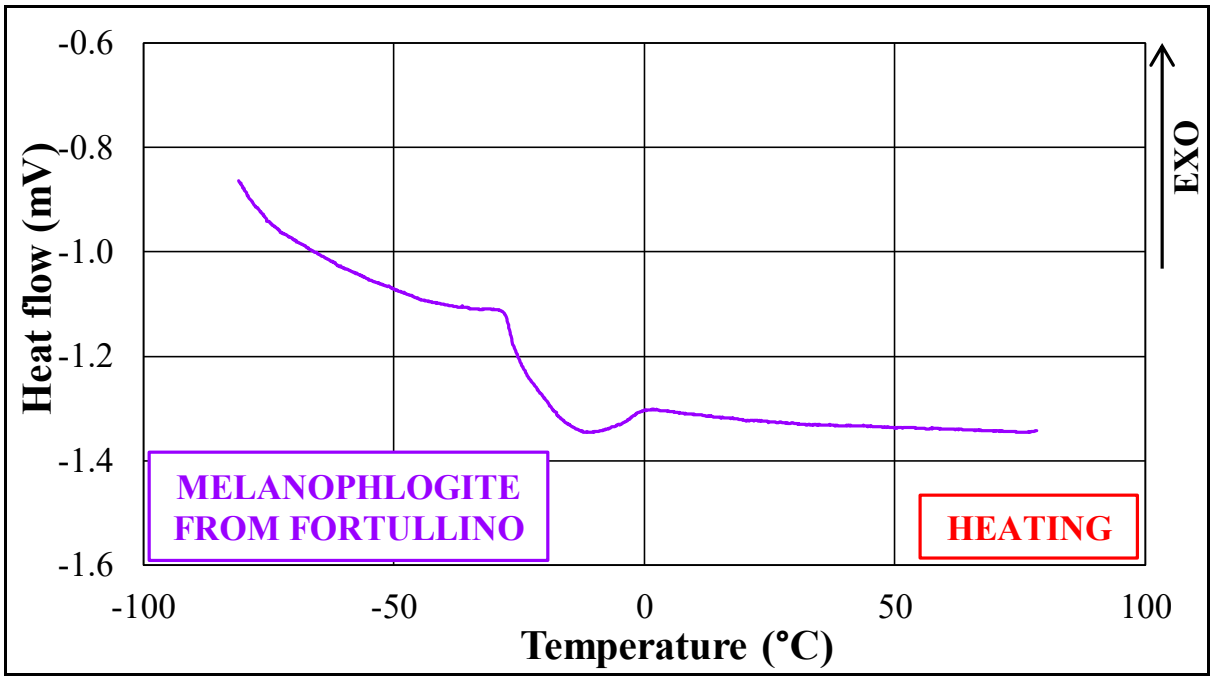

Figure 3.29. DSC at varying temperature on the chemically purified melanophlogite sample from Fortullino: heating from –90 to 80 °C, at 5 °C/min.

The reversibility of the phase transition is testified by endothermic and exothermic peaks, respectively during the heating and cooling ramps.

As for TGA, it has been not possible to done DSC measurements on melanophlogite from Varano Marchesi, due to the lack of a powdered sample pure enough.

In the first runs, the transition to cubic structure was hardly revealed for the very small change in slope during the heating between 50 and 90 °C.

As reported in Fig. 3.30, DCS measurements have been repeated from room temperature up to 145 and 95 °C, for samples from Fortullino and Racalmuto, respectively, in order to better constrain the phase transition. A continuous change in slope was found at about 95 and 60 °C for Fortullino and Racalmuto respectively. With the software *Calisto* used to control the instrument for DSC analysis, it is possible to process the experimental data to obtain some calorimetric parameters characteristic of the phase transition, such as the specific heat. For the melanophlogite sample from Fortullino, the evaluated specific heat is 0.194 J/(gK) (Fig. 3.30a), and the one from Racalmuto is 0.137 J/(gK) (Fig. 3.30b).

From the above results, we have that the temperature at which there is a higher peak of heat flow, that is when the phase transition takes place, is slightly different in the two localities, i.e. it suggests that an effect of the guest molecules on the transition exists. Moreover, the transition pinpointed by calorimetric behaviour in Fortullino occurs at a higher temperature than that by the unit cell parameters, indicating that the two processes, although possibly

related, are not the same. Last, the whole change here occurs in a continuous way, indicating a smooth second–order transition.

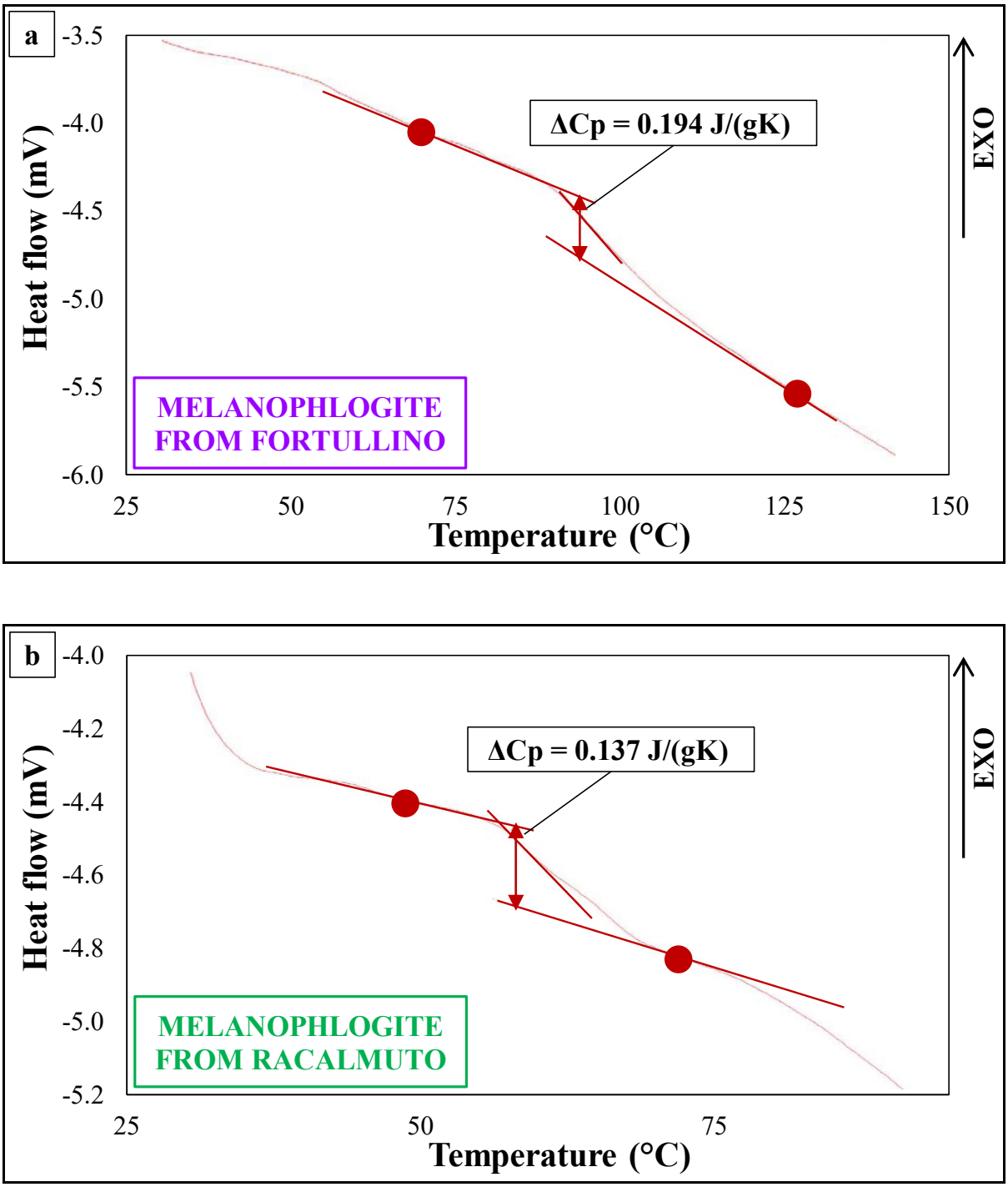

Figure 3.30. DSC runs on: (a) melanophlogite from Fortullino, from room temperature up to 145 °C; and (b) melanophlogite from Racalmuto, from room temperature up to 95 °C, always at a heating rate of 5 °C/min.

3.2. SYNTHESIZED SAMPLES

An important goal of this thesis was the synthesis of melanophlogite, to reproduce the conditions of natural genesis in laboratory, and to provide the basis for further practical applications in the gas storage. Beyond synthesis, we aimed to synthesize a sample as pure as possible and in quantities of hundreds of milligrams. Previous attempts of the synthesis were done by Gies *et al.* (1982), Gies (1984), Gunawardane *et al.* (1987), and Fyfe & Gies (1990).

In previous investigations, it was found that for crystallization of clathrasils, the guest species inside the structural voids play an indispensable role, since the cage–like framework structures cannot be constructed without them (Qiu *et al.*, 1998; Cooper *et al.*, 2004; van der Donk *et al.*, 2008). Large molecules, which fit into the large cages, play the structure–directing role, acting as templates for crystallization and controlling the topology of framework to crystallize.

Because the presence of large molecules serving as SDA is a precondition for seed formation, the formation of larger cages around SDA is considered a preliminary step for crystallization (van Koningsveld & Gies, 2004).

Small molecules, gaseous at room conditions, such as CH_4, N_2, O_2, H_2S, CO_2, and Ar, fit into small cages and can stabilize framework structures. These small gases are referred to as "help gases". For the formation of clathrate hydrates with some relatively large guest species, such as 2.2–dimenthylpentane and aminoadamatane, the presence of the above–mentioned small "help gases" is essential (Ripmeester *et al.*, 1987; Udachin *et al.*, 1997). For clathrasils, however, the "help gases" appear to play a minor role in the stability of clathrasil frameworks, because Si–O–Si bonds in the clathrasil framework are much more rigid than the O – H···O hydrogen bonds typical in the clathrate hydrate.

More in detail, synthesized melanophlogite has been reported for the first time by Gies *et al.* (1982). With similar approach, but simulating natural conditions by using a mixture of CO_2, CH_4, and N_2 as guest molecules, melanophlogite has crystallized under hydrothermal conditions from an aqueous silica solution (Fyfe & Gies, 1990).

A homogeneous 0.2 molar aqueous solution of silicic acids has been performed by adding $Si(OCH_3)_4$ tetramethylortosilicate (TMOS) to water under continuous agitation.

Hydrolysis has taken place according to the equation (Gies *et al.*, 1982):

$$Si(OCH_3)_4 + 4H_2O \rightarrow Si(OH)_4 + 4CH_3OH$$

Such solutions have filled into silica reaction tubes under addition of catalytic amount of NH_4F. Methane and carbon dioxide have been condensed into reaction tube by cooling the tube with liquid nitrogen and sealing it off under air (Gies *et al.*, 1982).

Reaction has taken place at 170 °C and a total pressure of about 150 bar. At this temperature, SiO_2 has been immediately precipitated as a gel. After one week at 170 °C, beginning precipitation of cristobalite at the inner surface of the reaction tube just above the solution has been observed. After six weeks, few isotropic cubes, identified as melanophlogite, could be distinguished from round aggregates of cristobalite. The size of melanophlogite cubes has been between 0.01 and 0.05 mm (Gies *et al.*, 1982).

Gunawardane *et al.* (1987) have synthesized five clathrasils: **MEP**–, **MTN**–, **DOH**–, **DDR**–, and **NON**– types (for FTCs, see Table 6.1 in the Chapter "**6.1**" of Appendix), from aqueous silica solutions and under hydrothermal conditions, in the presence of their characteristic guest molecules and in the absence of atmospheric gases. In the presence of air during the synthesis implementation, the presence of N_2, CO_2, and Ar in the products has been detected by mass spectrometry analyses, whereas, in the absence of "help gases" during the synthesis procedures, the small cages have been found to be empty. No appreciable differences in the crystallization rates of dodecasil–1H (**DOH**) and dodecasil–3C have been observed, with air as "help gas". In the case of melanophlogite (**MEP**) and nonasils (**NON**), longer annealing was required for the crystallization in the absence of atmospheric gases. Air also facilitates crystallization of dodecasil–3C in some conditions, and, in the absence of air, ZSM–48 (***MRE**) has been appeared as the major phase, along with dodecasil–3C. Therefore, although the interaction energy between the "help gas" and the host structure in clathrasils is small, this factor becomes significant at the stability limit of different framework types (Momma, 2014).

The presence of guest molecules in the solution leads to the formation of low density porous tectosilicates possessing polyhedral cavities (i.e. clathrasils). The guest molecules act as templates during crystallization process, and the size and shape of the cages in clathrasils depend mainly on the size and shape of the guest molecules present during synthesis (Gunawardane *et al.*, 1987).

Gunawardane *et al.* (1987) synthesized melanophlogite successfully, in the absence of "help gases", in aqueous silicic acid solution, with methylamine as the guest species. Presence of ethylenediamine appeared to hinder the formation of melanophlogite under these conditions. Methylamine as guest can promote crystallization of melanophlogite at lower temperature (160–200 °C) irrespective of the presence or absence of air (Table 3.5) (Gunawardane *et al.*, 1987).

GUEST	MEDIUM	TEMPERATURE (°C)			
		160	180	200	240
Methylamine *	en/H_2O	–	–	–	Cristobalite
Methylamine *	H_2O	MEP	MEP	MEP	–
Methylamine **	H_2O	MEP	MEP	MEP	D3C

Table 3.5. Results of melanophlogite synthesis (Gunawardane *et al.*, 1987). en = ethylenediamine, MEP = melanophlogite; D3C = dodecasil–3C; – = no crystallization; * = in vacuum; ** = in air.

As indicated by Gunawardane *et al.* (1987), much longer period (8–10 weeks) were necessary for the crystallization in vacuum. Crystal growth of melanophlogite appears faster in the presence of "help gases". It seems likely the occupation of small cages [5^{12}] by "help gases" in melanophlogite facilitates crystal growth. In a synthesized melanophlogite, the larger of the two cage type, [$5^{12}6^2$] is always occupied by CH_3NH_2, CO_2, N_2O, N_2 or a mixture of these species depending on the guests present during synthesis. The smaller [5^{12}] cages, in contrast, are either partly or fully occupied by CH_4, N_2, Kr or Xe when present during synthesis or they may remain empty when none of these molecules are present (Gunawardane *et al.*, 1987). The presence of CH_3NH_2 inside the [$5^{12}6^2$] cages has been reported also by Fyfe & Gies (1990).
Here, the synthesis procedure follows closely that by Gunawardane *et al.* (1987). In detail, we planned not to use "help gases", but to perform the experiments in chemically purified water and in a sealed container, either quartz vial or autoclave, together with methylamine as templating agent. The syntheses lasted between 12 up to 16 weeks, that is more in respect to 8–10 weeks reported in literature (Gunawardane *et al.*, 1987), at temperatures between 160 and 190 °C.
Four synthesis experiments have been done, two in quartz vials, and two in autoclave.

3.2.1. SYNTHESIS IN QUARTZ VIALS

3.2.1.1. 1st TEST

First attempts of synthesis of melanophlogite have been done, with tetramethylorthosilicate $Si(OCH_3)_4$ (TMOS) and tetraethylorthosilicate $Si(OC_2H_5)_4$ (TEOS) as crosslinking agents, methylamine as guest molecules source, and chemically purified water as medium.
The implementation of the procedures of synthesis proved quite difficult, since, in literature, information are scarcely present, and lacking in important practical details. During the first attempts, as means of containment, the vials have been chosen, created from quartz tubes, with different diameters and thickness. The vials have been worked with the flame.

The vials have been closed in vacuum, after cooling the reagents inside with liquid nitrogen, and working the quartz tubes with the flame, so to seal the vials. Finally, the vials have been placed in a kiln, at a temperature close to 170 °C and for almost 12 weeks, that is in the thermal range and the period suggested for crystallization of melanophlogite (Gunawardane *et al.*, 1987). Thanks to the small dimension of the kiln, we can assume that the thermal gradient was quite limited.

The preservation of the vials is related to the internal pressure during the thermal increasing ramp, and the following thermal treatment. At the beginning, to favour the manufacturing of the vials, quartz pipes of diameter of a little bit more than 10 mm and thickness of about 1 mm have been used, and TMOS as crosslinking agent. However, the vials wholeness was not guaranteed during the thermal increase, and consequently it was not possible to reach even the lowest limit of the thermal range suggested for melanophlogite crystallization, that is 160 °C (Gunawardane *et al.*, 1987), since the vials exploded, due to the lack of containment of the relatively thin quartz vials. Consequently, diametrical size reduction and thickness increase have been adopted to improve the vials wholeness: diametrical size of about 4 mm and 6 mm for internal and external diameters, respectively, and thickness of about 2 mm seem a proper combination of dimensional factors to contain the pressures developed in the vials.

After the explosions of the vials, it has been decided to use TEOS, instead of TMOS, as a safer reagent to employ as crosslinking agent. A safety issue was in fact considered, in the case of contact with the operators, after unexpected explosions of the vials, during the thermal increasing ramp or the thermal treatment, considering the scarce control exerted on the pressures generated inside the vials.

Moreover, the total amount of chemical reagents has been greatly decreased: 0.45 ml is the highest volume of reagents in a vial, in the vial containing the highest concentration of methylamine and the highest ratio between water and TEOS. All the other vials contain less than 0.45 ml of reagents.

The decreased amounts of reagents could decrease the yield potentially obtainable from the synthesis. It was decided to focus on the higher yield only after a preliminary determination of the optimum conditions of melanophlogite synthesis: the synthesis in vials enables to test different samples with various concentrations of methylamine and ratios between water and TEOS within a single run. In case of a successful synthesis, it was decided to focus on the optimum sample to obtain a higher yield with the use of an autoclave as mean of containment, which allows employing greater amounts of reagents, and reaching higher temperature than what is possible with the vials.

After the first aborted attempts, a new set of twenty vials has been organized, with four increasing methylamine concentrations and, for each of them, five ratios between chemically purified water and TEOS, as indicated in Table 3.6.

The thermal treatment has been of almost 12 weeks, and at a temperature close to 170 °C.

From twenty vials of the first run, cubic shape crystals of synthesized melanophlogite have been individuated exclusively in five vials (MEP_17, MEP_18, MEP_22, MEP_23 and MEP_24), corresponding to the methylamine concentrations of 0.9 and 1.2, and ratios between chemically purified water and TEOS of 4:1, 2:1 and 1:1 (Table 3.6), that is the higher methylamine content, and water prevailing or equal to TEOS.

METHYLAMINE CONCENTRATION (ml/ml solution)	H_2O:TEOS	VIALS IDENTIFICATION	MEP
0.3	4:1	MEP_7	NO
	2:1	MEP_8	NO
	1:1	MEP_9	NO
	1:2	MEP_10	NO
	1:4	MEP_11	NO
0.6	4:1	MEP_12	NO
	2:1	MEP_13	NO
	1:1	MEP_14	NO
	1:2	MEP_15	NO
	1:4	MEP_16	NO
0.9	4:1	MEP_17	YES
	2:1	MEP_18	YES
	1:1	MEP_19	NO
	1:2	MEP_20	NO
	1:4	MEP_21	NO
1.2	4:1	MEP_22	YES
	2:1	MEP_23	YES
	1:1	MEP_24	YES
	1:2	MEP_25	NO
	1:4	MEP_26	NO

Table 3.6. Methylamine concentration and H_2O:TEOS ratio in the first set of synthesis in vials. Melanophlogite yield: NO = not found; YES = few rare crystals.

The crystals of synthesized melanophlogite, which are not visible to the naked eye, can be identified by observations with an optical microscope (Fig. 3.31).

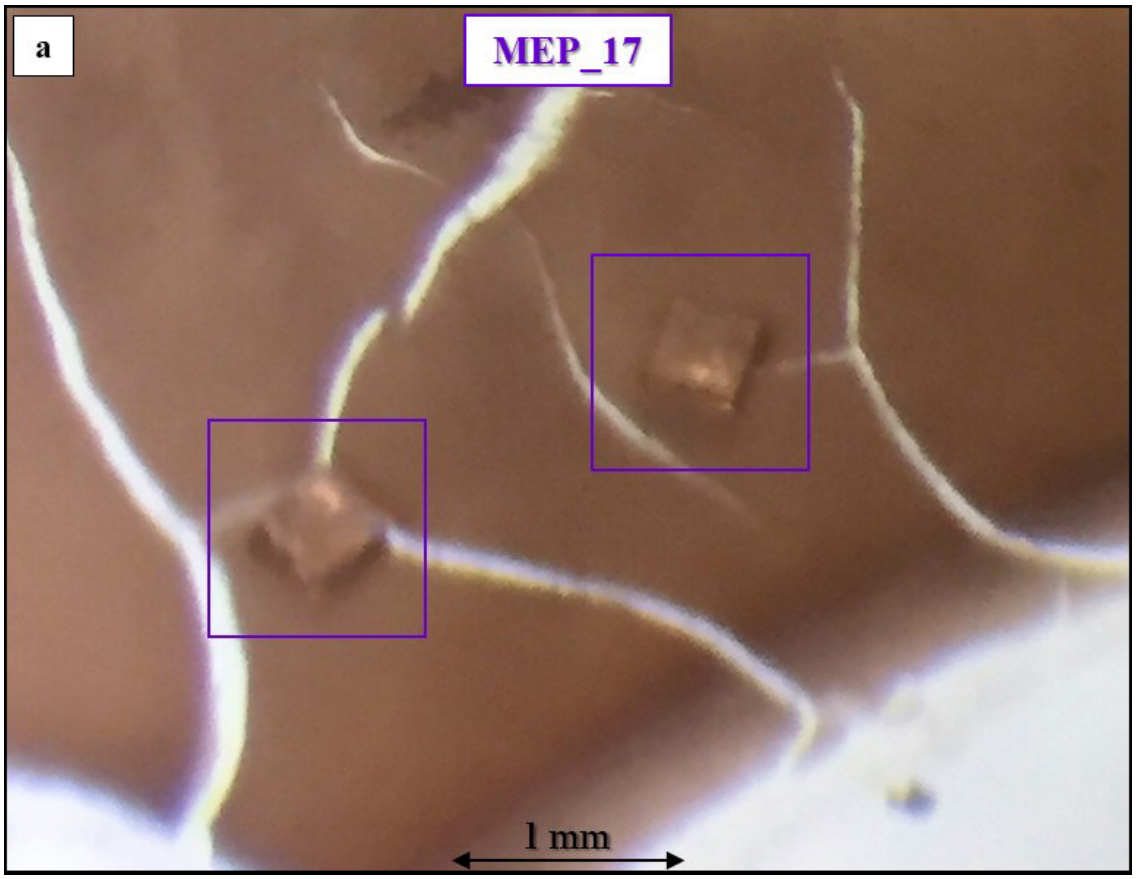
a
MEP_17
1 mm

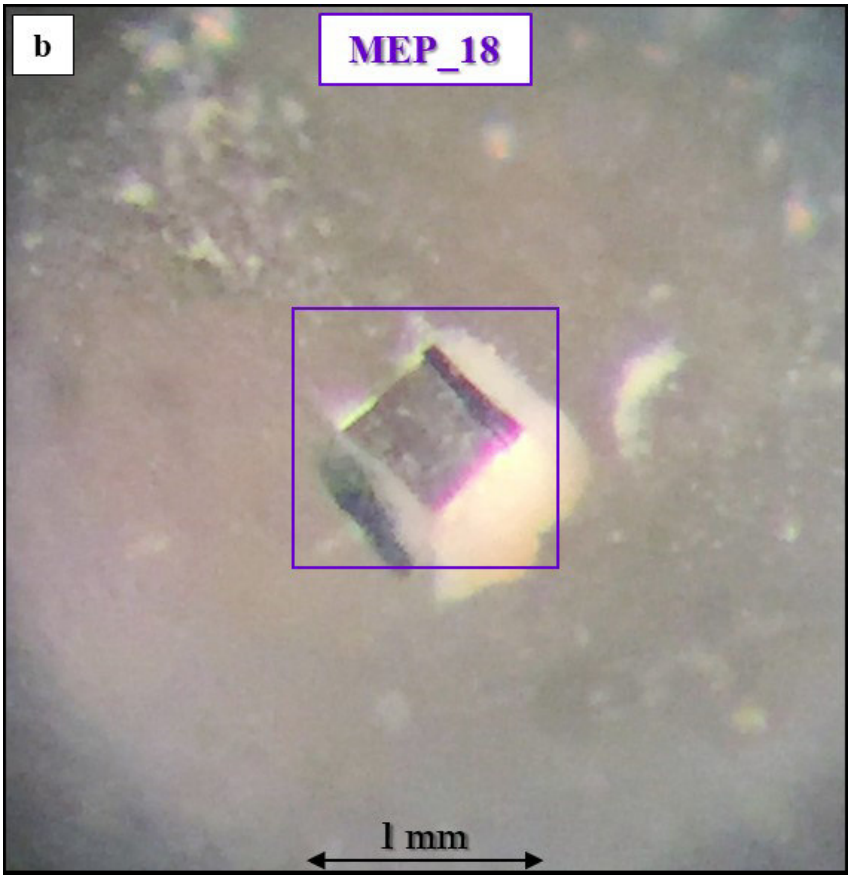
b
MEP_18
1 mm

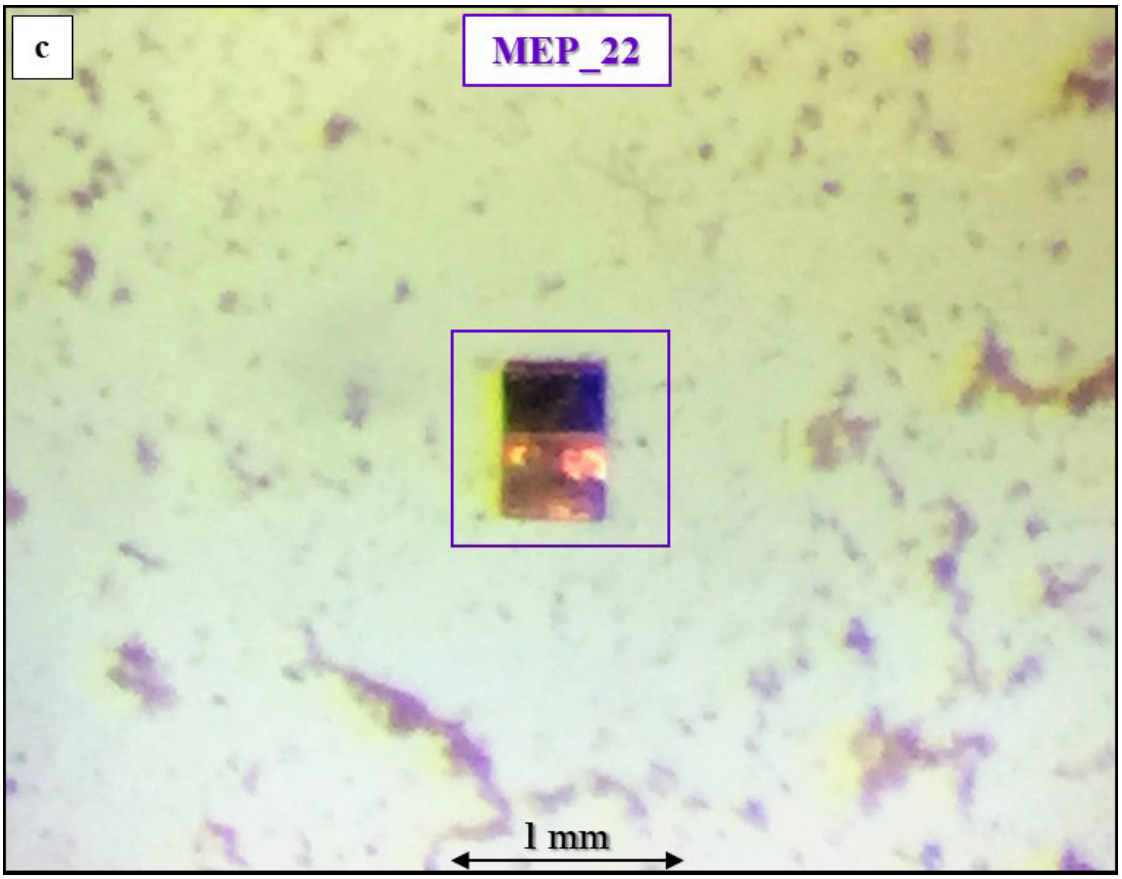
c
MEP_22
1 mm

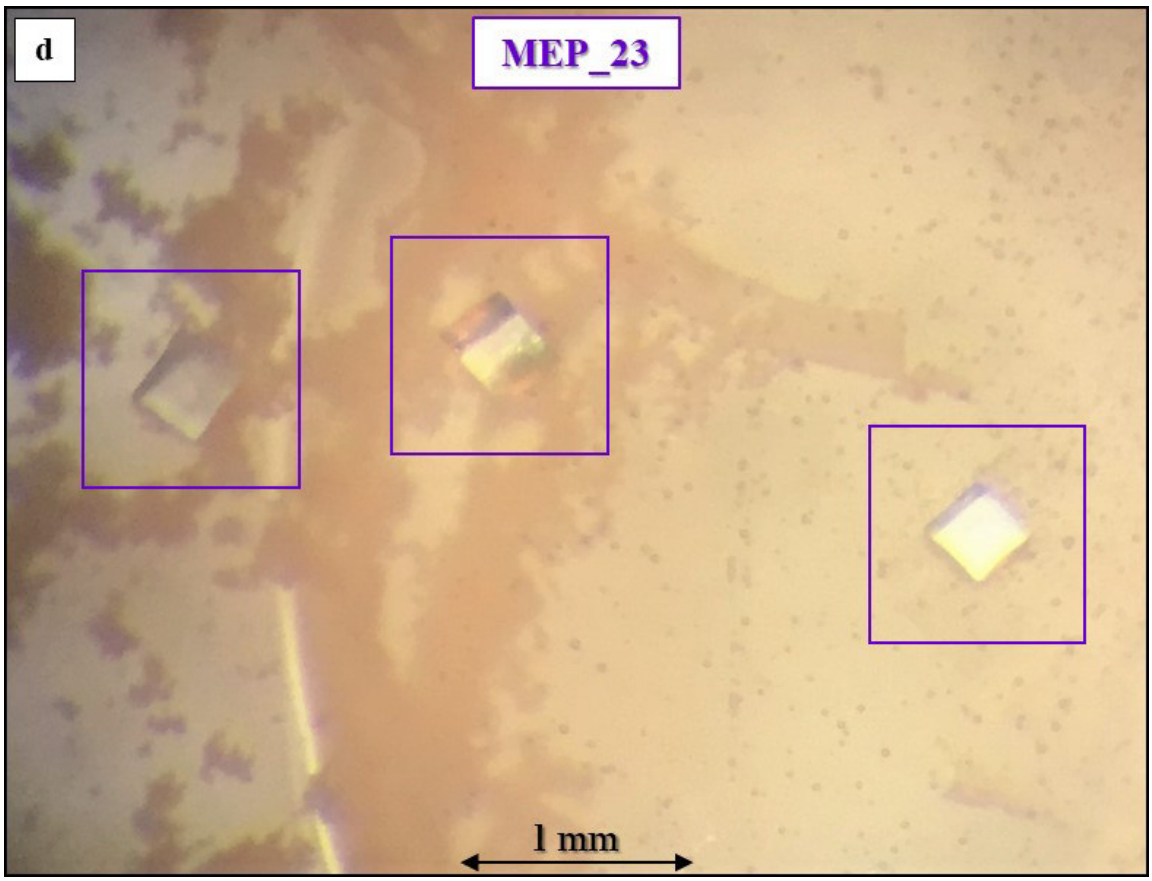
d
MEP_23
1 mm

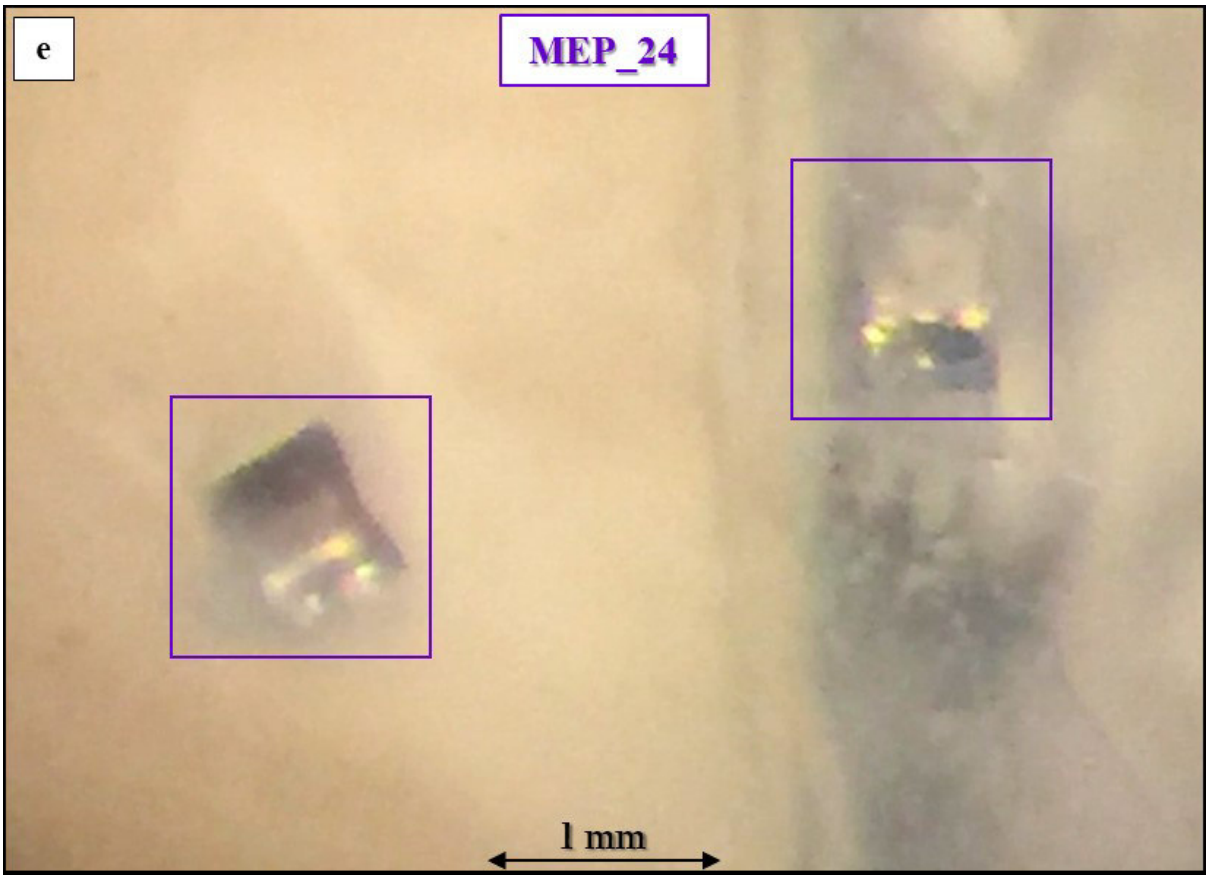

Figure 3.31. Cubic shape crystals of synthesized melanophlogite, observed using the optical microscope, in MEP_17 (a), MEP_18 (b), MEP_22 (c), MEP_23 (d), and MEP_24 (e) quartz vials.

Diffraction patterns have been collected for the synthesized material, recovered from all the vials in which melanophlogite has been crystallized. Preliminary diffraction patterns have been collected with the Bruker D2 Phaser diffractometer, over the 5–50 °2θ range, with a counting time of 0.5 sec/step and 0.018 ° as 2θ step. Further collections have been then taken over the 5–40 °2θ range, with higher counting times of 1.5 and 3 sec, and 0.018 ° as 2θ step; longer exposures were necessary, since they have revealed to be covered by a strong amount of amorphous. No other phase was found in the diffraction patterns.

A qualitative XRPD investigation to estimate the melanophlogite extent has been done on the diffraction pattern taken for the synthesized material recovered from MEP_24 vial, since it appeared to be that with the greatest number of cubic shaped crystals of melanophlogite (Fig. 3.32). The diffraction pattern has been collected over the 5–60 °2θ range, with a counting time of 14.5 sec/step and 0.018 ° as 2θ step.

The qualitative XRPD analysis has been done using the DIFFRAC.EVA Suite, and has shown the predominant presence of amorphous fraction, with very weak melanophlogite diffraction peaks. This is in perfect accordance with the observations done with the optical microscope,

in which very few crystals of melanophlogite, dispersed in an amorphous matrix have been detected.

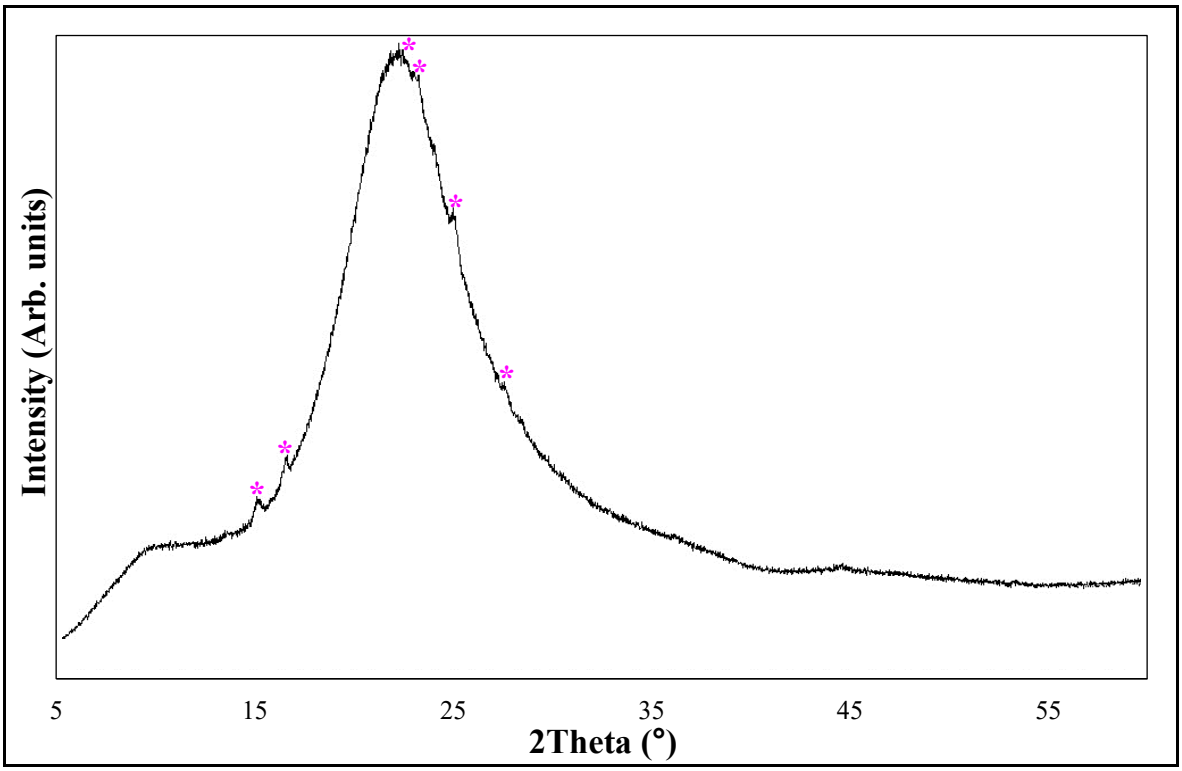

Fig. 3.32. The qualitative XRPD analysis carried out on the diffraction pattern taken for the synthesized material from MEP_24 quartz vial, at room temperature, after 13 hours and 30 minutes of exposure, with a counting time of 14.5 sec/step and 0.018 ° as 2θ step. * = melanophlogite diffraction peaks.

Considering the predominant presence of amorphous, no further quantitative investigation has been carried out to quantify the fraction of melanophlogite.

Some crystals of synthesized melanophlogite have been isolated from the synthesized material from all the vials in which mineral crystallization process has occurred, to carry out SC–XRD measurements.

3.2.1.2. 2nd TEST

From the results of the synthesis carried out in vials, it appears that higher methylamine concentrations and higher ratios between chemically purified water and TEOS can promote crystallization of melanophlogite.

A second set of vials has been prepared, with higher methylamine contents, and water to TEOS ratios higher or equal to one (Table 3.7).

Moreover, a second collection of vials is necessary to verify the reproducibility of the synthesis carried out with the first one, and to test the goodness of the synthesis procedures followed. The thermal treatment has been of almost 12 weeks, and at a temperature close to 170 °C.

METHYLAMINE CONCENTRATION (ml/ml solution)	H_2O:TEOS	VIALS IDENTIFICATION	MEP
1.2	4:1	MEP_27	YES
	2:1	MEP_28	NO
	1:1	MEP_29	NO
1.8	4:1	MEP_30	NO
	2:1	MEP_31	YES
	1:1	MEP_32	YES
2.4	4:1	MEP_33	YES
	2:1	MEP_34	YES
	1:1	MEP_35	YES
4.8	4:1	MEP_36	YES
	2:1	MEP_37	YES
	1:1	MEP_38	YES

Table 3.7. Methylamine concentration and H_2O:TEOS ratio in the second set of synthesis in vials. Melanophlogite yield: NO = not found; YES = few rare crystals.

As reported in Table 3.7, the vials prepared with the higher methylamine concentrations (2.4 ml/ml solution and 4.8 ml/ml solution) have shown melanophlogite crystallization for all the investigated ratios between chemically purified water and TEOS.

This seems to verify the hypothesis that higher concentrations of methylamine and higher ratios between chemically purified water and TEOS promote the crystallization.

To note, the synthesis MEP_29, which corresponds to the same methylamine concentration and water to TEOS ratio than MEP_24, here does not give melanophlogite, showing that oversaturation of methylamine is needed to obtain crystallization.

In this second set of synthesis in quartz vials, the crystals of synthesized melanophlogite are visible to the naked eye, thanks to their submillimetric dimensions, inside the vials, in the regions in which there are still liquid reagents, as shown in Fig. 3.33.

Sometimes, cubic shape crystals can be found strongly inter–penetrated, as shown in Fig. 3.34.

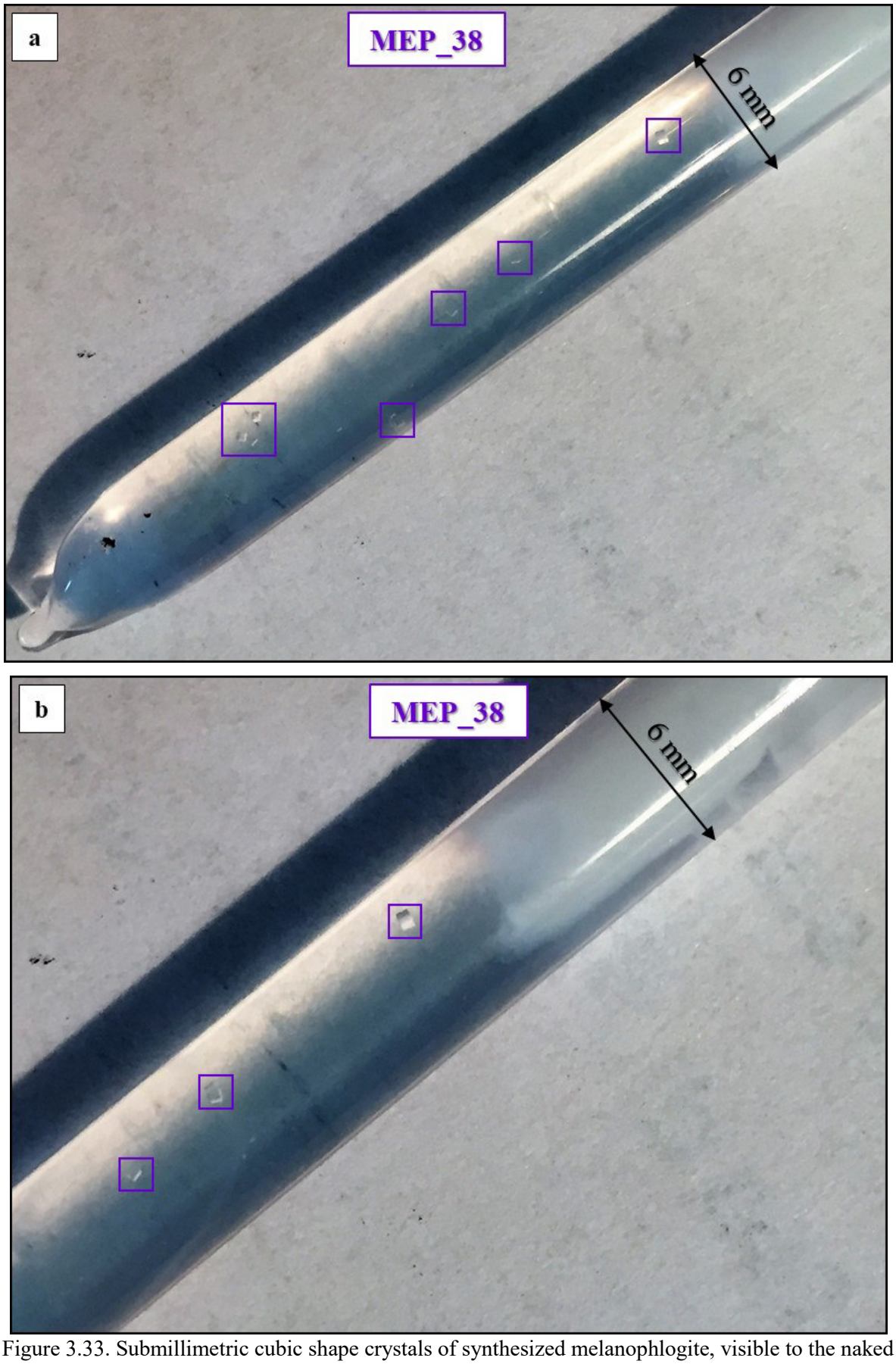

Figure 3.33. Submillimetric cubic shape crystals of synthesized melanophlogite, visible to the naked eye, in MEP_38 quartz vial, (a) and (b).

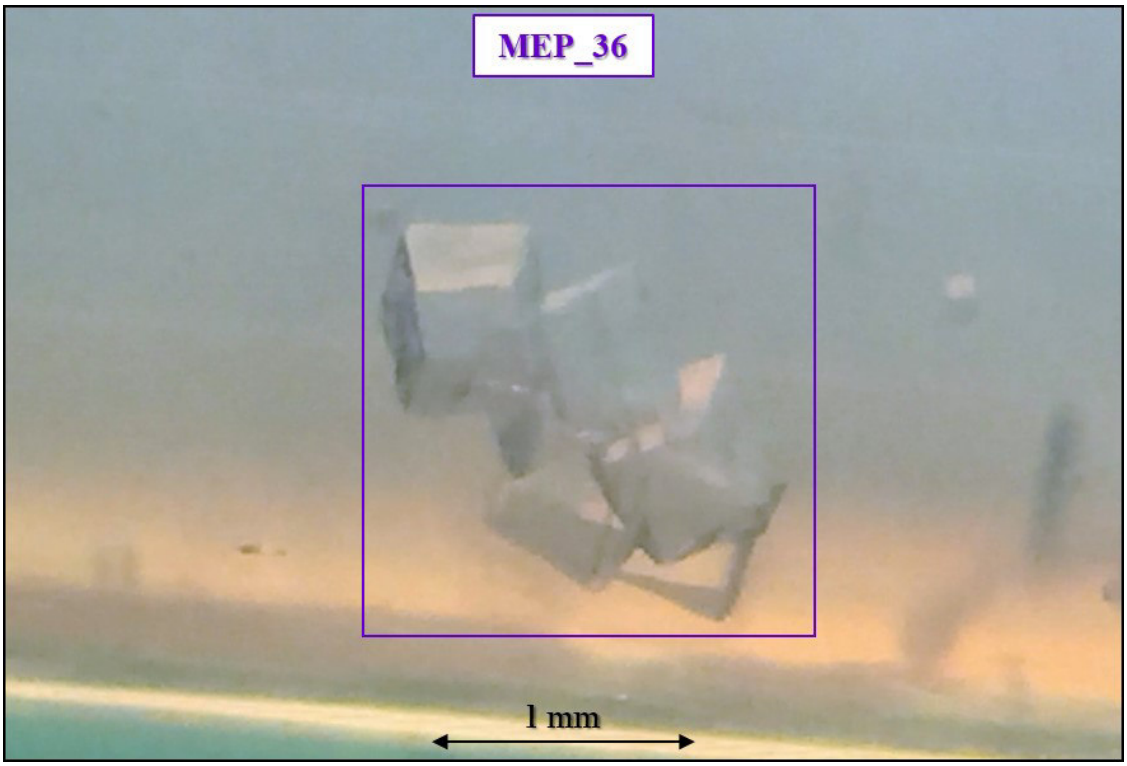

Figure 3.34. Cubic shape crystals of synthesized melanophlogite, observed using the optical microscope, in MEP_36 quartz vial.

Diffraction patterns have been taken for the synthesized material, recovered from all the vials with melanophlogite, in order to carry out a qualitative XRPD with DIFFRAC.EVA Suite. Preliminary diffraction patterns have been taken with the Bruker D2 Phaser diffractometer, over the 5–50 °2θ range, with a counting time of 1 sec/step and 0.018 ° as 2θ step; also in this second run, further collections have been taken over the 5–50 °2θ range, with a higher counting time of 10 sec, and 0.018 ° as 2θ step, to highlight melanophlogite diffraction peaks, since they have revealed themselves to be covered by a strong amount of the amorphous fraction.

To quantify the amorphous fraction, a quantitative XRPD analysis has been done on samples of the synthesized material, from the three vials prepared with the highest concentration of methylamine (that is 4.8 ml/ml solution), which, at sight, show the highest concentration of melanophlogite. A percentage equal to 20 wt.% of synthetic α–Al_2O_3 corundum was added as internal standard.

The diffraction patterns have been collected with the Bruker D2 Phaser diffractometer, over the 5–50 °2θ range, with a counting time of 2.5 sec/step and 0.018 ° as 2θ step.

As reported in Fig. 3.35, the Rietveld refinements have been done with the cubic symmetry *Pm*3*n* for melanophlogite, and with the trigonal symmetry *R*–3*c* for corundum (Lutterotti & Scardi, 1990).

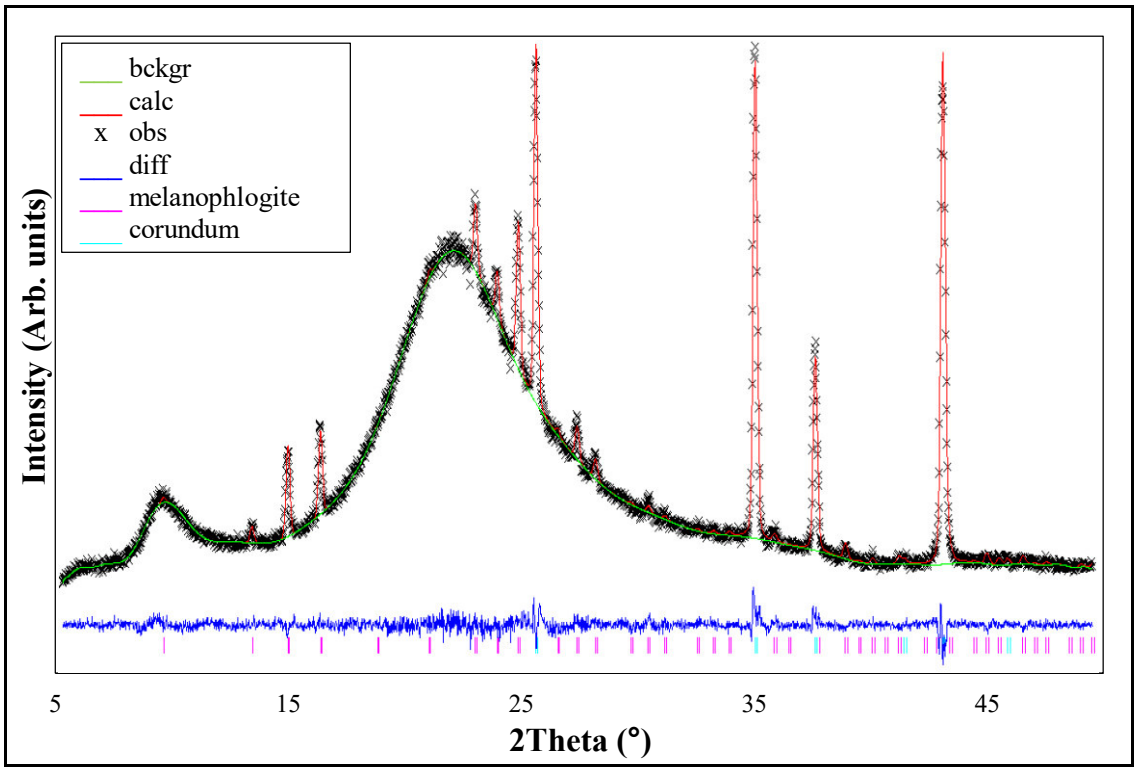

Figure 3.35. Rietveld refinement on diffraction pattern taken for a mixture of synthesized material from MEP_36 quartz vials, with the addition of a percentage equal to 20 wt.% of an internal standard, at room temperature. The difference between calculated and observed patterns (in red and marked with crosses, respectively) is in blue and the background in green. Melanophlogite and corundum are indicated with pink and light blue bars, respectively.

As suggested by the results of the quantitative XRPD analysis (Table 3.8), the synthesized material recovered from the three vials prepared considering the highest methylamine concentration, which should promote the crystallization of melanophlogite, is almost completely amorphous. In fact, also in the case of the second set of quartz vials, only a few crystals have been found dispersed in an amorphous matrix.

QUARTZ VIAL	MELANOPHLOGITE (wt.%)	AMORPHOUS (wt.%)
MEP_36	2.70 ± 0.05	97.30 ± 0.05
MEP_37	4.27 ± 0.07	95.73 ± 0.07
MEP_38	1.27 ± 0.02	98.73 ± 0.02

Table 3.8. Results of quantitative XRPD analysis on diffraction pattern, taken for a mixture of synthesized material with the addition of a percentage equal to 20 wt.% of an internal standard, at room temperature.

Some crystals of synthesized melanophlogite have been isolated from the synthesized material from all the vials with melanophlogite, to carry out SC–XRD measurements.

3.2.2. SYNTHESIS IN AUTOCLAVE

The results from the vials syntheses represent the starting point for the attempting an upscaling, employing an autoclave as mean of containment, to obtain a higher quantity of synthesized melanophlogite, instead of few crystals dispersed in an amorphous matrix. The two runs with vials allowed to define the optimal conditions of synthesis of melanophlogite, in terms of reagents, proportions between them, and temperature and duration of the thermal treatment, which are the basis for the synthesis in autoclave.

3.2.2.1. 1st TEST IN AUTOCLAVE

From the results obtained in the vials, it appeared that higher methylamine concentrations and higher ratios between chemically purified water and TEOS can promote crystallization of melanophlogite.

Consequently, it has been decided to employ the highest concentration of methylamine and the highest ratio between chemically purified water and TEOS, among those previously tested: 4.8 ml of methylamine/ml solution, and 4:1 as ratio between chemically purified water and TEOS.

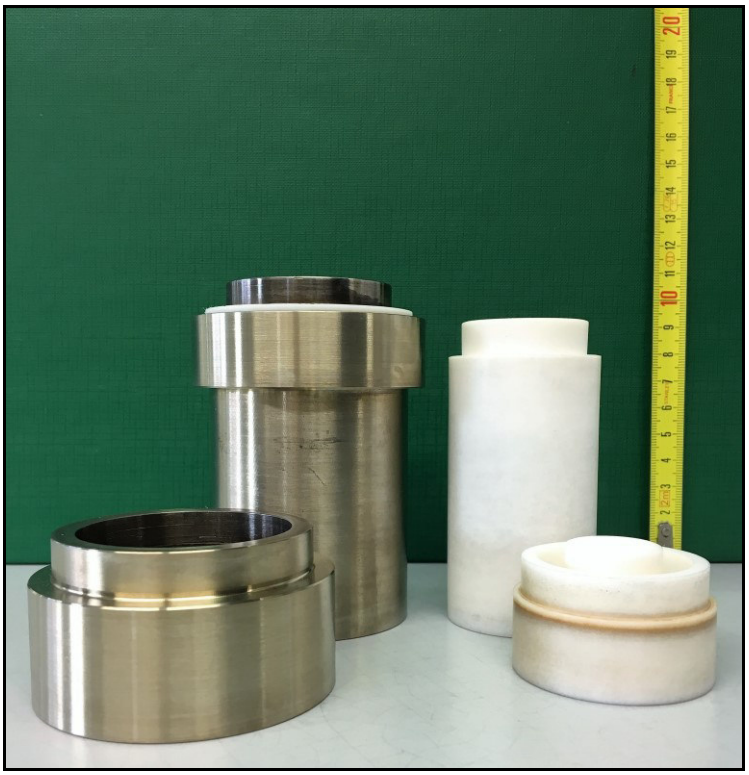

Figure 3.36. The autoclave used for the synthesis of melanophlogite, with the outer container of stainless steel, and the inner container of Teflon.

An autoclave has been used (Fig. 3.36) to simulate the hydrothermal synthesis conditions characteristic of the natural crystallization. The external coating of the autoclave is made up of stainless steel, and the inner container is made up of Teflon. This device of containment allows reaching pressures and temperatures higher than the ones that are possible with the quartz vials. Moreover, it is possible to obtain a higher quantity of synthesized material, and, in this light, it has been decided to fill the inner container for about 2/3 of its height.
The filling was done in the presence of air. In Table 3.9, the amounts of reagents are reported.

REAGENT	VOLUME OF REAGENT (ml)
Methylamine	12.72
Chemically purified water	0.65
TEOS	2.00

Table 3.9. The amounts of reagents calculated for the synthesis of melanophlogite in autoclave.

Once closed, always in the presence of air, the autoclave is placed in a kiln, which is the same where the quartz vials have undergone to the thermal treatment, and heated at a temperature close to 170 °C, as suggested in literature (Gunawardane *et al.*, 1987), at a heating rate which is not constant during the thermal ramp, but faster in the early phases and slower closer to the final temperature, i.e. the one chosen for the thermal treatment. After being well stabilized, the autoclave has been annealed for almost 16 weeks (precisely 111 days), which is more than 8–10 weeks, that is the period suggested in the literature (Gunawardane *et al.*, 1987). During the thermal treatment, a daily control of the temperature has been done, to verify the thermal stability inside the kiln.
At the end of the thermal treatment, the kiln has been turned off, and the temperature has been lowered, without setting any rate of thermal decreasing, but taking care to keep the oven door closed, so as not to cause any thermal shock, especially in the first phases of cooling to room temperature. When the temperature inside the kiln has reached a value close to room temperature, then the kiln door can be open, in order to facilitate and accelerate the final phase of cooling to room temperature.
Once stabilized at room temperature, the autoclave has been placed under a chemical hood, considering the hazardous nature of methylamine and TEOS, and has been opened. Inside the inner container, a considerable fraction of liquid phase has been found, and then removed manually. The inner container has been left opened, under the chemical hood, at room temperature, to dry the synthesized material. It has been decided to dry the sample at room

temperature to avoid changes in the characteristics of the synthesized material, for instance promoting the release of the guest molecules of the synthesized melanophlogite.

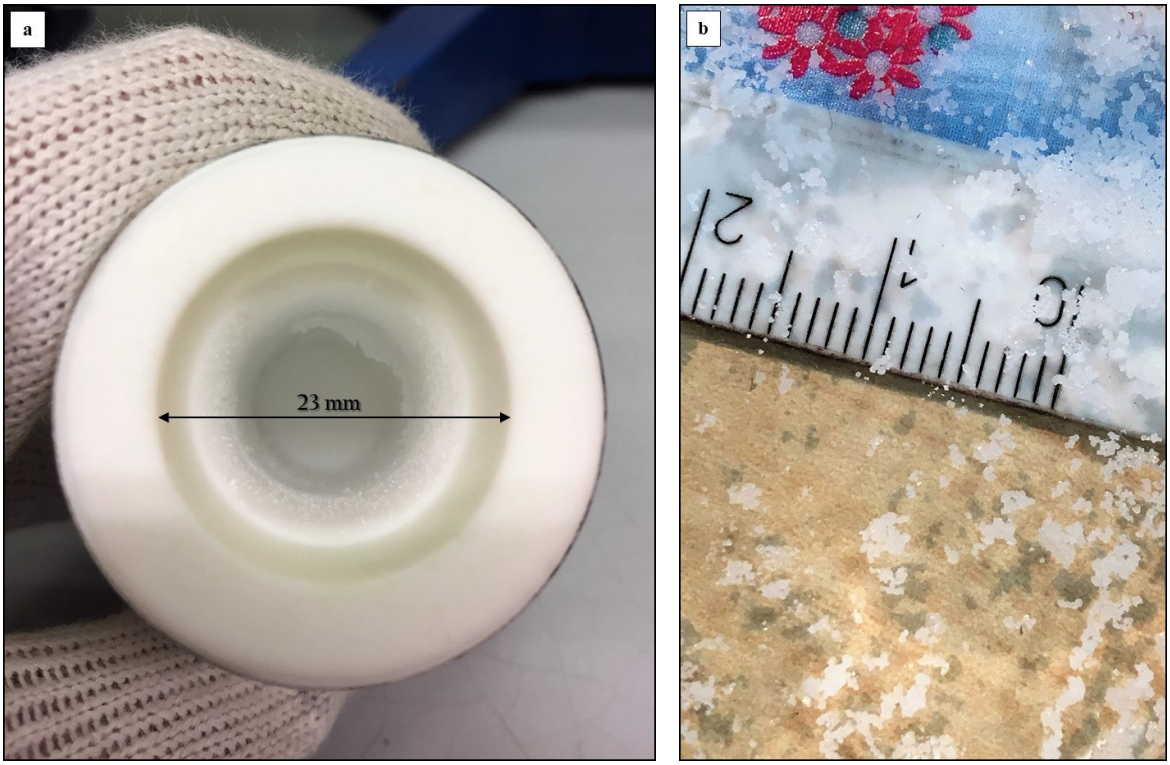

Figure 3.37. The synthesized material, obtained from the synthesis in autoclave, after the drying phase: still in the inner container (a), and placed in a becker (b).

The synthesized material, completely dry but still in the inner container, is presented in Fig. 3.37a. It appears different from the synthesized in the quartz vials, which, to the naked eye, appears as an amorphous matrix, and only after observation with an optical microscope reveals few cubic shaped melanophlogite crystals dispersed. On the contrary, in the synthesis in autoclave, the synthesized material shows a pervasive crystallinity, with submillimetric cubic shape crystals of melanophlogite, which are well visible even to the naked eye (Fig. 3.37b).

Observations with the optical microscope have supported the hypothesis of the predominant crystalline nature of the synthesized material, which reveals to be made up almost completely of crystals, with a cubic shape and very different size, as shown in Fig. 3.38. The crystals of melanophlogite synthesized in autoclave show a large dimensional range, differently from the material obtained from the syntheses in the quartz vials.

From the inner container of Teflon, a quantity slightly higher than 650 mg of synthesized material, weighed once well dry, has been recovered. A possible explanation for the higher

yield in the autoclave run might be the larger size of the autoclave, which promotes slower cooling and possibly better crystallization.

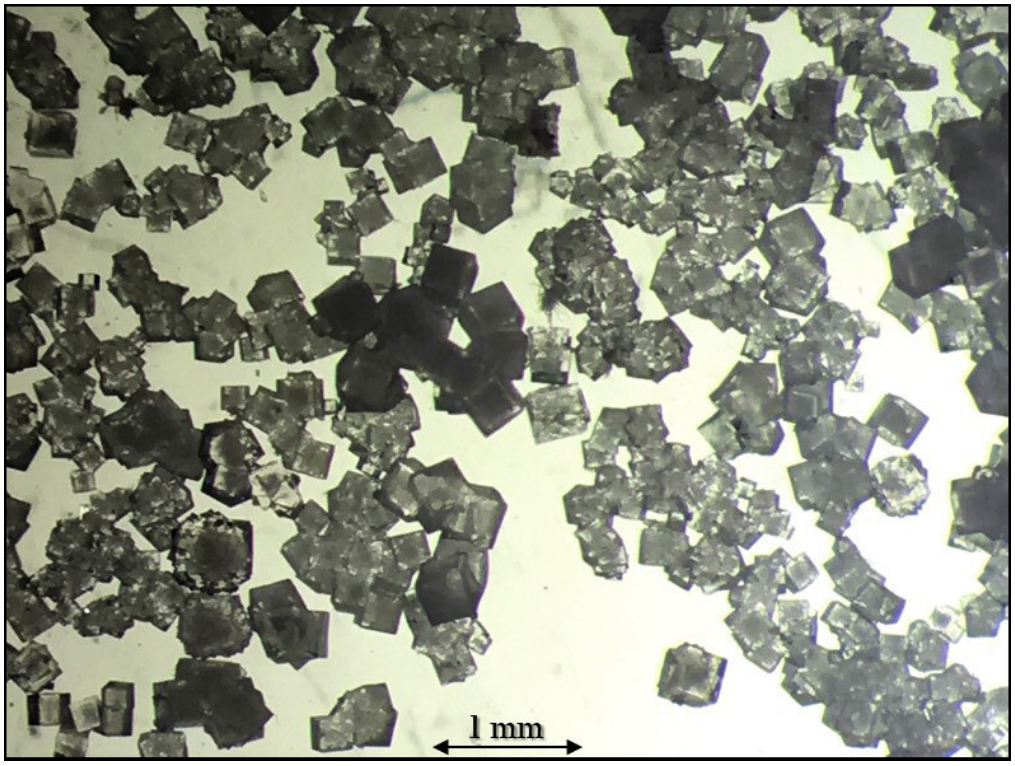

Figure 3.38. Synthesized material observed with the optical microscope: it is made up almost entirely of cubic shape crystals of melanophlogite.

XRD analyses have been carried out, at room temperature, to quantify the presence of the amorphous fraction.

The quantitative XRD analysis has been done on the powdered sample, with the addition of a percentage equal to 20 wt.% of an internal standard. For this purpose, a synthetic α–Al_2O_3 corundum has been employed.

The diffraction patterns have been collected with the Bruker D2 Phaser diffractometer, over the 8–50 °2θ range, with a counting time of 2.5 sec/step and 0.018 ° as 2θ step.

The Rietveld refinements have been carried out with the cubic symmetry *Pm*3*n* for melanophlogite (Gies, 1983), and with the trigonal symmetry *R*–3*c* for corundum (Lutterotti & Scardi, 1990).

As shown in Fig. 3.39, the Rietveld refinement has shown convergence without significant residuals. The intensity and the position of the diffraction peaks of melanophlogite is perfectly consistent with the structural model *Pm*3*n*.

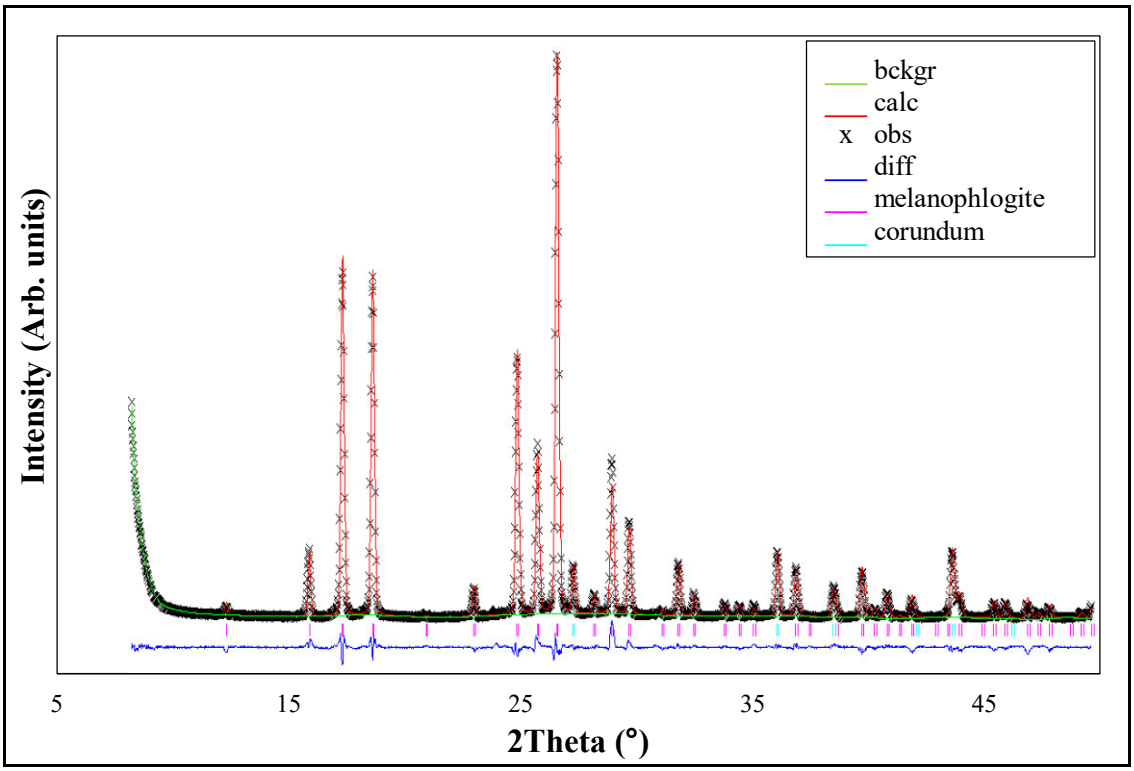

Figure 3.39. Rietveld refinement on diffraction pattern taken for a mixture of synthesized material with the addition of a percentage equal to 20 wt.% of an internal standard, at room temperature. The difference between calculated and observed patterns (in red and marked with crosses, respectively) is in blue and the background in green. Melanophlogite and corundum are indicated with pink and light blue bars, respectively.

As suggested by the results of the quantitative XRD analysis (Table 3.10), the synthesized material obtained from the synthesis in autoclave is almost completely made up of melanophlogite, with an amorphous fraction lower than 10%. As the synthesized material is almost pure melanophlogite, it can be further characterized without taking into account other crystalline phases, like carbonates.

MELANOPHLOGITE (wt.%)	AMORPHOUS (wt.%)
90.372 ± 0.001	9.628 ± 0.002

Table 3.10. Results of quantitative XRD analysis on diffraction pattern, taken for a mixture of synthesized material with the addition of a percentage equal to 20 wt.% of an internal standard, at room temperature.

Likely for the first time, since there are no references in the literature, it was here possible to synthesize melanophlogite, in quantities of hundreds of milligrams. Higher quantity allows to carry out a most complete characterization, thanks to an optimized hydrothermal synthesis in autoclave, and, in addition, succeeding in realizing an upgrade from the synthesis in quartz vials, in terms of purity and quantity characterizing the synthesized material.

3.2.2.1.1. SC–XRD AT ROOM TEMPERATURE

To define the symmetry of the synthesized melanophlogite, which could be a cubic one, as suggested by the morphology seen at the optical microscope, it has been decided to carry out SC–XRD analyses, at room temperature. At this purpose, some crystals of synthesized melanophlogite, either from vials (MEP_24) and from the synthesis in autoclave, have been chosen of different size, thinking that the ones of smallest dimensions could actually be single crystals, instead of mosaicized or twinned, as previously observed in the natural samples.

The major problem which prevents the experimental data refinement is that the synthesized material is not cubic, at room temperature. The phase transition takes place at a temperature slightly higher than room temperature, but the unit cell parameters are practically typical of a cubic symmetry. This aspect prevents to identify the *c* axis of a potential tetragonal symmetry, assuming that a tetragonal, or a lower symmetry, is the correct one. In these cases, in fact, the phase transition can promote the twinning phenomenon, and consequently the crystals result to be made up of individuals with the *c* axis oriented in the three possible directions of space. It becomes quite impossible to refine with a tetragonal (or a monoclinic) unit cell, obtaining a mediated structure.

Single crystal diffraction data have been collected with the Bruker AXS Smart diffractometer. The crystals, recovered from vials and autoclave, are only apparently single ones, as suggested by observations with the optical microscope, in which crystals of synthesized melanophlogite with a cubic shape are clearly noticeable. In fact, crystals, both from vials and autoclave, have revealed themselves to be mosaicized or twinned, and all of them have shown superstructural reflexes.

In the only melanophlogite crystal of such an adequate quality to allow attempting a data collection, the absence of the inversion center has been observed, and this aspect suggests a *P*–43*n* symmetry.

Consequently, this structure could be refined in the cubic symmetry, obtaining rather high R values: R_{int} = 10.55 % and R_{all} = 8.56 % (see “MEP_AUT.cif” file as additional document).

The unit cell volumes are 2409.3(1.1) and 2408.8(3.9) $Å^3$, for synthesized melanophlogite from vial (MEP_24) and autoclave, respectively: the synthesized crystals have shown very similar unit cell parameters and associated volumes, no matter the synthesis procedure.

3.2.2.1.2. RAMAN SPECTROSCOPY

Raman spectroscopy can be very useful to identify the guest molecules in the structural cages of melanophlogite. A preliminary Raman spectrum of the synthesized material has been collected with the portable Enspectr RaPort–Raman Handheld Analyser, to ascertain and identify the guest species in the structural cavities of synthesized melanophlogite (Fig. 3.40).

The synthesized material has not been grinded, but analysed as recovered from the inner container of Teflon, after drying.

Considering the position of the Raman modes characteristic of melanophlogite, it is possible to state that the silicate pattern is the same both in natural and synthesized samples.

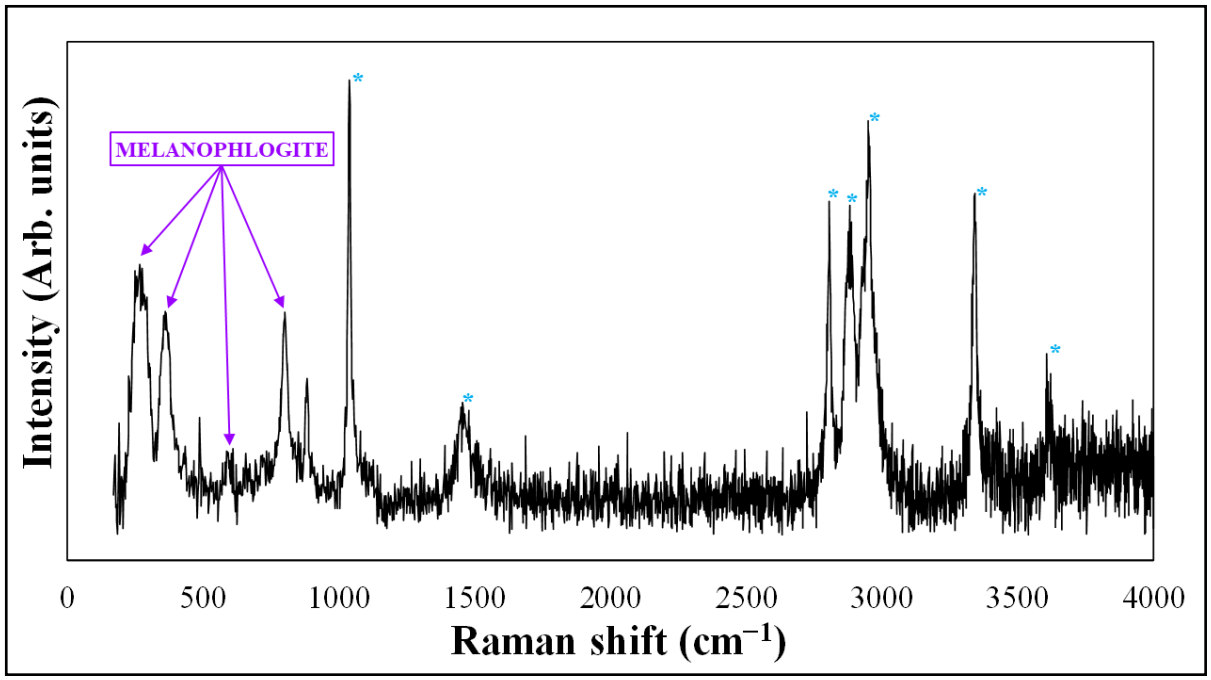

Figure 3.40. Raman spectrum of synthesized material from autoclave. * in light blue = Raman modes of methylamine.

Compared with previous results reported in literature (During *et al.*, 1968), it has been possible to confirm the presence of methylamine, thanks to its characteristic Raman modes, in the synthesized material recovered from autoclave. This result is in accordance to what previously reported by Gunawardane *et al.* (1987), and Fyfe & Gies (1990), which have detected methylamine in pentagondodecahedral [$5^{12}6^2$] cages of synthesized melanophlogite.

In a few broader peaks, there are small differences between the experimental Raman modes and what reported in the literature (Durig *et al.*, 1968), but, in other peaks, such difference is not apparent.

Moreover, the difference is an increase in frequency in the encaged methylamine, whereas for other encaged small molecules the difference is a decrease.

Differently from other small molecules, it looks like that methylamine in the synthesized melanophlogite has different interactions between guest molecules and host silica framework.

	PEAK POSITION (cm^{-1})				
LIQUID METHYLAMINE	1040	1429	2807	2885	3320
ENCAGED METHYLAMINE	1041.8	1451	2807.2	2882.7	3345

Table 3.11. Peak position of methylamine in liquid and encaged in synthesized melanophlogite.

It appears that methylamine has entered in the structural cages of synthesized melanophlogite, even though with a configuration still to be clarified, and act as templating agent.

3.2.2.1.3. TGA

A quantity, slightly lower than 6.5 mg, of powdered sample of synthesized material has been heated from 50 to 880 °C, with a heating rate of 5 °C/min.

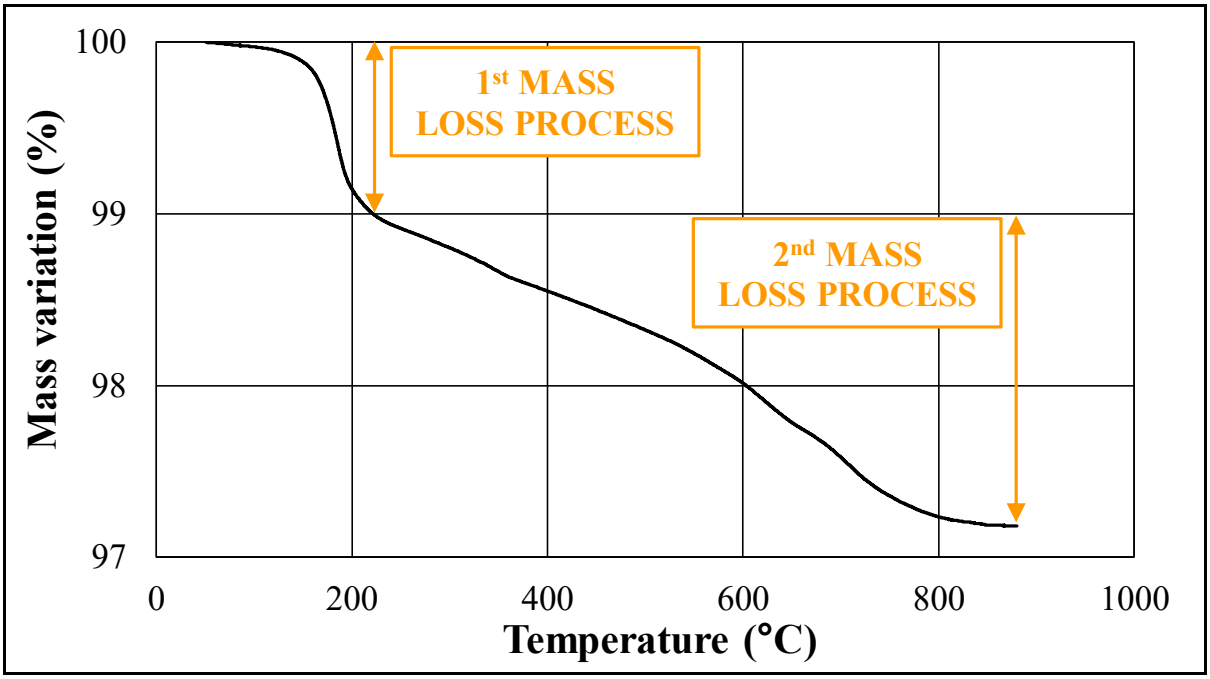

Figure 3.41. TGA on the synthesized material, carried out from 50 to 880 °C and with a heating rate of 5 °C/min.

As reported in Fig. 3.41, a very small mass variation is observable for temperatures lower than 100 °C. On the contrary, at temperatures between 100 and 220 °C, the mass variation is much more pronounced, and a loss by 1 % is achieved. Between 220 and 600 °C, another 1 %

mass loss occurs. At temperatures between 600 and 800 °C, the weight decreases somewhat faster. In the final phase of the thermal treatment, i.e. at temperatures higher than 800 °C, the mass loss apparently does not occur anymore. The overall mass variation has been of 2.8 %. The theoretical overall mass variation, calculated considering all the structural cages filled by methylamine, is 9 %. If methylamine occupies all the cages, some further weight loss could be expected at higher temperature, since not even a third of the theoretical mass variation has been released. However, the absence of mass variation at temperatures higher than 800 °C could simply be interpreted as the methylamine does not fill completely the cages.

3.2.2.1.4. DSC

A quantity slightly lower than 4.5 mg of powdered synthesized material has been thermally treated, in the following way: 1) heating from –85 to 175 °C, at 5 °C/min (Fig. 3.42a); 2) cooling from 175 to –75 °C, at 5 °C/min (Fig. 3.42b); 3) heating from –85 to 25 °C at 5 °C/min (Fig. 3.42c).

A peak has been located between –40 and –20 °C, and its reversibility has been confirmed, thanks to the presence of endothermic peaks during the heating phases, and an exothermic peak during the cooling down. A likely interpretation, as shown in the Discussion section, is that the peak is related to a first–order phase transition. The splitting of endothermic and exothermic peaks suggests that the phase transition could take place with two consecutive steps.

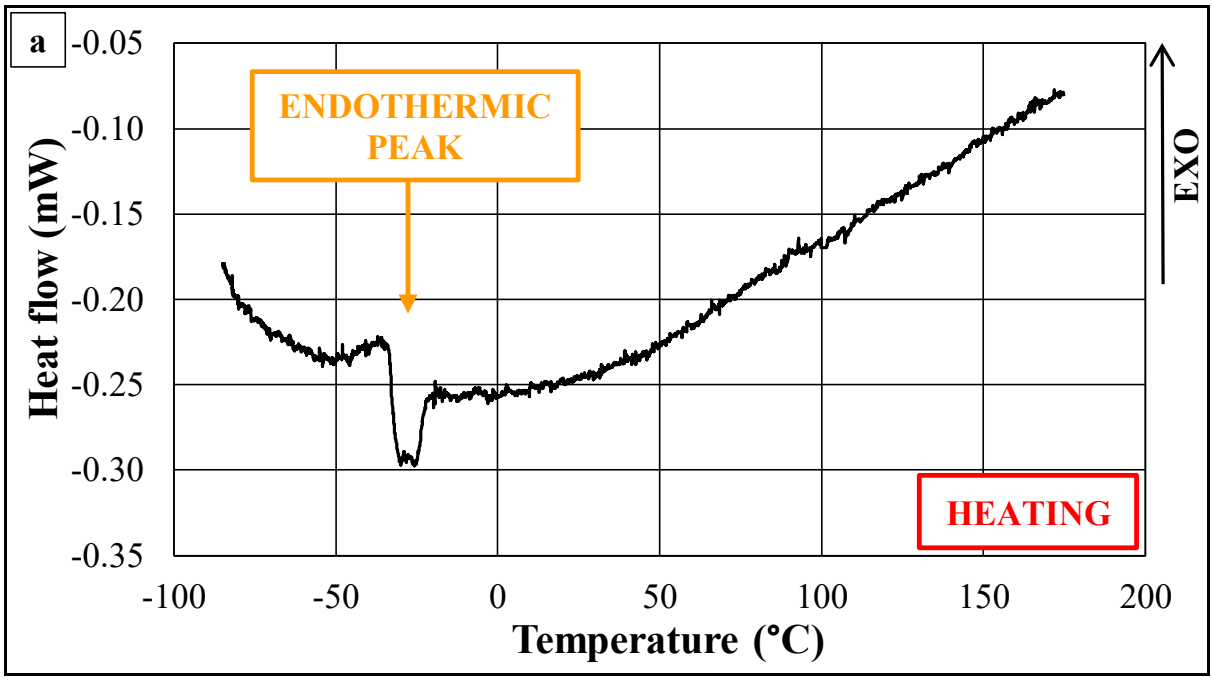

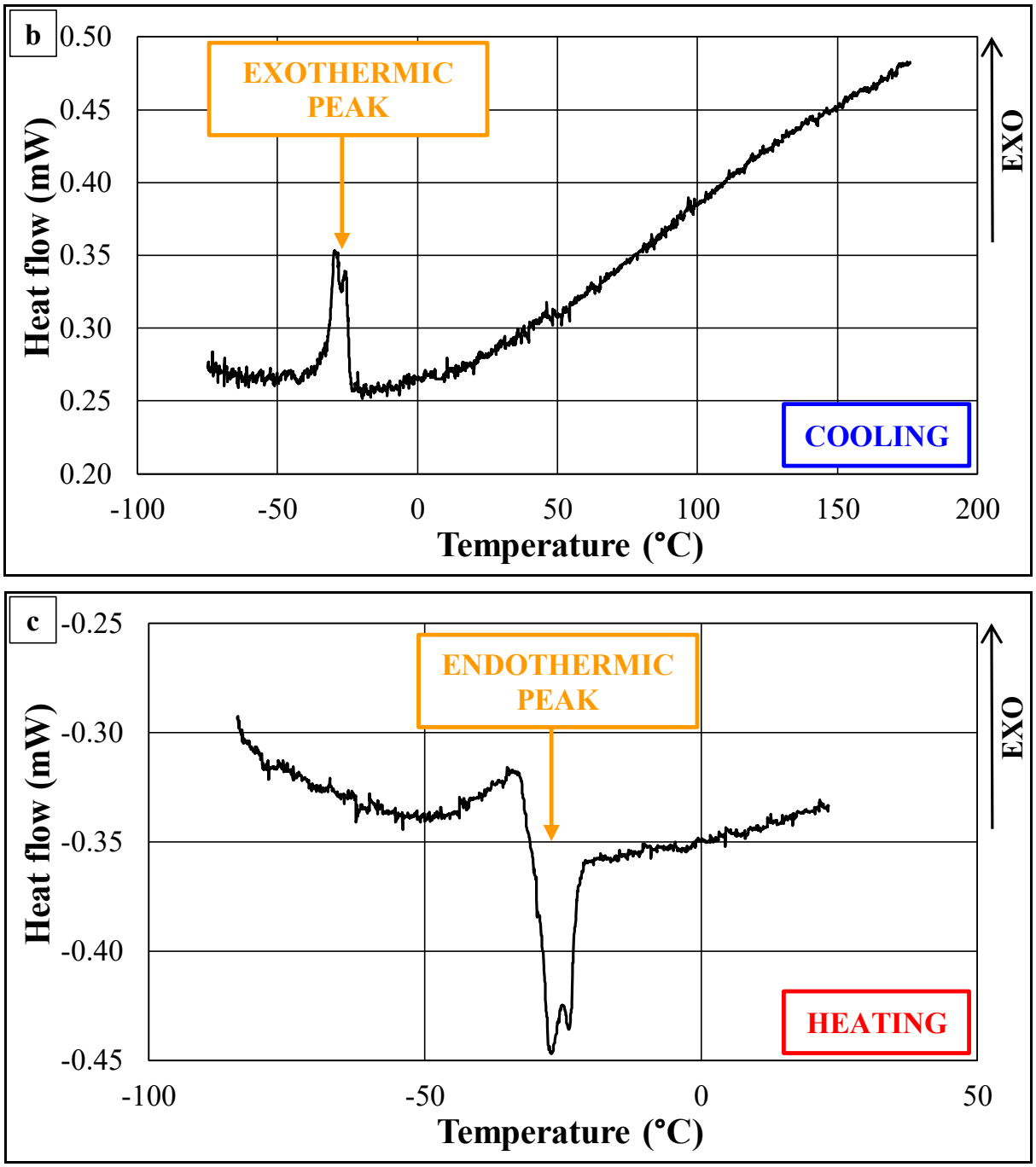

Figure 3.42. DSC on synthesized material from autoclave: (a) a first heating, from –85 to 175 °C, (b) a cooling, from 175 to –75 °C, and (c) a second heating, from –85 °C to room temperature, always with a heating rate of 5 °C/min.

A multi–instrumental INS investigation at ILL (Grenoble, France) has been already planned and currently in progress on synthesized melanophlogite, to clarify the interactions between the guest molecules and the silicate framework, in particular in order to gain a deeper insight into the dynamical properties of the host framework, as well as onto the diffusion mechanism of the guest species.

3.2.2.2. 2nd TEST IN AUTOCLAVE

A second test has been carried out in autoclave, to verify the goodness and the reproducibility of the synthesis of melanophlogite in autoclave.

The same conditions fixed for the first test have been considered.

The only changed parameter is the temperature at which the thermal treatment has been carried out. In fact, we have decided to set a higher temperature with respect to the one chosen during the first test, exploiting the potential of the autoclave, which allows to reach temperatures higher than those which have been allowed with the quartz vials. The final temperature has been set between 180 and 185 °C, that is within the thermal range indicated for melanophlogite crystallization (Gunawardane *et al.*, 1987).

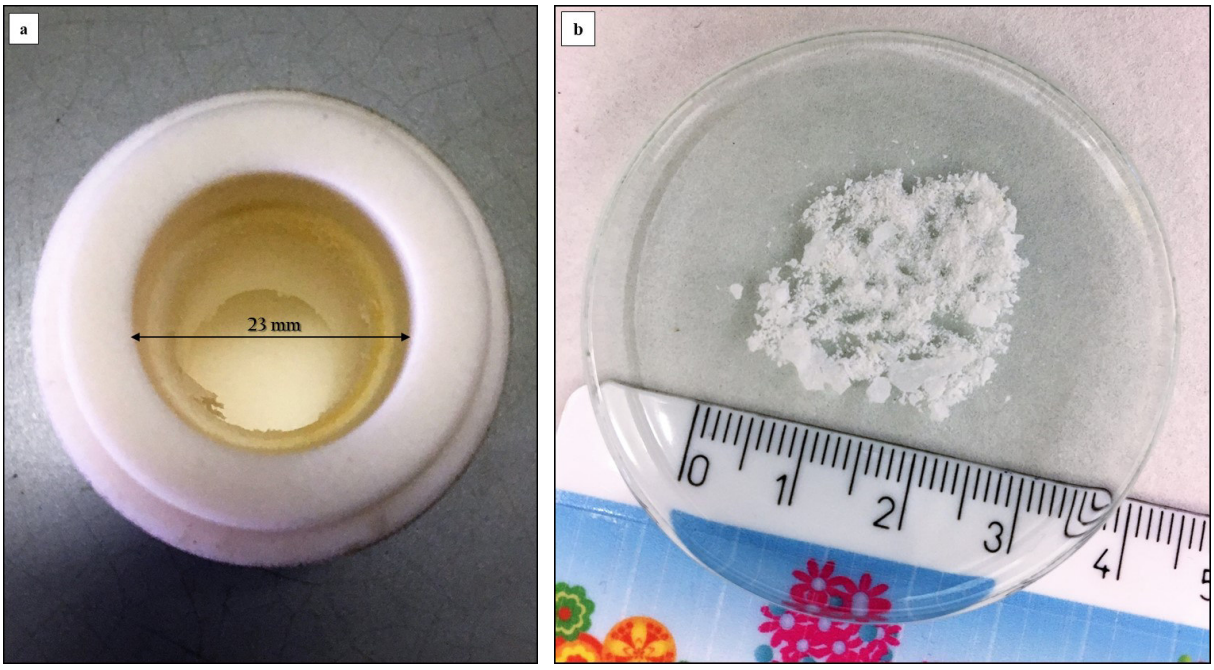

Figure 3.43. The synthesized material, obtained from the second test of synthesis in autoclave, after the drying phase: still in the inner container (a), and placed on a watch glass (b).

In Fig. 3.43a, the synthesized material, after the drying phase, is shown, still in the container. It appears very different if compared with the synthesized material of the first test of synthesis in autoclave. Once recovered from the container and put on a watch glass, the material appeared not crystalline to the naked eye (Fig. 3.43b).

Observations carried out with an optical microscope have shown that the synthesized material is quite different from the one obtained from the first test of synthesis in autoclave, since it has not revealed itself to be made up of cubic crystals (Fig. 3.44).

From the inner container of Teflon, a quantity slightly higher than 75 mg of synthesized material, weight once well dry, has been recovered. This quantity is much lower than the one obtained from the first test of synthesis in autoclave (a quantity slightly higher than 650 mg), and this is another remarkable difference between the two tests of synthesis of melanophlogite.

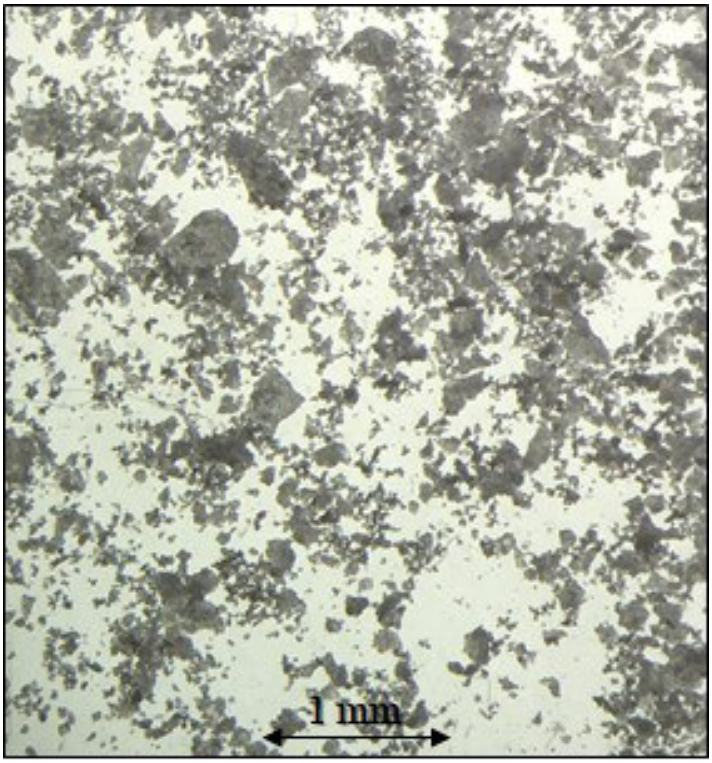

Figure 3.44. Synthesized material, obtained from the second test of synthesis in autoclave, observed with the optical microscope.

3.2.2.2.1. XRPD AT ROOM TEMPERATURE

XRD has been carried out on the powdered sample of synthesized material, to make a qualitative analysis and, consequently, identify which crystalline phases have potentially formed during the thermal treatment.

The qualitative analysis has been done using the DIFFRAC.EVA Suite.

The diffraction pattern has been collected with the Bruker D2 Phaser diffractometer, over the 5–50 °2θ range, with a counting time of 1 sec/step and 0.018 ° as 2θ step.

The qualitative analysis has revealed that the synthesized material is a mixture of cristobalite and quartz (Fig. 3.45). It appears quite clear that the temperature chosen for the thermal treatment has been too high, even though within the thermal range suggested to promote crystallization of melanophlogite (Gunawardane *et al.*, 1987).

Consequently, it is advisable to make further tests of synthesis in autoclave, to determine with more accuracy the thermal range in which melanophlogite crystallizes, maintaining methylamine, as templating agent, in concentration of 4.8 ml/ml solution, and 4:1 as ratio between chemically purified water and TEOS, which are medium and crosslinking agent respectively, and in the amounts already tested, and reported in Table 3.9. Probably, as suggested by the results of XRPD analyses, the thermal range indicated in literature is too wide, taking into account the proportions and the quantities of reagents above–mentioned.

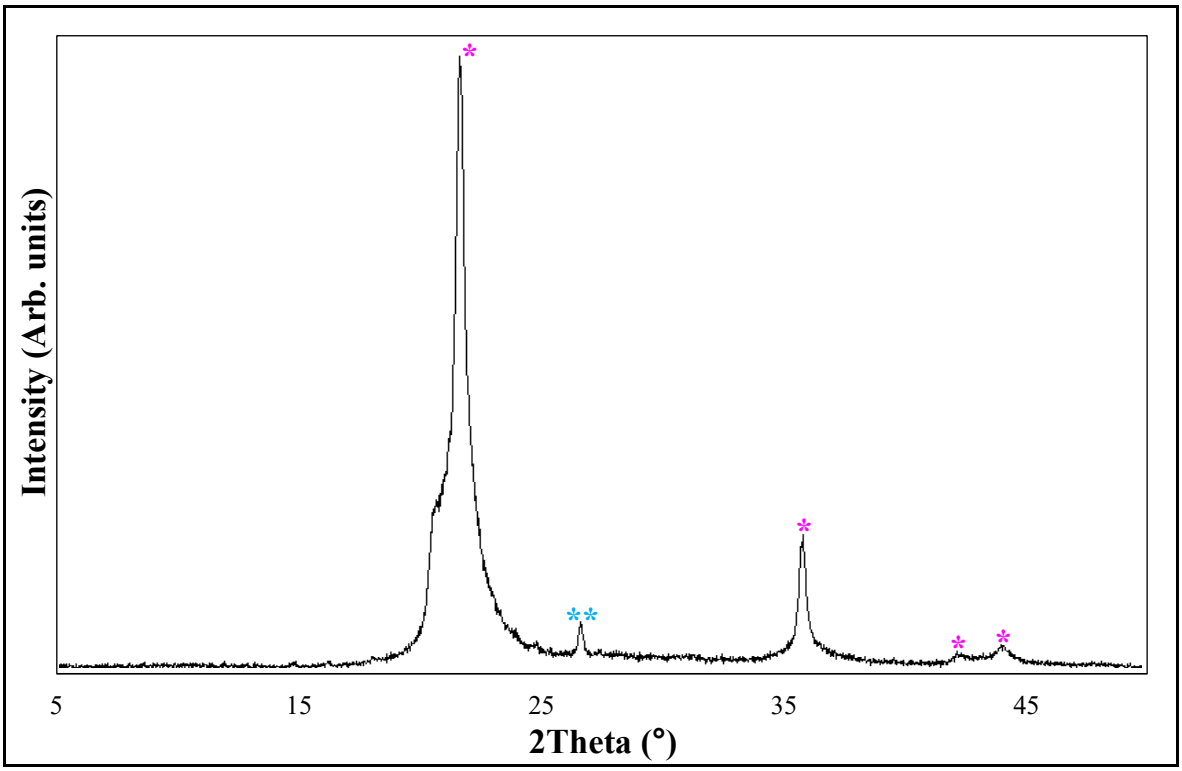

Fig. 3.45. Results of the qualitative XRPD analysis done on the diffraction pattern taken for the synthesized material, at room temperature. * in pink = cristobalite diffraction peaks; ** in light blue = quartz diffraction peak.

The concentration of methylamine and the ratio between chemically purified water and TEOS could have influence on the temperature of crystallization of melanophlogite, but further tests of synthesis in autoclave are required to validate that.

XRPD have shown that silica polymorphs stable at higher temperature, i.e. cristobalite and quartz, have crystallized instead of melanophlogite, suggesting that the synthesis in autoclave have been done correctly, but at too high temperature. In fact, the synthesized material has revealed itself to be crystalline, and not amorphous, and this aspect leads to think that the synthesis in autoclave has been well organized. However, it is necessary to define accurately the thermal range in which the process of crystallization of melanophlogite occurs.

4. DISCUSSION

4.1 PHASE TRANSITIONS IN MELANOPHLOGITE

The synchrotron radiation diffractions showed clearly split peaks at temperature below 60 °C. Moreover, further split occurs at lower temperature (i.e. –30 °C), so that single peaks in the higher symmetry become a triplet at temperatures lower than –30 °C. This was interpreted as an evidence of the occurrence of at least two phase transitions: from cubic to orthorhombic, and from orthorhombic to monoclinic structures, considering a decreasing temperature.

The transition from cubic to lower symmetry favours the unit cell volume contraction, and changes the thermal expansion coefficient. Below 200 °C almost no weight loss, hence, guest phase loss, is observed. Therefore, we ascribe changes in the thermal expansion and/or phase transition, to a contribution different from the loss of guest molecules. At about 60°C we find a difference in thermal expansion: for melanophlogite from Fortullino, the thermal expansion coefficient $\alpha = 1/V_{25}(\partial V/\partial T)$ is $7.2(1.4)\times10^{-5}$, between 25 and 60 °C, and $3.1(2)\times10^{-5}$, between 60 and 200 °C. A similar result can be obtained from the thermal expansion in melanophlogite from Mt. Hamilton: Nakagawa *et al.* (2005) have found $\alpha = 7.8(1.2)\times10^{-5}$ and $3.3(4)\times10^{-5}$, respectively below and above 60 °C. The same change in slope at the lower temperature was also observed in a degassed sample from Fortullino by Liu *et al.* (1997). Nakagawa *et al.* (2005) related the turning point at 60 °C to a phase transition from tetragonal to cubic symmetry, occurring with a slight unit cell distortion together with a cell doubling of a_0 and b_0. Also Fyfe & Gies (1990) and Liu *et al.* (1997) observed the transition by their ^{29}Si NMR data, which show a substantial involvement of the framework tetrahedra; Liu *et al.* (1997) suggested that the low symmetry phase is orthorhombic. Here, our synchrotron radiation diffraction data suggest that the lower temperature phase is orthorhombic, or, if of lower symmetry, this could hardly be detected for the very low deviations from the orthorhombic lattice close to the transition. It is not clear whether the different symmetry of the lower phase was misinterpreted, due to the very small structural changes involved, or it is real and somehow related to the different guest molecules in the different melanophlogite samples. Still, the presence of the transition at 60 °C is unambiguously determined in several melanophlogite samples from different localities. Likely, the higher temperature transformation has a counterpart at 1.2 GPa (Tribaudino *et al*, 2010; Gatta *et al.*, 2014).

The higher temperature phase transition was revealed also in DSC runs: a step in the calorimetric profile is observed at 80 and 60 °C, for samples from Fortullino and Racalmuto. There is a difference between the 60 and 80 °C transition temperatures from the unit cell and DSC runs for melanophlogite from Fortullino. Such difference may be explained by the rather complex nature of this phase transition, which would be purely ferroelastic. As shown by this work and previous single crystal investigations at room conditions, in melanophlogite the transitions occurs by the formation of superstructural reflections, doubling the a_0 and b_0 parameters in the tetragonal refinements by Nakagawa *et al.* (2001). Although the exact nature of the unit cell axis doubling is not clear, there is a suggestion that it involves some kind of rearrangement in the guest phases. As it is, the two processes, cell distortion and axis doubling, may occur separately, and the DSC might reveal mostly changes in the encaged molecules beginning at slightly higher temperature.

DSC have shown clearly the presence of another phase transition at about –30 °C, found in natural Fortullino and in synthetic melanophlogite. To our knowledge, this is the first time such low temperature transition is observed. A lower temperature monoclinic or triclinic structure for melanophlogite was suggested by quantum mechanical calculation in guest–free melanophlogite by Liang *et al*. (2011), but never experimentally verified. It is not clear whether this second transition is present in any melanophlogite. In a calorimetric analysis by Geiger *et al*. (2008) the authors did not find evidence of a discontinuity in heat capacity at about –25 °C in guest–free melanophlogite, and in those from Mt. Hamilton and Racalmuto. However, in guest–bearing Racalmuto melanophlogite, the authors found a higher rate of increase in heat capacity at temperatures higher than –25 °C (Geiger *et al.*, 2008).

Unfortunately, we did not have enough sample of melanophlogite from Racalmuto to perform low temperature DSC analysis.

The energetics involved are rather different for the two transitions. In the transformation at higher temperature, we have a continuous change, with very little endothermic behavior, and no peak in calorimetric analysis. In the second transformation, at lower temperature we have a sharp peak in the heat flow, with double dip.

Our accurate low temperature data obtained by synchrotron radiation can provide further evidence to characterize these transitions, via an analysis of the spontaneous strain.

The spontaneous strain is the deformation in the unit cell due to the transition, which sums to that related to thermal expansion.

It is physically described by a second–order tensor (Carpenter *et al.*, 1998). In cubic–to–orthorhombic ferroelastic phase transitions, only the diagonal terms of the tensor differ from zero (ε_{11}, ε_{22} and ε_{33}).

The diagonal terms are calculated from the cell parameters at each temperature in the low symmetry orthorhombic phase (a_{orth}, b_{orth} and c_{orth}) with respect to those that the cubic phase would have at the same temperature [$\varepsilon_{11} = (a_{orth} - a_{cub})/a_{cub}$; $\varepsilon_{22} = (b_{orth} - b_{cub})/b_{cub}$; $\varepsilon_{33} = (c_{orth} - c_{cub})/c_{cub}$]. In the transition to the monoclinic symmetry, the tensor acquires an off–diagonal term, ε_{13} (Schlenker, 1978).

An overall scalar spontaneous strain can be calculated as $\varepsilon_{ss} = (\varepsilon_1^2 + \varepsilon_2^2 + \varepsilon_3^2)^{1/2}$, with ε_1, ε_2 and ε_3 corresponding to ε_{11}, ε_{22} and ε_{33} in the transition to orthorhombic, or to the diagonalized components in the transition to monoclinic. A volume strain can be calculated as $V_s = (V - V_0)/V_0$, to show whether the transition occurs without a change in unit cell volume, i.e. for pure shear, or some further deformation occurs. Volume strain likely has a bearing in this investigation: an issue from the above data was that the overall thermal expansion decreases with temperature, contrary to the expectation of an increase, mostly at lower temperature. The significant contraction related to significant volume strain for phase transitions explains the anomalous thermal expansion.

In practice, the spontaneous strain is assessed from the extrapolated high temperature unit cell (here, the cubic one) and that at a given temperature (Ohashi & Burnham, 1973).

Therefore, a linear fit was done from the cubic unit cell data between 67 and 87 °C. The fit was then extrapolated to lower temperature, to provide a cubic reference unit cell for lower temperature melanophlogite. The strain at each temperature was assessed from the Winstrain program (Angel, 2003), comparing the measured unit cell with the reference cubic at the temperature.

The spontaneous strain tensor shows three in orthorhombic and four in monoclinic symmetry independent components, which are shown in Fig. 4.1. The volume strain was also calculated from the measured and cubic extrapolated volumes.

As shown in Fig. 4.1, the scalar spontaneous strain shows three well defined regions, one corresponding to the orthorhombic structure between –25 and 67 °C, the other two in the monoclinic field, between –125 and –25 °C, and the third at lower temperature. The turnover at –25 °C corresponds to the temperature of the peak in DSC, giving further confirmation of the phase transition to the monoclinic structure. A possible further phase transition at –125 °C is revealed by further changes in unit cell parameters and volume strain. The rather complex

picture shows that different processes, possibly coupled, act to modify the crystal structure of melanophlogite.

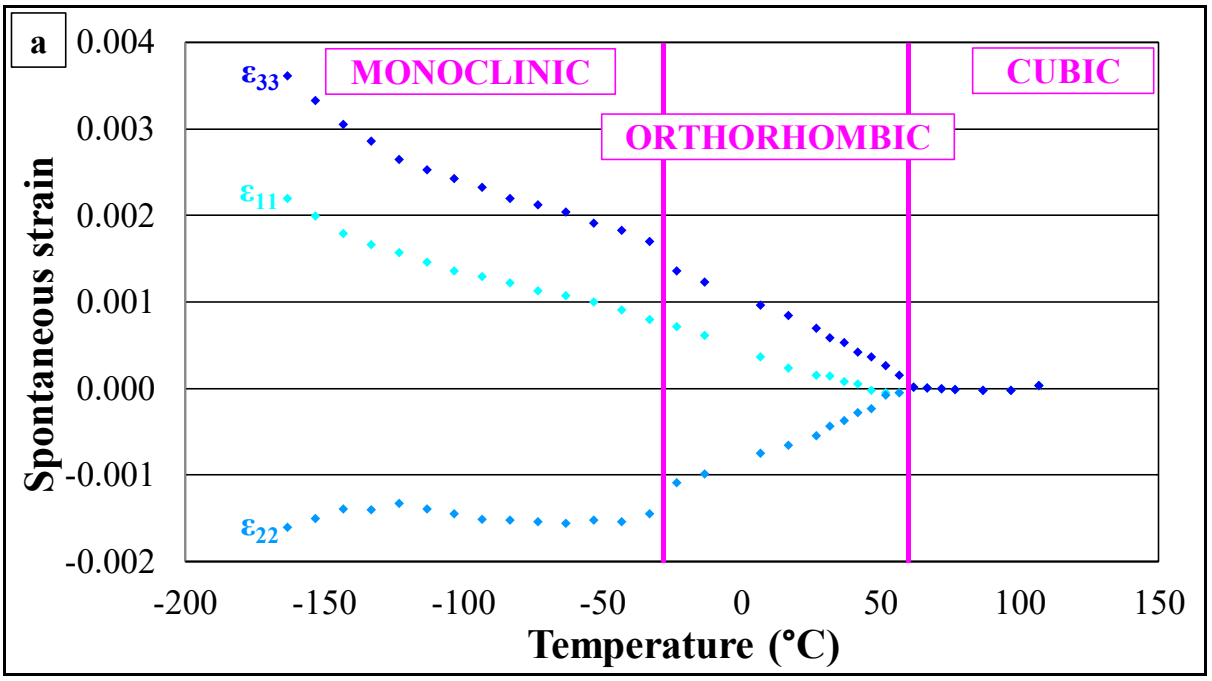

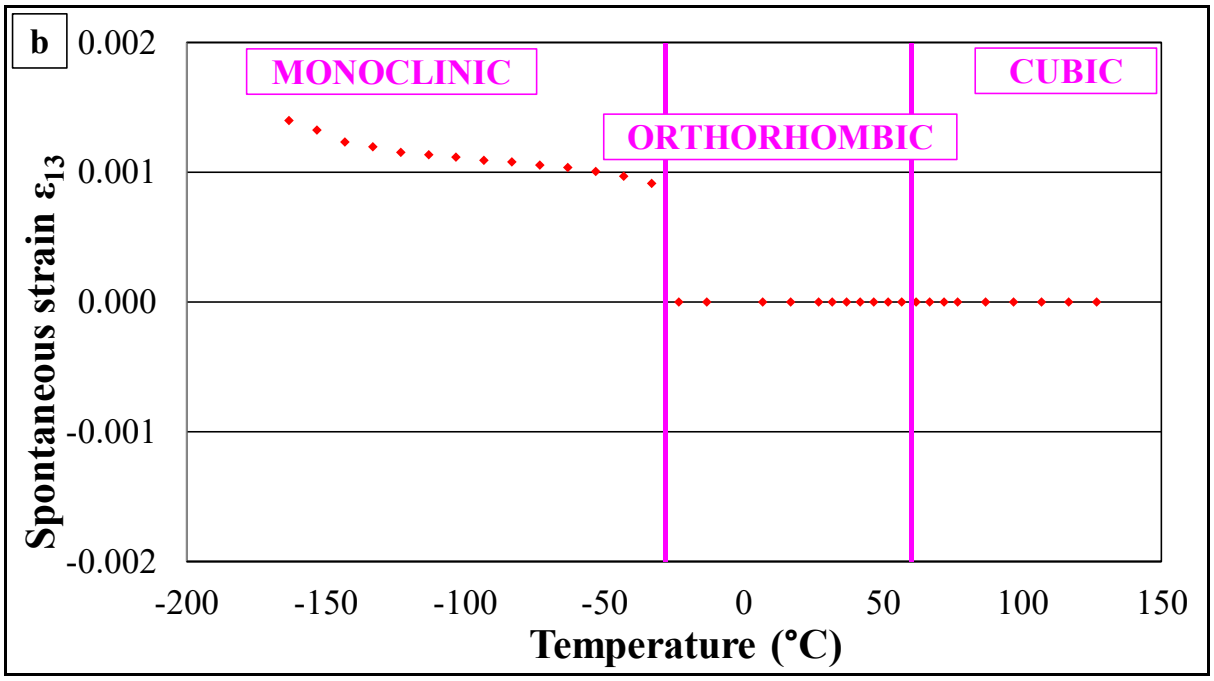

In the orthorhombic region, the strain increases continuously, so as the three diagonal components. The volume strain at the lower orthorhombic condition, i.e. at –25 °C is about 0.10 %, whereas it becomes 0.44 % at –163 °C. The spontaneous strain at –25 °C is just a bit higher, 0.18 %, showing that volume strain pays an important contribution to the transition.

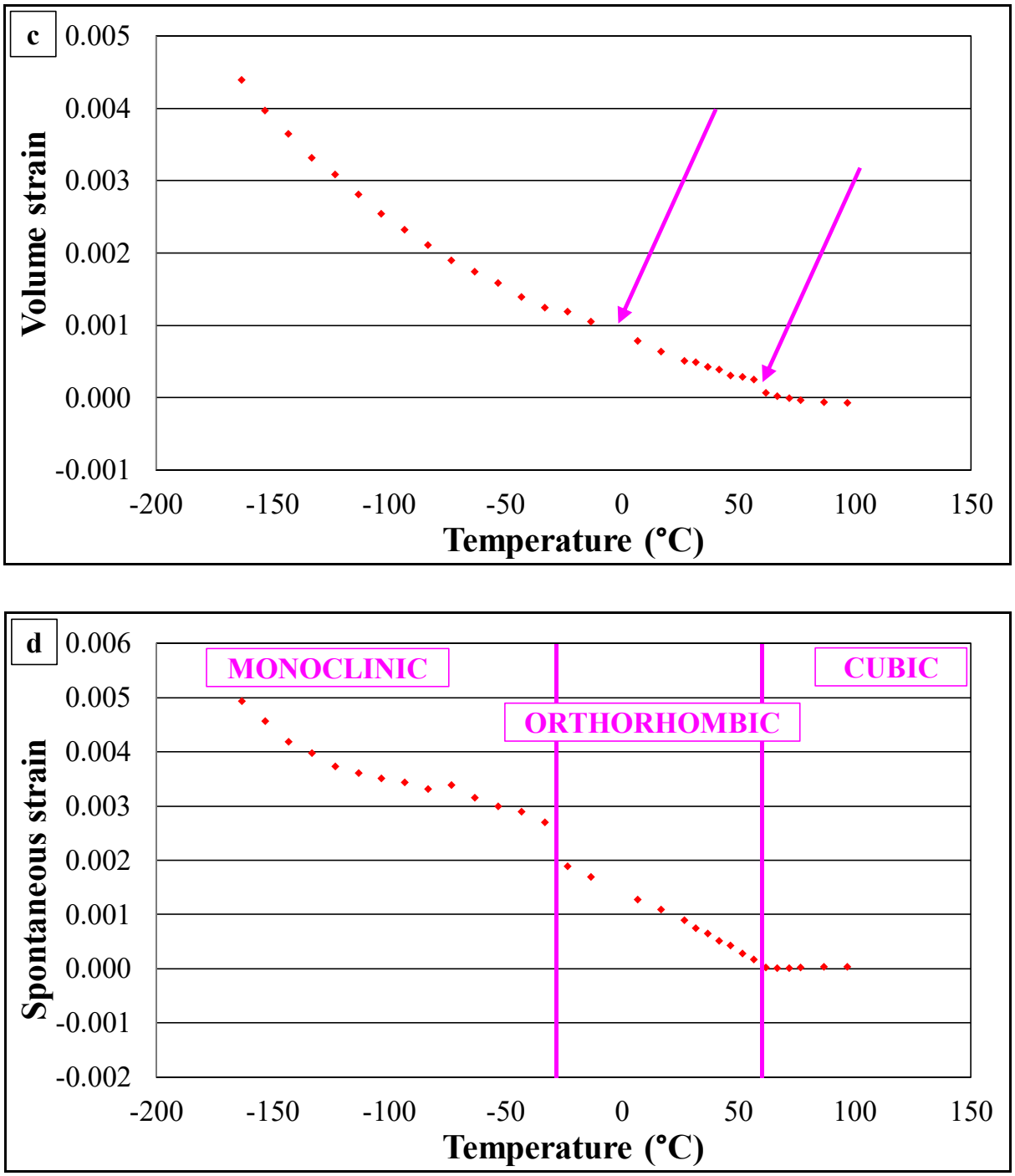

Figure 4.1. (a) and (b): components of the spontaneous strain; (c) the volume strain; (d) the spontaneous strain, calculated from a cubic reference.

At temperatures lower than –25 °C two of the tensor components change little, whereas ε_{22} stops its decrease. Moreover, at –25 °C the ε_{13} component appears, with a step at the transition, but changes little at lower temperature. At temperatures lower than –125 °C, the ε_{11} and ε_{33} components change their slope whereas ε_{22} decreases somewhat. Further analysis of the lower temperature behaviour is hindered by the lack of a low temperature structural model.

To relate the spontaneous strain data with an order parameter to describe the thermodynamics of the transitions one should consider that the cubic to lower temperature phase is marked by the appearance of critical cell doubling reflections, together with the above deviation from the isometry. These reflections were always found in any XRD at room temperature, either in the synthetic or natural samples. They disappear in the cubic phase (Žák, 1972; Gies, 1983). As discussed in Tribaudino *et al.* (2008), it is not obvious that cell doubling and deformation processes act together, although some kind of coupling may be present.

As discussed above, the unit cell from powder diffraction were refined in the unit cell at 13 Å, without taking into account the cell doubling. In fact, cell doubling reflections could not be observed even in synchrotron radiation runs. Here we have the contribution related to the transformation of the unit cell, i.e. by the deformation of the framework, no matter for the involved structural feature.

The deviation modeled from the lattice parameters through the analysis of the spontaneous strain is related to the order parameter of a phase transition as $\varepsilon_{ss} \propto Q$ in a zone center phase, or $\varepsilon_{ss} \propto Q^2$ in a zone boundary transition. The excess free energy of a phase transition with temperature is expressed as a function of the order parameter as:

$$G = (1/2)\, a(T - T_c)Q^2 + (1/4)\, bQ^4 + (1/6)\, cQ^6 \quad (1)$$

which represents the standard 2–4–6 Landau potential, where a, b and c are the Landau coefficients, and T_c is the critical temperture at which the transition takes place. At equilibrium:

$$\Delta G/\partial Q = 0 = a(T - T_c)Q + bQ^3 + cQ^5 \quad (2)$$

and:

$$T = T_c - (b/a)Q^2 - (c/a)Q^4 \text{ or } T = T_c - AQ^2 - BQ^4 \quad (3)$$

The order of the transition can be obtained by the value of the A term. In a *T*–induced transition in which the critical temperature is higher than the temperature of the low-symmetry phase, the A switches from negative in first– to positive in second–order transitions, respectively. In the case of a null quadratic term, the transition is tricritical.

Here the higher temperature phase transition will be investigated. In this transition, we have that together with unit cell distortion a cell doubling occurs, hence a zone boundary transition. Cell distortion could then be modeled via $\varepsilon_{ss} \propto Q^2$. From (3), it comes:

$$T = T_c - A\varepsilon_{ss} - B\varepsilon_{ss}^2 \quad (4)$$

The A, B and T_c can be fitted from the experimental spontaneous strain, as:

$$T = 337.7(8) - 40(2)*10^3*\varepsilon_{ss} - 29(11)*10^5*\varepsilon_{ss}^2$$

The transition shows therefore a second–order character and a T_c = 65 °C, R^2 = 0.998. The behavior differs only trivially from a linear fit (R^2 = 0.997, T_c = 67 °C). This optimum fit could be obtained only assuming that $\varepsilon_{ss} \propto Q^2$: if $\varepsilon_{ss} \propto Q$, i.e. assuming a zone center transition, a reliable fit would not be obtained (R^2 = 0.93 forcing a linear fit), confirming that unit cell distortion is related to the cell doubling. A second–order character was also found examining the results from melanophlogite from Mt. Hamilton by Nakagawa *et al.* (2005), and in Tribaudino *et al.* (2010).

Instead, the lack of a suitable structural model hinders an investigation of the second and possibly third phase transitions at –25 and –125 °C. However, the clear step observed in the ε_{13} and ε_{22} components of the strain tensor, as well as the calorimetric data, prompt for a first–order transition at –25 °C.

A similar series of phase transitions was found in $NaTaO_3$ perovskite (Darlington & Knight, 1999) and lawsonite (Carpenter *et al.*, 2003).

4.2 DEGASSING IN MELANOPHLOGITE

The TGA on the sample from Fortullino has shown a detailed picture of the degassing process. The degassing begins at rather low temperature, about 200 °C, but it is not complete even after the end of the first run at 1000 °C. The rate of the degassing increases at temperatures higher than 500 °C. Our experiments suggest that CO_2 has different degassing kinetics depending on temperature. A similar behaviour was found in a silica clathrasil with dodecasil 1H cages (van der Donk *et al.*, 2008), in which the TGA shows that the gas loss begins readily, at 100–200 °C, and at 600–700 °C the loss becomes faster. In the synthesized sample, a higher degassing by 1 wt.% occurs below 200 °C, and the degassing becomes faster at temperature in excess of 600 °C. Contrarily to the natural sample, in the synthetic one at 800 °C the degassing looks completed, but the weight loss suggests that the cages are only partially occupied.

The degassing has a significant effect also on the DSC and possibly XRPD. The DSC measurements carried out on melanophlogite samples from Fortullino and Racalmuto have shown an endothermic behaviour, up to 200−250 °C, and a slightly exothermic behaviour, at higher temperature. The onset of the slightly exothermic behaviour at lower temperature begins at the same temperature of the onset of degassing, i.e. at 180−250 °C. To sum it up, in DSC, the onset of degassing is related to a switch from an increasingly endothermic

behaviour to one in which the heat flow changes little and is somewhat more exothermic, found also in zeolites, e.g. Seraj *et al.* (2016).

Powder diffraction data show in the sample from Fortullino, at temperatures higher than 200 °C, a continuous decrease in the thermal expansion, and at temperatures higher than 300 °C, almost no volume expansion. Quartz and/or cristobalite, which appeared at the end of the Raman runs by Likhacheva *et al.* (2018), but not in the study by Liu *et al.* (1997), were not observed even at the end of the runs, in excess of 1000°C. This could be related by some difference in our powdered samples with respect to Likhacheva *et al.* (2018). Skinner & Appleman (1963) noted that applied stress (such as grinding) resulted in the formation of quartz. Kanzaki (in prep.) has suggested that exact reverting temperature might depend on specific states (i.e. grain size and grinding) of each melanophlogite sample.

DSC, HT–XRPD and TGA data collected for melanophlogite from Fortullino are compared in Fig. 4.2.

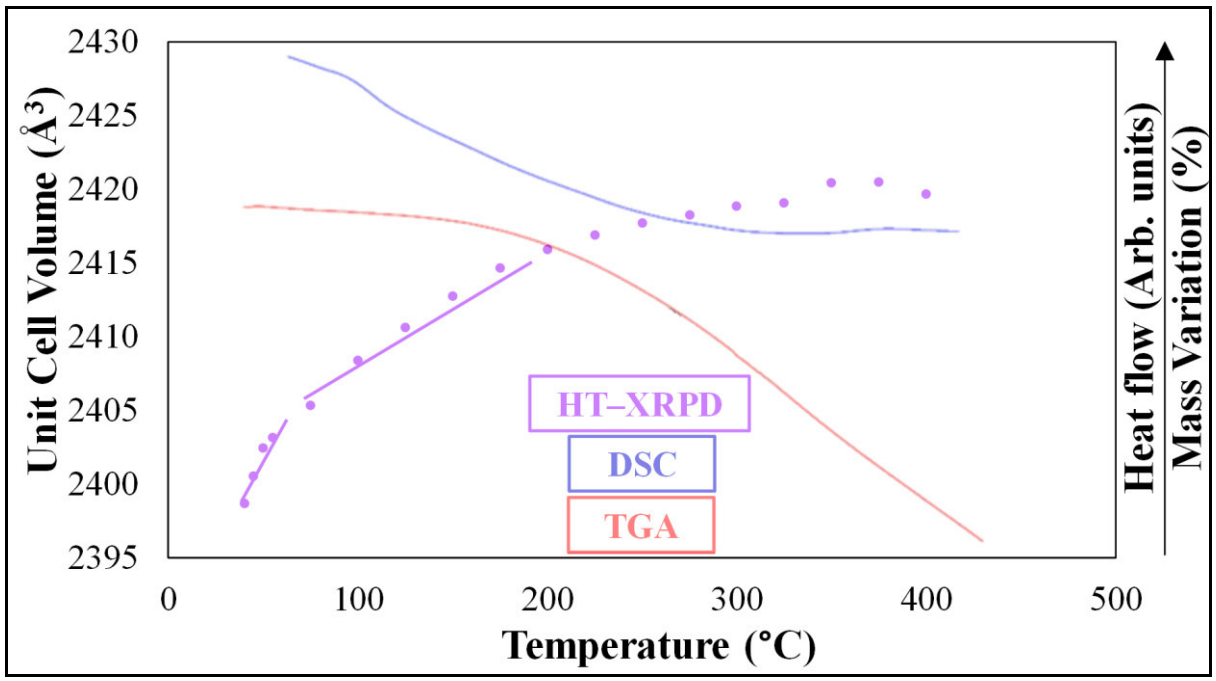

Figure 4.2. HT–XRPD, DSC, and TGA experimental data collected for melanophlogite from Fortullino.

It appears that DSC and TGA show a somewhat opposite behaviour: changing heat flow in DSC has a counterpart below 200 °C in a lack of mass variation, whereas a decrease in mass occurs without a change in the heat flow. The degassing involves the encaged molecules, which can be best studied by Raman spectroscopy. Although this was not done in this work, the Raman high temperature behaviour of melanophlogite from Mt. Hamilton was recently

studied by Likhacheva *et al.* (2018). The Raman data by Likhacheva *et al.* (2018) are crucial to clarify the faster degassing at temperatures higher than 500 °C. The authors have shown that the C–H bands blue–shift by about 3 cm^{-1} from room temperature to about 500 °C, whereas the shift stops upon further temperature increase. The interpretation of the blue–shift by Likhacheva *et al.* (2018) is that thermally–induced strengthening of the collisions between enclathrated CH_4 molecules and the cages walls leads to the decrease of the efficient C–H bond length and the corresponding increase of the C–H stretching frequency. In view of our results, this could be basically related to preliminary degassing, possibly with interaction between encaged species during molecular diffusion within the crystal. As diffusion further goes on, and the number of void increases, such interaction becomes less effective, and degassing may proceed to a faster rate. The slightly different thermogravimetric behaviour of the synthetic melanophlogite could be related to a partial occupancy in the cages.

The degassing affects also the silicate framework, which, in the absence of high temperature structural data, can be investigated by the evolution of the unit cell with temperature. A major feature is that the volume changes less during degassing. A framework crumpling was found, as the cages become empty, and the unit cell parameters after the degassing are smaller by 0.4 % (Liu *et al.*, 1997; Likhacheva *et al.*, 2018). However, extrapolating to 400 °C the volume between 60 and 200 °C, i.e. in the cubic range before degassing, the difference between the observed volume and the expected one is by about 0.8 %, i.e. more than what is observed by comparing empty and filled melanophlogite samples. Besides, cell parameters refined here before and after gas release did not show significant differences. A possible suggestion is that, together with some volume decrease induced by degassing, we have a differential thermal expansion at higher temperature, which should be visible also in the guest–free phase. This could be triggered by a phase transition at 200 °C, or, simply, the decreasing expansion at temperatures higher than 200 °C may indicate that the clathrate expansion has reached a limit, related to the lack of further tilt of the framework in melanophlogite structure. In guest–free melanophlogite, Liu *et al.* (1997) actually showed by ^{29}Si NMR that, between 60 and 200 °C, a number of different local tetrahedral configuration coexist, leading at 200 °C also at a local scale to the configuration which is expected for the high temperature cubic phase, i.e. one with only three different NMR peaks for the three different Si unique crystallographic sites. The authors interpreted this tentatively as a phase transition from *m*3 to *m*3*m* point group at about 200 °C, which could agree by group theory considerations, but this could be also come from disorder at a local level in an average cubic *m*3*m* symmetry. That is, long–range order in the cubic phase is achieved at about 60 °C, but at a local level a short–range order, locally

with *m*3 configurations, is present, and at a short–range level the symmetry would become *m*3*m* only at higher temperature, i.e. above 200 °C. In Raman spectra by Likhacheva *et al.* (2018), the main peak at 267 cm^{-1}, which is a peak related to framework vibrations, shows a different behaviour below and above 200 °C: above 200 °C the blue–shift stops, and for further heating the frequency of the peak does not change.

5. CONCLUSIONS AND APPLICATIONS TO EARTH SCIENCES

This work results show that melanophlogite, contrarily to previous indications, shows a significant degassing at relatively low temperature. However, full degassing occurs only at temperature higher than 1000°C, confirming the specific nature of melanophlogite as a clathrasil able to retain at least some encaged molecules up to higher temperature.

Synchrotron radiation data showed that the supposed low temperature tetragonal symmetry is not present in Fortullino melanophlogite, and an orthorhombic structure at room temperature is suggested instead.

Also, another phase transition, yet undiscovered, was found at about –25 °C.

This work results may pose some constrain to the geological conditions where melanophlogite is found.

The experimental results, combined to field observations, indicate that a narrow stability field and the lack of tectonic activity are necessary to promote the growth of melanophlogite and avoid its transformation to cristobalite and quartz.

At first, one must consider that melanophlogite in nature always has encaged molecules. Guest–free melanophlogite has never been found in nature, but an assemblage of quartz pseudomorphic on the cubic former melanophlogite has been found instead. In fact, melanophlogite becomes easily amorphous at very low stress (Skinner & Appleman, 1963), and it readily reacts at higher temperature to become cristobalite, or quartz. Guest–free melanophlogite can be obtained in laboratory, degassing the natural melanophlogite, but it is very sensitive to strain and likely to amorphize also at long–range. Xu *et al.* (1997) have shown that guest–free melanophlogite becomes amorphous by *in–situ* high pressure XRD analysis at about 8 GPa, whereas guest–bearing melanophlogite is still crystalline at 17 GPa (Yagi *et al.*, 2007; Tribaudino *et al.*, 2010; Liang *et al.*, 2011; Gatta *et al.*, 2014).

Natural melanophlogite occurs always in open veins. In Varano Marchesi and Racalmuto sites (Grassellini Troysi & Orlandi, 1972; Adorni & Tateo, 2007; Tribaudino *et al.*, 2008), together with melanophlogite, coexisting pseudomorphic quartz was found. Both melanophlogite and pseudomorphs are in the same geological setting, i.e. the obvious suggestion is that in pseudomorphic ones melanophlogite was crystallized with its guest molecules, and then degassing has occurred. Guest molecules behave as template agent and stabilize the mineral structure; their loss makes the mineral extremely reactive to amorphization or transition to other silica phases.

In all the localities of natural melanophlogite, the host rocks were subjected to temperature not higher than 200 °C, and degassing could have been promoted by longer stay at an increased temperature, or helped by some deformation of natural melanophlogite.

Also, the range of possible stability is rather narrow. A lower temperature limit to the formation of melanophlogite may be given by our synthesis results: melanophlogite crystallization required temperature in excess of 160 °C, but at higher temperature it readily became an assemblage of quartz and cristobalite. Moreover, the crystallization in a cubic morphology and the ubiquitous occurrence of transformation twinning indicate that natural and synthetic melanophlogite were all obtained in the stability field of the cubic polymorph, i.e. beyond 60–80°C. This brackets the temperature of formation of melanophlogite; moreover, to preserve the phase, no loss of gases by tectonic shear must have occurred. It is not therefore surprising that melanophlogite is a rare mineral.

As concerns potential applications, the synthesis done in this work provides the basis. It is still to verify the rate of exchange between melanophlogite and other species, so to obtain best filling and loss of the guest phases.

6. APPENDIX

6.1. POROUS SILICA STRUCTURES

In Table 6.1, the currently known pure silica materials of zeolite–type structures, representing approximately ~ 20 % of the known zeolite topologies, are reported.

PURE SILICA MATERIAL	FTC	SPACE GROUP	FD
SSZ–24	**AFI**	*P6/mcc*	16.9
Octadecasil	**AST**	*Fm–3m*	15.8
SSZ–55	**ATS**	*Cmcm*	16.1
Zeolite beta	***BEA**	$P4_122$	15.3
ITQ–14	**BEC**	$P4_2/mmc$	15.1
CIT–5	**CFI**	*Imma*	16.8
Chabazite	**CHA**	*R–3m*	15.1
Deca–dodecasil–3R	**DDR**	*R–3m*	17.9
Dodecasil–1H	**DOH**	*P6/mmm*	17.0
UTD–1	**DON**	*Cmcm*	17.1
UE–1	**EUO**	*Cmme*	17.1
Dealuminated zeolite–Y	**FAU**	*Fd–3m*	13.3
Ferrierite	**FER**	*Immm*	17.6
GUS–1	**GON**	*Cmmm*	17.7
SSZ–42, ITQ–4	**IFR**	*C2/m*	17.2
ITQ–32	**IHW**	*Cmce*	18.5
ITQ–7	**ISV**	$P4_2/mmc$	15.0
ITQ–3	**ITE**	*Cmcm*	15.7
ITQ–13	**ITH**	*Amm2*	17.4
ITQ–12	**ITW**	*C2/m*	17.7
ITQ–24	**IWR**	*Cmmm*	15.6
ITQ–29	**LTA**	*Pm–3m*	14.2
ZSM–11	**MEL**	*I–4m2*	17.4
Melanophlogite	**MEP**	*Pm–3n*	17.9
Silicalite, ZSM–5	**MFI**	*Pnma*	18.4
ZSM–48	***MRE**	*Imma*	19.7
MCM–35	**MTF**	*C2/m*	20.7
ZSM–39, dodecasil–3C, CF4	**MTN**	*Fd–3m*	17.2
ZSM–23	**MTT**	*Pmmm*	18.2
ZSM–12	**MTW**	*C2/m*	18.2
ITQ–1, MCM–22, SSZ–25	**MWW**	*P6/mmm*	15.9
Nonasil	**NON**	*Fmmm*	17.6
RUB–41	**RRO**	*P2/c*	17.9
RUB–3	**RTE**	*C2/m*	17.2
RUB–10	**RUT**	*C2/m*	18.1

RUB–24	**RWR**	*I*4$_1$/*amd*	19.2
SSZ–73	**SAS**	*I*4/*mmm*	14.9
Sigma–2	**SGT**	*I*4$_1$/*amd*	17.5
Sodalite	**SOD**	*Im*–3*m*	16.7
SSZ–35, ITQ–9, MU–26	**STF**	*C*2/*m*	16.9
SSZ–23	**STT**	*P*2$_1$/*n*	17.0
SSZ–74	**–SVR**	*Cc*	17.2
Theta–1	**TON**	*Cmcm*	18.1

Table 6.1. Pure silica zeolite–type structures: FTC is the acronym for "framework type code", and FD the one for "framework density" (Momma, 2014).

6.2. STRUCTURE AND PROPERTIES OF CLATHRASILS

6.2.1. STRUCTURE

Although the crystal structures of the clathrasils are well described on the basis of type of cages present inside them, another description of the structures based on periodic building units (also indicated as PerBUs) highlights different aspects of their structural similarities and provides an interesting insight into their crystal growth process (van Koningsveld & Gies, 2004). In the description based on type of cages, [5^{12}] is the most common kind in **DDR**, DD3H, **DOH**, **MEP**, and **MTN**. However, a set of "half–cages", or 12–ring double cups, made of thirty T–atoms and indicated as T30 units, is the smallest part of the PerBUs of the above–mentioned five framework topologies, and constitutes the bottoms of the cages, in which the structure–directing template molecules are entrapped. For instance, the [$5^{12}6^8$] in **DOH**, [$5^{12}6^4$] in **MTN**, [$4^3 5^{12} 6^1 8^3$] in **DDR** and DD3H, [$5^{18} 6^2 8^3$] and [$5^{15} 6^1 7^3$] in DD3H and [$5^{12}6^2$] in **MEP**. T30 units can be connected into two types of layers: PerBU1 and PerBU2, in which the T30–units form a pseudo–hexagonal layer and an orthogonal layer, respectively. The "extended" PerBU1 and PerBU2 are obtained by addition of T6–rings connected to them. Neighbouring PerBU1s can be connected via oxygen bridges along the normal to the layers in three ways: (1) AB (or BC or CA) sequence with + (2/3a + 1/3b) shift; (2) AC (or CB or BA) sequence with – (2/3a + 1/3b) shift; (3) AA (or BB or CC) sequence with no lateral shift. The **DOH** and **MTN** framework topologies are obtained via AA and ABC stacking of the PerBU1, respectively. The extended PerBU1s can be connected in three further sequences: (1) AB (or BC or CA); (2) AC (or CB or BA); (3) AA (or BB or CC). The **DDR** structure is obtained via ABC stacking of the extended PerBU1, and the DD3H structure is obtained

through AAB stacking. The only previously known connection mode of orthogonal PerBU is that of extended PerBU2s with no lateral shift. The resulting framework structure is the cubic **MEP**.

The fact that these clathrasils are constructed from the same T30 unit, which is the cage region where the SDAs are entrapped, indicates that such half–open cups provide a site for interactions with SDA. Moreover, the T30 unit generates new speculations concerning precursors in solution. Although many intermediate sequences, in which the stacking sequence has a long periodicity or repeats in a disordered manner, are theoretically possible, no such "intermediate" materials are reported. Therefore, the size and the shape of the organic guest molecules represent the structure–directing force, leading to the specific framework structure types and preventing stacking disorder from occurring (van Koningsveld & Gies, 2004). This structure–directing influence of the clathrasil templates is different from what is known for zeolites with channel–type voids, such as zeolite beta (***BEA**) and NU–86, which are only known to occur as disordered frameworks.

6.2.2. THERMODYNAMIC PROPERTIES

Zeolitic pure silica materials are metastable with respect to α–quartz, the thermodynamically stable phase at ambient conditions (Momma, 2014).

Experimentally, the entropy differences between the various crystalline siliceous polymorphs and α–quartz are known to be small and span a narrow range (Navrotsky *et al.*, 2009).

Petrovic *et al.* (1993) have been calculated the formation enthalpy of the high–silica zeolites ZSM–5 (**MFI**), ZSM–11 (**MEL**), ZSM–12 (**MTW**), and SSZ–24 (**AFI**) and of cubic and hexagonal symmetries of faujasite (**FAU**), determining that the energy range in the above–mentioned silica zeolites is quite narrow (7–14 kJ mol^{-1} above quartz).

Piccione *et al.* (2000) have considered a larger range of materials (**AST**, ***BEA**, **CFI**, **CHA**, **IFR**, **ISV**, **ITE**, **MEL**, **MFI**, **MWW**, and **STT**), obtaining a similar range of energies (6.8–14.4 kJ mol^{-1} above quartz).

The excess enthalpies of the silica zeolites with respect to α–quartz are comparable to that of silica glass, with values of ~ 9 kJ mol^{-1} above quartz (Richet *et al.*, 1982).

Because amorphous silicas derived from gels are higher in energy than fused glass by 0–10 kJ mol^{-1}, silica zeolites and amorphous silicas occupy an overlapping energy (Navrotsky *et al.*, 2009).

In Fig. 6.1, the trend of formation enthalpies among zeolitic silica phases, mesoporous silica, and aluminophosphates is shown.

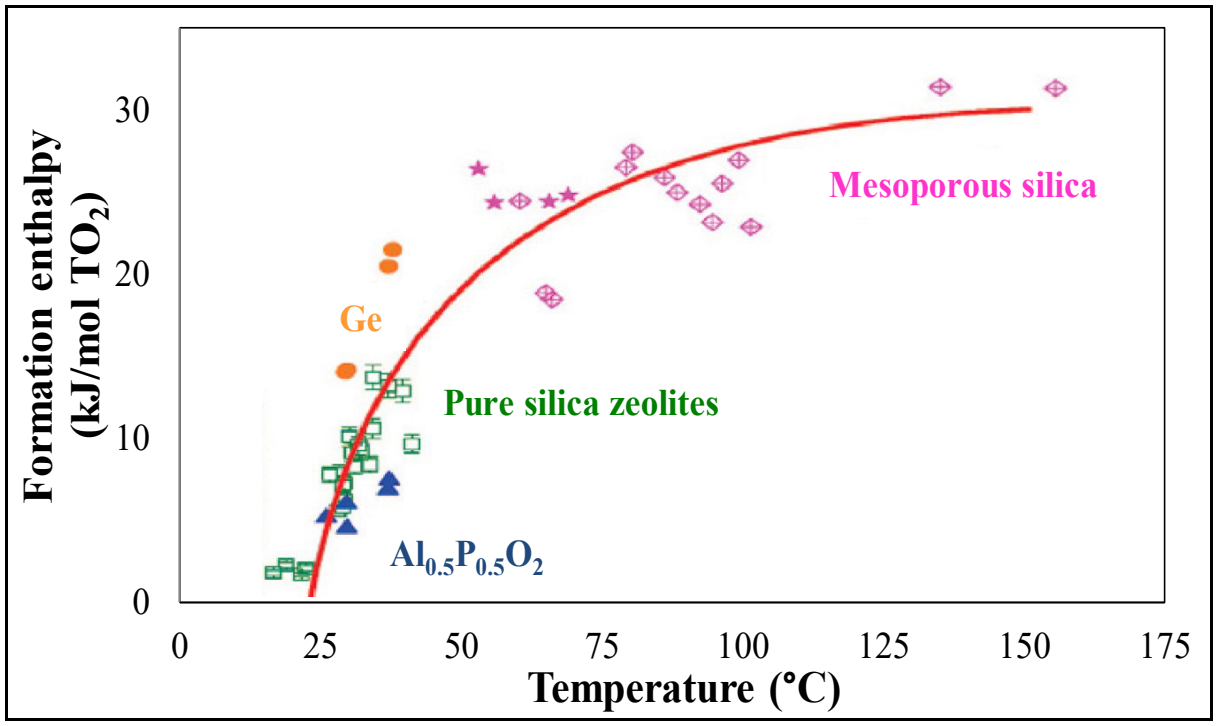

Figure 6.1. Formation enthalpies for silica zeolites, Ge and Al phosphate zeotypes, and mesoporous silica: green symbols, dense and zeolitic silica phases; blue symbols, aluminophosphates; orange symbols, Ge–zeolites; magenta symbols, cubic and hexagonal mesoporous silica, marked with stars and diamonds respectively (Navrotsky *et al.*, 2009).

Considering a larger energy scale, the formation enthalpy relative to α–quartz increases with increasing molar volume but seems to reach an upper limit at values close to 30 kJ mol^{-1}.

On the contrary, on a finer scale, the energy seems to be not correlated to the molar volume, and this suggests that complex interactions among different factors of the framework structure affect the framework stability. The presence of strained rings can contribute to the excess energy. For instance, the formation enthalpy for **MEI** is ~ 3 kJ mol^{-1} higher than that of **EMT**, despite of similar values for the molar volume of the two above–mentioned framework topologies: the former has three–membered rings, the latter does not. On the contrary, **FAU** has enthalpy and molar volume values similar to those of **MEI** but does not have three–membered rings.

Bushuev & Sastre (2010) have done a comprehensive computational study on the energetics of pure silica zeolites, considering all the topologies in the IZA database known at that time and reproducing experimental enthalpies of pure silica zeolites with respect to quartz.

Based on statistical distributions of thermodynamic properties, the upper energetic limit for synthesized pure silica zeolites has been proposed to be ~ 16 kJ mol^{-1} SiO_2 above α–quartz, and the densities of excess energy of pure zeolites lie in the region where $\Delta E/V < 0.5$ kJ cm^{-3}. Contributions of van der Waals and three–body O–Si–O interactions to the excess energies have been found to be significant. On the contrary, the three body Si–O–Si and electrostatic interactions play more significant roles in the stability of zeolites. The van der Waals, three–body O–Si–O and Si–O–Si interactions seem to be independent of molar volume because of short–range nature of these interactions. On the other hand, the excess energies from long–range electrostatic interactions tend to increase with molar volumes, and this tendency qualitatively explains the large–scale trend of formation enthalpy versus molar volumes (Fig. 6.1).

Piccione *et al.* (2001) have reported entropies of pure silica zeolites of ***BEA**–, **FAU**–, **MFI**–, and **MTT**–types, using heat capacity measurements obtained from an adiabatic calorimetry. The entropies of the transition to quartz at room temperature span a very narrow range of (3.2 ÷ 4.2) J K^{-1} mol^{-1} above quartz, despite a difference in the molar volumes of **FAU** and quartz of a factor two. Thus, the entropy contribution to the overall thermodynamics of SiO_2 phase transformations is much smaller than the enthalpy contribution. The entropies vary linearly with the molar volume for dense siliceous polymorphs, on the contrary achieve a constant value of (45.1 ± 0.7) J K^{-1} mol^{-1} for silica zeolites. The small entropy differences of the different silica frameworks reflect the strong tetrahedral bonding in the framework.

The heat capacities of ***BEA**–, **FAU**–, **MFI**–, and **MTT**, ranging from –260 to 125 °C, have been reported by Boerio–Goates *et al.* (2002) in detail.

The heat capacities of three of the polymorphs (**FAU**, **MFI**, and **MTT**) are greater than that of quartz over the entire temperature region of study, while that of ***BEA** drops below that of quartz for temperatures higher than –35 °C. In addition, the excess heat capacity of all four polymorphs relative to quartz is greater than that exhibited by amorphous silica for temperatures lower than –75 °C.

Because amorphous forms of a substance have higher heat capacities at low temperature than their crystalline counterparts, this result is unexpected and remains unsolved.

6.2.3. POTENTIAL TECHNOLOGICAL APPLICATIONS

6.2.3.1. GAS STORAGE

Two promising applications of clathrasils are gas storage and use as membranes for gas separations. Because of the small windows characteristic of their frameworks (respect to the larger ones in zeolites), only the small pentagondodecahedral [5^{12}] cages can allow diffusion fast enough in the clathrasil frameworks, thinking about potential practical applications. The relatively high densities of some aluminosilicates make them less practical for on–board hydrogen storage, and consequently promote the development of zeolite–like materials with higher Si/Al ratios. Anyway, they remain attractive to scientists for their potential and the well–characterized framework structures, analogous to some other candidates of hydrogen storage, such as clathrate hydrates and metal–organic frameworks (MOFs) (Langmi *et al.*, 2003; Vitillo *et al.*, 2005; Dong *et al.*, 2007; Jhung *et al.*, 2007; van den Berg *et al.*, 2007).

From molecular dynamics simulations, a window of clathrasil cages larger than six–membered rings is permeable to H_2 (van den Berg *et al.*, 2004 (a)). In both volume and window size, the [5^{12}] cage is very important for the purpose of trapping H_2 at ambient conditions. The H_2–containing **DDR**–type clathrasil, DD3R, has been synthesized at 180 °C in the presence of 50 bar of gaseous hydrogen, and a concentration of 0.8 ± 0.1 H_2 molecules per [5^{12}] cages of DD3R has been determined by means of PGAA and ^{1}H MAS NMR spectroscopy (van den Berg *et al.*, 2007). The hydrogen storage capacity (0.2 wt.%) should be improved by increasing the concentration of [5^{12}] cages in the framework topology, although the H_2 in the [5^{12}] cages has been released only above 825 °C. For improving the hydrogen capacity of zeolites, a large volume of micropores and a suitable diameter near the kinetic diameter of a hydrogen molecule are important (Dong *et al.*, 2007). Classical molecular mechanics simulations on hydrogen storage capacities of twelve pure silica zeolites has shown that flexible non–pentasils **RHO**, **FAU**, **KFI**, **LTA** and **CHA** display the highest maximal capacities, ranging from 2.86 to 2.65 mass %, which correlate well with the experimental results obtained at low temperature (Vitillo *et al.*, 2005). For **FAU**–, **MFI**– and **MOR**–type zeolites with similar Al concentration, hydrogen adsorption capacity, isosteric heat of adsorption, surface coverage, and micropore occupancy have been reported to increase in the order of **FAU** < **MFI** < **MOR** (Jhung *et al.*, 2007). Irrespective of the framework structure, the adsorption capacity, heat of adsorption, surface coverage, and micropore

occupancy of these three zeolites increase with increasing Al content of zeolites. These results suggest that the ideal zeolite for an efficient hydrogen storage material is one with a high electrostatic field and narrow pores without intersections. At low H_2 pressure, hydrogen adsorption capacities have been reported to correlate with the isosteric heat of adsorption (Frost *et al.*, 2006), which reflects the interaction energy between hydrogen and host materials. The heat of adsorption of the above–mentioned **FAU**–, **MFI**– and **MOR**–type of zeolites is roughly in the order of 6–7 kJ mol^{-1} when the adsorbed amount is 40 mL g^{-1} , and when adsorbed amount is smaller, it ranges up to 11.7 kJ mol^{-1} (Jhung *et al.*, 2007). These values are comparable to other candidates of hydrogen storage, such as MOFs (Dincă *et al.*, 2006; Frost *et al.*, 2006) and carbon materials (Yang *et al.*, 2007).

6.2.3.2. MEMBRANES FOR GAS SEPARATION

The permeation and separation of gas mixtures through zeolitic membranes are controlled via balancing the effects of adsorption and diffusion in micropores. For instance, Dong *et al.* (2000) have studied the gas permeation selectivity between hydrogen and light hydrocarbons (C_1–C_4) with all–silica **MFI** zeolite (silicalite) membranes at 25–500 °C and feed pressures of 0.1–0.4 MPa. At temperatures lower than 100 °C, the membrane have shown excellent separation properties, prohibiting the permeation of hydrogen and increasing the permeance of hydrocarbons with increasing molecular masses. This behaviour is due to the increasing adsorption strength of the component in the hydrophobic silicalite with increasing molecular mass, and the permeation is primarily determined by preferential adsorption at these temperatures. At 500 °C, the membrane becomes permselective for hydrogen and smaller hydrocarbons because diffusion in the pores controls the permeance and the preferential adsorption effect is negligible at such a high temperature.

Hydrogen production from fossil fuels involves the separation of H_2 from small molecules, such as CH_4, CO_2, CO, H_2O, and H_2S at high temperature, at which permeation is controlled by diffusion, and zeolitic membranes can selectively permeate and separate H_2 from these small molecules (Dong *et al.*, 2008). Clathrasils and pure silica zeolites have the advantage of high thermal stability, whereas zeolites with low Si/Al ratios are generally unsuitable for operating at high temperatures and moist atmospheres. The **MFI**– and **DDR**–types of high–silica zeolites have been extensively studied for H_2 separation (Burggraaf *et al.*, 1998; Dong *et al.*, 2000; Algieri *et al.*, 2003; Min *et al.*, 2003; Hong *et al.*, 2005; Dong *et al.*, 2008; Kanezashi *et al.*, 2008; Zheng *et al.*, 2008). Clathrasils with six–membered rings as their

largest openings, such as **SOD**, **MTN**, and **DOH**, are also considered as promising candidates for hydrogen storage and purification. For the diffusion of H_2 to occur through six–membered rings, framework flexibility is very important because it allows the ring to adapt to the hydrogen passage (van den Berg *et al.*, 2004 (b)). The self–diffusion of H_2 in pure silica **MTN** and **SOD** by means of molecular dynamics simulations was previously investigated (van den Berg *et al.*, 2005). The H_2 diffusion rate in **MTN** has been found to be considerably lower than that in **SOD**. Although the flexibilities of the **MTN** and **SOD** frameworks do not differ greatly and their activation energies are roughly equal, it was suggested that a large cage volume leads to a lower diffusion rate because of a smaller chance of finding hydrogen molecules near the cage's six–membered rings.

The removal and recovery of CO_2 from fuel and natural gases are of great interest because CO_2 is the main component of greenhouse gases. The hydrophobicity of high–silica zeolites offers an advantage of retaining their adsorption capacity in water. The all–silica **DDR** has high selectivity of adsorption for CO_2 over CH_4 (Himeno *et al.*, 2007; van den Bergh *et al.*, 2008). Molecular simulations on pure silica zeolites have indicated that **CHA** and **DDR** yield the best permeation selectivities among twelve zeolite topologies for the separation of CO_2 and CH_4 (Krishna & van Baten, 2007). **MFI**, **LTA**, and **DDR** exhibited high separation performances of CO_2/N_2 and CH_4/N_2, comparable to those of MOFs (Liu & Smit, 2009). **DDR** has been also reported to be a very effective molecular sieve for the separation or purification of propane–propene mixtures (Gascon *et al.*, 2008).

6.3. METHANE HYDRATES

Methane hydrates and associated free gas deposits have relevance as an unconventional energy resource only insofar as natural gas is a viable fuel to power the world's economies. Natural gas is typically made up of methane, ethene, butane, and propane, but the focus here is on methane, which constitutes 70 % to over 90 % of most conventional natural gas. Although methane has ~ 80 % of the heat content of crude oil, natural gas remains impractical for applications that rely on a liquid fuel stable at ambient pressure and temperature. Nonetheless, the U.S. Energy Information Administration projects an increase of more than 90 % in annual, absolute global consumption of natural gas between 2003 and 2030, corresponding to a ~ 2 % increase (from 24 to 26 %) in natural gas use relative to other energy sources.

The world's largest–known reserves of conventional natural gas lie in Iran, Qatar, and Western Siberia. Compared to liquid fuels that need intense refining, raw natural gas has a much shorter path from extraction to reaching a usable form, as it requires only separation of the different gases. The critical challenge is transportation of gas, which requires either specialized pipelines or extreme cooling to form liquid natural gas. Less than 10 % of global natural gas production is transported as liquid natural gas, and a significant increase in liquid natural gas capacity will be necessary to accommodate rising global natural gas consumption in areas that cannot be served by direct pipelines. Due in part to transportation issues, the small amount of natural gas produced from methane hydrates in the initial commercial projects might be used to power infrastructure on site instead of being transported to markets.

Natural gas is regarded as a relatively clean hydrocarbon–based fuel because methane combustion yields fewer pollutants than either oil or typical coal, with markedly lower emissions of CO_2, nitrogen oxides, SO_2, and particulates. Methane is ~ 20 times more powerful than CO_2 as greenhouse gas and it's typically oxidized in the atmosphere in less than 10 years. Natural outgassing of methane hydrates is estimated to account for ~ 1–2 % of present day atmospheric methane. Conventional fossil fuel production and use accounts for 15 to 18 %, and rice production, wetlands, ruminants, and landfills for up to ~ 75 %. Methane emissions will certainly increase if methane hydrate reservoirs are exploited for natural gas, but a more critical concern is possible catastrophic release of methane to the atmosphere or ocean from shallow gas hydrate deposits as a results of extraction activities or even climate change. For marine gas hydrates, some released methane would probably be oxidized in the sediments and water column; some might dissolve in the ocean and alter pH, carbonate solubility, and oxygen levels in the vicinity of the emission; and a fraction might reach the atmosphere either immediately or over time. For permafrost gas hydrates, the potential for direct outgassing of methane to the atmosphere is considerably larger.

Methane hydrate is a conventional hydrocarbon resource (natural gas) that is found in an unconventional form (frozen), at shallower (tens hundreds of meters), more readily accessible depths than conventional oil and gas and in locations both within and outside some of the permafrost and marine areas that supply conventional fuels. The methane contained in gas hydrate deposits can originate through the same, deep–seated thermal cracking (thermogenic) processes that produce oil and conventional natural gas from sedimentary organic carbon. More often, though, the carbon isotope signature ($\delta^{13}C$) of the hydrated methane indicates a biogenic source, namely microbial degradation of sedimentary organic matter. Even within a major petroleum basin like the Gulf of Mexico, the volumetrically most extensive gas hydrate

deposits (i.e. those located in pore space in regional strata, not concentrated in discrete faults and seeps) may be dominated by biogenic ($\delta^{13}C$ values between –110 and –50‰), and not thermogenic ($\delta^{13}C$ values between –50 and –20‰), methane.

Gas hydrates were studied primarily to enhance safety and productivity in the petroleum industry. Without thermodynamic or kinetic inhibitors or measures to closely control pressure and temperature (Sloan, 1998), conventional wells and pipelines can clog with artificial gas hydrates that damage equipment, halt production, and endanger workers. If natural gas is not carefully dried, even some consumer gas lines can be subject to gas hydrate formation. Naturally occurring gas hydrates have also become an important focus for the private sector. As conventional offshore hydrocarbon exploration has shifted to progressively deeper water (greater than 300 to 500 m), there has been increased awareness of potential hydrate–associated geohazards (Hovland & Gudmestad, 2001), such as uncontrolled degassing from shallow sediments, seafloor collapse, and sediment fluidization.

Commercial–scale production of methane from gas hydrate or proximal free gas deposits will require safe, efficient, cost–effective, and environmentally sound extraction technologies. Some experience garnered from producing natural gas in conventional reservoirs can be readily applied to gas hydrate reservoirs. For instance, extracting free gas from beneath capping, gas hydrate–bearing sediments is similar to production of natural gas from beneath much deeper structural traps in conventional reservoirs.

Direct mining of solid methane hydrate will probably remain economically and logistically impractical due to the relatively low concentrations of gas hydrate per unit volume of sediment in most places and the difficulty of maintaining gas hydrate within its stability field. Instead, exploitation of the solid hydrate will involve controlled dissociation of the gas hydrate through perturbations to pressure, temperature, and/or chemical conditions in the reservoir (Holder *et al.*, 1984; Sloan, 1998; Collett, 2002). Dissociation increases pressure in the reservoir, meaning that the free gas released from the gas hydrate should in some cases flow freely to the wellhead (Max *et al.*, 2006). In contrast, energy must often be expended in conventional reservoirs. Owing to the relatively shallow nature of gas hydrate deposits, preventing blowouts, borehole collapse, and the accidental release of methane, which is a powerful greenhouse gas, is critical. Measures must also be adopted to avoid new gas hydrate formation in sediments or in wells as the liberated gas expands and cools. The strongly endothermic nature of gas hydrate dissociation (~ 55 kJ mol^{-1} at 0 °C for pure methane hydrate) means that ice formation could also pose a production challenge.

Injection of heated fluids (liquids or steams), possibly enhanced by hydrofracturing of the formation, is the simplest technique for driving dissociation of methane hydrate to liberate gas for extraction. While conductive heating of the sediments is limited by the low thermal diffusivity of saturated sediments (nominally 3 to 7 * 10^{-7} m^2 s^{-1}), forced injection of hot fluids or steams could expose larger amounts of gas hydrate to destabilizing temperatures. Because dissociation is largely a surface phenomenon (Max *et al.*, 2006), more energy must be expended to extract methane from the interior of deposits than from those close to the injection well. The thermal stimulation method has several disadvantages. Heating and pumping large quantities of fluids in places with cold ambient temperatures (permafrost or deep sea) would be expensive. There would also be the potential for permeable zones other than the target area to capture significant fluid flow and heat from the injection event and, conversely, it might be difficult to penetrate massive, low–permeability gas hydrate deposits (if they exist) with the fluids. Last, there would be the possibility of unintended gas hydrate dissociation and mechanical weakening of the sediments adjacent to the thermal stimulation borehole.

For a quite long time, it has been known that depressurization requires less energy input and has lower overall production costs than thermal stimulation alone (Holder *et al.*, 1984). Initially, the free gas that often underlies gas hydrate deposits would be extracted, thereby lowering the pressure in the overlying sediments and leading to dissociation, gas expansion, and then a drop in formation temperature. In an ideal reservoir, such depressurization should case relatively uniform dissociation progressing upward from the base of the gas hydrate stability zone. Dissociation would continue until the reservoir pressure drops to the equilibrium pressure corresponding to the now–reduced formation temperature (Sloan, 1998). Continued production would require heating of the reservoir to prevent gas hydrate from forming again and to drive new dissociation.

Methods developed to prevent the formation of gas hydrate plugs in hydrocarbon pipelines may also be applied to produce methane from gas hydrate (Sloan, 1998). Injection of inhibitors like methanol, glycol, or brine could drive dissociation, but carries unknown environmental risks. Brines, which also occur naturally, might be the obvious choice to enhance production where depressurization combined with limited thermal injection is the primary production technique.

A more exotic mechanism for production of methane from gas hydrates is substitution of CO_2 for methane in the gas hydrate molecule. Natural gas hydrate reservoirs could thus be used for simultaneous energy extraction and sequestration of waste CO_2 generated by burning fossil

fuels. The thermodynamics and kinetics are favourable for the exchange of methane for CO_2, but the process occurs rapidly only near the surface of the gas hydrate masses, leaving the deeper crystals untouched. Thermal perturbations and the processing of CO_2 to form emulsions of very fine droplets prior to injection (McGrail *et al.*, 2004) might allow more methane to be released from natural deposits.

Since the 1980s, there have been claims of natural gas production from gas hydrate in the Messoyakha field in Russia, but subsequent analyses indicate that gas hydrates may not have contributed to recovered gas at the site (Collett & Ginsburg, 1998). The first verifiable production of natural gas from gas hydrate probably occurred during depressurization and thermal injection tests conducted at the Mallik permafrost well in 2002 (Dallimore & Collett, 2005). This test was promising not for the amount of gas produced, but rather for information it provided about extraction techniques, production rates, well control, and the capacity of models to predict the rate and pattern of gas extraction.

7. REFERENCES

Adorni F. & Tateo F. (2007) – A New Melanophlogite Occurrence from The Case Montanini Quarry Parma, Northern Appenines, Italy. Axis, 3, 1.

Adorni F., Tateo F. & Adorni B. (2004) – La melanoflogite di Case Montanini (S. Andrea B., Medesano), Appenino Parmense. *Rivista Mineralogica Italiana*, 3, 126–136.

Algieri C., Bernardo P., Golemme G., Barbieri G. & Drioli E. (2003) – Permeation properties of a thin silicalite–1 (MFI) membrane. *Journal of Membrane Science*, 222, 181–190.

Althoff, P.L. (1977) – Structural refinements of dolomite and a magnesian calcite and implications for dolomite formation in the marine environment Mg–calcite. *American Mineralogist*, 62, 772–783.

Angel R.J. (2003) – Winstrain user manual. http://www.rossangel.com/text_strain.htm.

Artoni A., Papani G., Rizzini F., Calderoni M., Bernini M., Argnani A., Roveri M., Rossi M., Rogledi S. & Gennari R. (2004) – The Salsomaggiore structure (Northwestern Apennine foothills, Italy): a Messinian mountain front shaped by mass–wasting products. *GeoActa*, 3, 107–128.

Baerlocher C., McCusker L.B. & Olson D.H. (2007) – Atlas of Zeolites Framework Types (Amsterdam: Elsevier Science).

Baerlocher C., Olson D.H. & Meier W.M. (2001) – Atlas of Zeolites Framework Types (formerly: Atlas of Zeolite Structure Types) (Amsterdam: Elsevier Science).

Barsotti G. (1999) – Storia Naturale dei Monti Livornesi. Geologia: i minerali e la rocce, Belforte editore.

Beard A.D., Howard K., Carmody L. & Jones A.P. (2013) – The origin of melanophlogite, a clathrate mineral, in natrocarbonatite lava at Oldoinyo Lengai, Tanzania. *American Mineralogist*, 98, 1998–2006.

Binggeli N., Keskar N. & Chelikowsky J. (1994) – Pressure–induced amorphization, elastic instability, and soft modes in alpha–quartz. *Physical Review B*, 49, 3075–3081.

Bnmner G.O. & Meier W.M. (1989) – Framework density distribution of zeolite–type tetrahedral nets. *Nature*, 337, 146–147.

Boccaletti M., Elter P. & Guazzone G. (1971) – Plate tectonics models for the development of the western Alps and northern Apennines. *Nature*, 234, 108–111.

Boerio–Goates J., Stevens R., Hom B.K., Woodfield B.F., Piccione P.M., Davis M.E. & Navrotsky A. (2002) – Heat capacities, third–law entropies and thermodynamic

functions of SiO_2 molecular sieves from T = 0 K to 400 K. *Journal of Chemical Thermodynamics*, 34, 205–227.

Bracci G. & Orlandi P. (1985) – Minerali del territorio comunale di Rosignano Marittimo. Supplemento 1, Quaderni del Museo di Storia Naturale di Livorno, 6, 195–206.

Burggraaf A.J., Vroon Z.A.E.P., Keizer K. & Verweij H. (1998) – Permeation of single gases in thin zeolite MFI membrane. *Journal of Membrane Science*, 144, 77–86.

Bushuev Y.G. & Sastre G. (2010) – Feasibility of pure silica zeolites. *Journal of Physical Chemistry C*, 114, 19157–19168.

Carpenter M.A., Salje E.K.H. & Graeme–Barber A. (1998) – Spontaneous strain as a determinant of thermodynamic properties for phase transitions in minerals *European Journal of Mineralogy*, 10, 621–691.

Carpenter M.A., Meyer H.W., Sondergeld P., Marion S. & Knight K.S. (2003) – Spontaneous strain variations through the low temperature phase transitions of deuterated lawsonite. *American Mineralogist*, 88, 534–546.

Chae H.K, Klemperer W.G., Payne D.A., Suchicital C.T.A., Wake D.R. & Wilson S.R. (1991) – Clathrasils: New minerals for nonlinear optical applications. *Materials for Nonlinear Optics (ACS Symposium Series)*, 455 (Washington, DC: American Chemical Society), 528–540.

Chazallon B., Focsa C., Charlou J., Bourry C. & Donval J. (2007) – A comparative Raman spectroscopic study of natural gas hydrates collected at different geological sites. *Chemical Geology*, 244, 175–185.

Chen P., Zha C., Chen X., Shu J., Hemley R.J. & Mao H. (2011) – Raman study of phase transition in compressed methane using moissanite anvil cells. *Physical Review B*, 84, 104110.

Coasne B., Haines J., Levelut C., Cambon O., Santoro M., Gorelli F. & Gambarino G. (2011) – Enhanced mechanical strength of zeolites by adsorption of guest molecules. *Physical Chemistry Chemical Physics*, 13, 20096–20099.

Collett T.S. & Ginsburg G.D. (1998) – Gas hydrates in the Messoyakha gas field of the West Siberian Basin–A re–examination of the geologic evidence. *International Journal of Offshore and Polar Engineering*, 8, 22–29.

Collett T.S. (2002) – Energy resource potential of natural gas hydrate. *American Association of Petroleum Geologists Bulletin*, 86, 1971–1992.

Conti S., Artoni A. & Piola G. (2007) – Seep – carbonates in a thrust–related anticline at the leading edge of an orogenic wedge: The case of the middle–late Miocene

Salsomaggiore Ridge (Northern Apennines, Italy). *Sedimentary Geology*, 199, 233–251.

Coombs D.S., Alberti A., Armbruster T., Artioli G., Colella C., Galli E., Grice J.D., Liebau F., Mandarino J.A., Minato H., Nickel E.H., Passaglia E., Peacor D.R., Quartieri S., Rinaldi R., Ross M., Sheppard R.A., Tillmanns E. & Vezzalini G. (1997) – Recommended nomenclature for zeolite minerals: report of the subcommittee on zeolites of the International Mineralogical Association, Commission on New Minerals and Mineral names. *The Canadian Mineralogist*, 35, 1571–1606.

Cooper E.R., Andrews C.D., Wheatley P.S., Webb P.B., Wormald P. & Morris R.E. (2004) – Ionic liquids and eutectic mixtures as solvent and template in synthesis of zeolite analogues. *Nature*, 430, 1012–1016.

Cooper J.F. & Dunning G.E. (1972) – Melanophlogite from Mount Hamilton, Santa Clara County, California. *American Mineralogist*, 57, 1494–1504.

D'Alessio D., Tribaudino M., Mezzadri F., Mantovani L., Milanese C., Gaboardi M., Magnani G., Pontiroli D. & Riccò M. – Degassing and phase transitions in melanophlogite. In preparation.

D'Amour H., Denner W. & Schulz H. (1979) – Structure determination of α–quartz up to $68*10^8$ Pa. *Acta Crystallographica Section B*, 35, 550–555.

Dallimore S.R. & Collett T.S. (2005) – Scientific Results from the Mallik 2002 Gas Hydrate Production Research Well Program, Mackenzie Delta, Northwest Territories, Canada. *Geological Survey of Canada Bulletin*, 585, 140 pp.

Darlington C.N. & Knight K.S. (1999) – High–temperature phases of NaNbO3 and NaTaO3 *Acta Crystallographica B*, 55, 24–30.

Daqing Z., Shilun Q. & Wenqin P. (1990) – Synthesis of large single crystals of pentasil–type silica zeolites from non–alkaline medium. *Journal of the Chemical Society, Chemical Communications*, 1313–1314.

Dessau G., Jensen M.L. & Nakai N. (1962) – Geology and isotopic studies of Sicilian sulfur deposits. *Economic Geology*, 57, 410–438.

Dincă M., Dailly A., Liu Y., Brown C.M., Neumann D.A. & Long J.R. (2006) – Hydrogen storage in a microporous metal–organic framework with exposed Mn^{2+} coordination sites. *Journal of the American Chemical Society*, 128, 16876–16883.

Domenici V. & Lenzi A. (2004) – Storia mineraria del territorio Livornese (Descrizione di alcune giaciture mineralogiche del Comune di Rosignano Marittimo e zone limitrofe). *La biblioteca dei 500, Ulisse nella rete della Scienza*, ISSN 1722–4306.

Domenici V., Lenzi A. & Taccone R. (2006) – La Melanoflogite di località Fortullino: uno studio strutturale del minerale. *Atti del Primo Congresso Regionale di Scienze Naturali della Toscana "Codice Armonico"*, 44–48.

Dong J., Lin Y.S. & Liu W. (2000) – Multicomponent hydrogen/hydrocarbon separation by MFI–type zeolite membranes. *AIChE Journal*, 46, 1957–1966.

Dong J., Lin Y.S., Kanezashi M. & Tang Z. (2008) – Microporous inorganic membranes for high temperature hydrogen purification. *Journal of Applied Physics*, 104, 121301.

Dong J., Wang X., Xu H., Zhao Q. & Li J. (2007) – Hydrogen storage in several microporous zeolites. *International Journal of Hydrogen Energy*, 32, 4998–5004.

Durig J.R., Bush S.F. & Baglin F.G. (1968) – Infrared and Raman Investigation of Condensed Phases of Methylamine and its Deuterium Derivates. *Journal of Chemical Physics*, 49, 2106–2117.

Frezzotti M.L., Tecce F. & Casagli A. (2012) – Raman spectroscopy for fluid inclusion analysis. *Journal of Geochemical Exploration*, 112, 1–20.

Friedel G. (1890) – Sur la mélanophlogite. *Bulletin de la Société Française de Minéralogie*, 13, 356–372.

Friedel G. (1891) – Sur la mélanophlogite. *Bulletin de la Société Française de Minéralogie*, 14, 74–76.

Friedel G. (1892) – Sur une nouvelle publication relative a la mélanophlogite. *Bulletin de la Société Française de Minéralogie*, 15, 49–58.

Frost H., Düren T. & Snurr R.Q. (2006) – Effects of surface area, free volume, and heat of adsorption on hydrogen uptake in metal–organic frameworks. *Journal of Chemical Physics*, 120, 10285–10289.

Fyfe C.A. & Gies H. (1990) – A ^{29}Si NMR Study of Natural and Synthetic Melanophlogites, the Silica Analogues of the Clathrate Hydrates of Type I. *Journal of Inclusion Phenomena and Molecular Recognition in Chemistry*, 8, 235–239.

Gascon J., Blom W., van Miltenburg A., Ferreira A., Berger R. & Kapteijn F. (2008) – Accelerated synthesis of all–silica DD3R and its performance in the separation of propylene/propane mixtures. *Microporous and Mesoporous Materials*, 115, 585–593.

Gatta G.D., Bersani D., Lottici P.P. & Tribaudino M. (2014) – High–pressure Raman study of CH_4 in melanophlogite (type I clathrate). *Mineralogical Magazine*, 78, 1661–1669.

Geiger C.A., Dachs E. & Nagashima M. (2008) – Heat capacity and entropy of melanophlogite: Molecule–containing porosils in nature. *American Mineralogist*, 93, 1179–1182.

Gerke H. & Gies H. (1984) – Studies on Clathrasils. IV. Crystal structure of dodecasil 1H, a synthetic clathrate compound of silica. *Zeitschrift für Kristallographie*, 166, 11–22.

Gies H. & Czank M. (1986) – TEM–Untersuchungen zur Polytypie an Deca–Dodecasil 3R. *Zeitschrift für Kristallographie*, 174, 64–65.

Gies H. (1983) – Studies on Clathrasils. III. Crystal structure of melanophlogite, a natural clathrate compound of silica. *Zeitschrift für Kristallographie*, 164, 3–4, 247–257.

Gies H. (1984) (a) – Studies on Clathrasils. VI. Crystal structure of dodecasil 3C, another synthetic clathrate compound of silica. *Zeitschrift für Kristallographie*, 167, 73–82.

Gies H. (1984) (b) – Studies on Clathrasils. VII. A new clathrate compound of silica: synthesis, crystallographic, and thermal properties. *Journal of Inclusion Phenomena*, 2, 275–278.

Gies H. (1986) – Studies on Clathrasils. IX. Crystal structure of deca–dodecasil 3R, the missing link between zeolites and clathrasils. *Zeitschrift für Kristallographie*, 175, 93–104.

Gies H., Gerke H. & Liebau F. (1982) – Chemical composition and synthesis of melanophlogite, a clathrate compound of silica. *Neues Jahrbuch für Mineralogie–Monatshefte*, 3, 119–124.

Grassellini Troysi M. & Orlandi P. (1972) – Sulla melanoflogite del Fortullino (Livorno). *Atti Società Toscana di Scienze Naturali–Memorie Serie A*, 79, 245–250.

Greaves G.N., Meneau F., Sapelkin A., Colyer L.M., ap Gwynn I., Wade S. & Sankar G. (2003) – The rheology of collapsing zeolites amorphized by temperature and pressure. *Nature Materials*, 2, 622–629.

Gunawardane R.P., Gies H. & Liebau F. (1987) – The effect of "Help Gases" on the Formation and Stability of Clathrasils. *Zeitschrift für anorganische und allgemeine Chemie*, 546, 189–198.

Haines J., Cambon O., Levelut C., Santoro M., Gorelli F. & Gambarino G. (2010) – Deactivation of pressure–induced amorphization in silicalite SiO_2 by insertion of guest species. *Journal of the American Chemical Society*, 132, 8860–8861.

Hemley R.J., Jephcoat A.P., Mao H.K., Ming L.C. & Manghnani M.H. (1988) – Pressure–induced amorphization of crystalline silica. *Nature*, 334, 52–54.

Herzberg G. (1989) – Molecular Spectra and Molecular Structure I. Spectra of Diatomic Molecules, 2nd ed. Krieger Publishing Company, New York.

Herzberg G. (1991) – Molecular Spectra and Molecular Structure II. Infrared and Raman Spectra of Polyatomic Molecules, 2nd ed. Krieger Publishing Company, Malabar, Florida.

Higgins J.B. – Chapter 15. Silica zeolites and clathrasils. In: Heaney P.J., Prewitt C.T. & Gibbs G.V. (1994) – Silica: Physical Behavior, Geochemistry and Materials Applications. Reviews in Mineralogy, MSA (Mineralogical Society of America), 29, 507–543.

Himeno S., Tomita T., Suzuki K. & Yoshida S. (2007) – Characterization and selectivity for methane and carbon dioxide adsorption on the all–silica DD3R zeolite. *Microporous and Mesoporous Materials*, 98, 62–69.

Holder G.D., Kamath V.A. & Godbole S.P. (1984) – The potential of natural gas hydrates as an energy resource. *Annual Review of Energy*, 9, 427–445.

Hong M., Falconer J.L. & Noble R.D. (2005) – Modification of zeolite membranes for H_2 separation by catalytic cracking of methyldiethoxysilane. *Industrial & Engineering Chemistry Research*, 44, 4035–4041.

House K.Z., Schrag D.P., Harvey C.F. & Lackner K.S. (2006) – Permanent carbon dioxide storage in deep–sea sediments. *Proceedings of the National Academy of Sciences*, 103, 12291–12295.

Hovland M. & Gudmestad O.J. (2001) – Potential influence of gas hydrates on seabed installations. In: Paull C.K. & Dillon W.P. (eds). Natural Gas Hydrates: Occurrence, Distribution, and Detection. Monograph 124, American Geophysical Union, Washington, DC, 307–315.

Huang Y. & Havenga E.A. (2001) – Why do zeolites with LTA structure undergo reversible amorphization under pressure? *Chemical Physics Letters*, 345, 65–71.

Isambert A., Angot E., Hébert P., Haines J., Levelut C., Le Parc R., Ohishi Y., Kohara S. & Keen D.A. (2008) – Amorphization of faujasite at high pressure: an x–ray diffraction and Raman spectroscopy study. *Journal of Materials Chemistry*, 18, 5746–5752.

Jhung S.H., Yoon J.W., Lee J.S. & Chang J.S. (2007) – Low–temperature adsorption/storage of hydrogen on FAU, MFI, and MOR zeolites with various Si/Al ratios: effect of electrostatic fields and pore structures. *Chemistry*, 13, 6502–6507.

Kamb B. (1965) – A Clathrate Crystalline Form of Silica. *Science*, 148, 232–234.

Kanezashi M., O'Brien–Abraham J., Lin Y.S. & Suzuki K. (2008) – Gas permeation through DDR–type zeolite membranes at high temperatures. *AIChE Journal*, 54, 1478–1486.

Kanzaki M. In–situ high–temperature Raman spectroscopy study of a CO_2–containing melanophlogite. In preparation.

Kingma K., Hemley R., Mao H. & Veblen D. (1993) – New high–pressure transformation in alpha–quartz. *Physical Review Letters*, 70, 3927–3930.

Knorr K. & Depmeier W. (1997) – Room–temperature structure and geometrical analysis of the cubic–tetragonal phase transition in dodecasil 3C–THF. *Acta Crystallographica B*, 53, 18–24.

Kohler S., Irmer G., Kleebergg Monecke J., Herzig P.M. & Schulz B. (1999) – Melanophlogite from the Cascadia accretionary prism, offshore Oregon: First occurrence from an active submarine vent site. Beth 1. *European Journal of Mineralogy*, 11, 129.

Kolesov B.A. & Geiger C.A. (2003) – Molecules in the SiO_2–clathrate melanophlogite: A single–crystal Raman study. *American Mineralogist*, 88, 1364–1368.

Könnecke M. & Fuess H. (1995) – Phase transitions of the clathrasil dodecasil 3C (MTN) for the guest molecules pyrrolidine and t–butylamine. *Zeolites*, 15, 264–269.

Könnecke M., Miehe G. & Fuess H. (1992) – Static disorder of dodecasil 3C. A single–crystal study with synchrotron radiation. *Zeitschrift für Kristallographie*, 201, 147–155.

Kopasheva S.K. & Makarov J.J. (1975) – First occurrence of melanophlogite in the URSS. *Doklady Akademia Nuak*, 224, 905–908.

Krishna R. & van Baten J.M. (2007) – Using molecular simulations for screening of zeolites for separation of CO_2/CH_4 mixtures. *Chemical Engineering Journal*, 133, 121–131.

Langmi H.W., Walton A., Al–Mamouri M.M., Johnson S.R., Book D., Speight J.D., Edwards P.P., Gameson I., Anderson P.A. & Harris I.R. (2003) – Hydrogen adsorption in zeolites A, X, Y and RHO. *Journal of Alloys and Compounds*, 356–357 (3), 710–715.

Larson A.C., and Von Dreele, R.B. (1997) – GSAS: General Structure Analysis System. Report LAUR 86–748, Los Alamos National Laboratory, Los Alamos, New Mexico, USA.

Lazzeri K.E., Bebout G.E & Geiger C.A. (2017) – Nitrogen and carbon concentrations and isotopic compositions of the silica clathrate melanophlogite. *American Mineralogist*, 102, 686–689.

Liang, Y., Ogundare, F.O., Miranda, C.R., Christie, J.K. & Scandolo, S. (2011) – Structural properties and phase transitions in a silica clathrate. *Journal of Chemical Physics*, 134, 074506.

Liebau F. (1985) – Structural Chemistry of Silicates. Structures, Bonding, and Classification (Berlin: Springer).

Liebau F., Gies H., Gunawardane R.P. & Marler B. (1986) – Classification of tectosilicates and systematic nomenclature of clathrate type tectosilicates: a proposal. *Zeolites*, 6, 373 –377.

Likhacheva A.Y., Prasad P.S.R., Sarma D.S. & Goryainov S.V. (2018) – High–temperature Raman study of methane–rich melanophlogite up to 1000 °C: The framework stability on degassing. *Microporous and Mesoporous Materials*, 266, 149–154.

Liu B. & Smit B. (2009) – Comparative molecular simulation study of CO_2/N_2 and CH_4/N_2 separation in zeolites and metal–organic frameworks. *Langmuir*, 25, 5918–5926.

Liu S., Welch M.D. & Klinowski J. (1997) – NMR Study of Phase Transitions in Guest–Free Silica Clathrate Melanophlogite. *Journal of Physical Chemistry B*, 101, 2811–2814.

Long Y., He H., Zheng P., Wu G. & Wang B. (1987) – Single crystal growth, morphology, and structure of ZSM–39 and its variation CF–4. *Journal of Inclusion Phenomena*, 5, 355–362.

Lutterotti L. & Scardi P. (1990) – Simultaneous structure and size–strain refinement by the Rietveld method. *Journal of Applied Crystallography*, 23, 246–252.

Mak T.C.W. & McMullan R.K. (1965) – Polyhedral clathrate hydrates. X. Structure of the double hydrate of tetrahydrofuran and hydrogen sulphide. *Journal of Chemical Physics*, 42, 2732–2737.

Marinelli G. (1955) – Il giacimento di "marcasite" e magnesite nelle serpentine di Macchia Escafrullina (Rosignano Marittimo). *Atti Società Toscana di Scienze Naturali–Memorie Serie A*, 62(2), 419–443.

Marler B., Dehnbostel N., Eulert H.H., Gies H. & Liebau F. (1986) – Studies on Clathrasils. VIII. Nonasil–[4^15^8], $88SiO_2•8M^8•8M^9•4M^{20}$: synthesis, thermal properties, and crystal structure. *Journal of Inclusion Phenomena*, 4, 339–349.

Marroni M., Molli G., Montanini A., Ottria G., Pandolfi L. & Tribuzio R. (2002) – The external Ligurian units (Nothern Apennine, Italy): From rifting to convergence of a fossil ocean–continent transition zone. *Ofioliti*, 27, 119–131.

Max M.D., Johnson A.H. & Dillon W.P. (2006) – Economic Geology of Natural Gas Hydrate. Springer, The Netherlands, 341 pp.

McGrail B.P., Zhu T., Hunter R.B., White M.B., Patil S.L. & Kulkarni A.S. (2004) – A new method for enhanced production of gas hydrates with CO_2. *American Association of Petroleum Geologists Hedberg Conference Proceedings*.

McMullan R.K. & Jeffrey G.A. (1965) – Polyhedral clathrate hydrates. IX. Structure of ethylene oxide hydrate. *Journal of Chemical Physics*, 42, 2725–2731.

McNaught A.D. & Wilkinson A. (1997) – Compendium of Chemical Terminology. IUPAC Recommendations. Wiley–Blackwell, 2nd Revised Edition. ISBN 978–0865426849.

Min J.S., Kiyozumi Y. & Itoh N. (2003) – A sealant–free preparation technique for high–temperature use of a composite zeolite membrane. *Industrial & Engineering Chemistry Research*, 42, 80–84.

Momma K. (2014) – Clathrate compounds of silica. *Journal of Physics: Condensed Matter*, 26, 103203.

Momma K., Ikeda T., Nishikubo K., Takahashi N., Honma C., Takada M., Furukawa Y., Nagase T. & Kudoh Y. (2011) – New silica clathrate minerals that are isostructural with natural gas hydrates. *Nature Communications*, 2, 196.

Nakagawa T., Kihara K. & Fujinami S. (2005) – X–ray studies of structural changes in melanophlogite with varying temperature. *Journal of Mineralogical and Petrological Sciences*, 100, 247–259.

Nakagawa T., Kihara K. & Harada K. (2001) – The crystal structure of low melanophlogite. *American Mineralogist*, 86, 1506–1512.

Nannoni R. & Sammartino F. (1975) – Guida ai minerali dei Monti Livornesi. Bologna, Calderini editore.

Navrotsky A., Trofymluk O. & Levchenko A.A. (2009) – Thermochemistry of microporous and mesoporous materials. *Chemical Reviews*, 109, 3885–3902.

Navrotsky A., Xu H., Moloy E.C. & Welch M.D. (2003) – Thermochemistry of guest–free melanophlogite. *American Mineralogist*, 88, 1612–1614.

Ohashi Y. & Burnham C.W. (1973) – Clinopyroxene Lattice Deformations: The Role of Chemical Substitution and Temperature. *American Mineralogist*, 58, 843–849.

Peacor D.B. (1973) – High–temperature single–crystal study of the cristobalite inversion. *Zeitschrift für Kristallographie–Crystalline Materials*, 138, 274–298.

Petrovic I., Navrotsky A., Davis M.E. & Zones S.I. (1993) – Thermochemical study of the stability of frameworks in high silica zeolites. *Chemistry of Materials*, 5, 1805–1813.

Piccione P.M., Laberty C., Yang S., Camblor M.A. Navrotsky A. & Davis M.E. (2000) – Thermochemistry of pure – silica zeolites. *Journal of Physical Chemistry B*, 104, 10001–10011.

Piccione P.M., Woodfield B.F., Boerio–Goates J., Navrotsky A. & Davis M.E. (2001) – Entropy of pure–silica molecular sieves. *Journal of Physical Chemistry B*, 105, 6025–6030.

Qiu S., Yu J., Zhu G., Terasaki O., Nozue Y., Pang W. & Xu R. (1998) – Strategies for the synthesis of large zeolite single crystals. *Microporous and Mesoporous Materials*, 21, 245–251.

Ricci Lucchi, F. (1986) – The Oligocene to Recent foreland basins of the northern Apennines. In Allen P.A. & Homewood P., Eds., Foreland Basins, 105–140, Blackwell, Oxford.

Richet P., Bottinga Y., Denielou L., Petitet J.P. & Tequi C. (1982) – Thermodynamic properties of quartz, cristobalite and amorphous SiO_2: drop calorimetry measurements between 1000 and 1800 K and a review from 0 to 2000 K. *Geochimica et Cosmochimica Acta*, 46, 2639–2658.

Ripmeester J.A., Tse J.S., Ratcliffe C.I. & Powell B.M. (1987) – A new clathrate hydrate structure. *Nature*, 325, 135–136.

Ruppel C. (2007) – Tapping Methane Hydrates for Unconventional Natural Gas. *Elements*, 3, 193–199.

Sassen R. & MacDonald I.R. (1994) – Evidence of structure H hydrate, Gulf of Mexico continental slope. *Organic Geochemistry*, 22, 1029–1032.

Schlenker J.L., Dwyer F.G., Jenkins E.E., Rohrbaugh W.J., Kokotailo G.T. & Meier W.M. (1981) – Crystal structure of a synthetic high silica zeolite–ZSM–39. *Nature*, 294, 340–342.

Schlenker J.L., Gibbs G.V. & Boisen M.B. (1978) – Strain–tensor components expressed in terms of lattice parameters *Acta Crystallographica*, 34, 52–54.

Schrötter H.W. & Klöckner H.W. (1979) – Raman scattering cross sections in gases and liquids. In: Raman spectroscopy of gases and liquids, Weber A., ed. Springer–Verlag, Berlin, 123–137.

Seraj S., Ferron R.D. & Juenger M.C.G. (2016) – Calcining natural zeolites to improve their effect on cementitious mixture workability. *Cement and Concrete Research*, 85, 102–110.

Skinner B.J. & Appleman D.E. (1963) – Melanophlogite, a cubic polymorph of silica. *American Mineralogist*, 48, 854–867.

Sloan E.D. Jr (1998) – Clathrate Hydrates of Natural Gases. Marcel Dekker, New York, 641 pp.

Sloan E.D. Jr (2003) – Fundamental principles and applications of natural gas hydrates. *Nature*, 426, 353–363.

Smith J.V. (1984) – Definition of a zeolite. *Zeolites*, 4, 309–310.

Steinfink H., and Sans, F.J. (1959) – Refinement of the crystal structure of dolomite. *American Mineralogist*, 44, 679–682.

Thomson, P., Cox, D.E., and Hastings, J.B. (1987) – Rietveld Refinement of Debye–Scherrer Synchrotron X–ray Data from Al_2O_3. *Journal of Applied Crystallography*, 20, 79–83.

Toby, B.H. (2001) – EXPGUI, a graphical user interface for GSAS. *Journal of Applied Crystallography*, 34, 210–213.

Tribaudino M., Artoni A., Mavris C., Bersani D., Lottici P.P. & Belletti D. (2008) – Single–crystal X–ray and Raman investigation on melanophlogite from Varano Marchesi (Parma, Italy). *American Mineralogist*, 93, 88–94.

Tribaudino M., Gatta G.D. & Lee Y. (2010) – A high–pressure cubic–to–tetragonal phase–transition in melanophlogite, a SiO_2 clathrate phase. *Microporous and Mesoporous Materials*, 129, 267–273.

Tribaudino M., Bruno M., Nestola F., Pasqual D. & Angel R.J. (2011) – Thermoelastic and thermodynamic properties of plagioclase feldspars from thermal expansion measurements. *American Mineralogist*, 96, 992–1002.

Tse J.S. & Klug D.D. (1995) – Reversible amorphization and structural memory effect in clathrasil dodecasil–3C. *Supramolecular Chemistry*, 6, 165–170.

Tse J.S., Klug D.D., Ripmeester J.A., Desgreniers S. & Lagarec K. (1994) – The role of non–deformable units in pressure–induced reversible amorphization of clathrasils. *Nature*, 369, 724–727.

Udachin K.A. & Ripmeester J.A. (1999) – A complex clathrate hydrate structure showing bimodal guest hydration. *Nature*, 397, 420–423.

Udachin K.A., Ratcliffe C.I., Enright G.D. & Ripmeester J.A. (1997) – Structure H hydrate: a single crystal diffraction study of 2.2–dimethylpentane•5(Xe, H_2S)•34H_2O. *Supramolecular Chemistry*, 8, 173–176.

van den Berg A.W.C. & Areán C.O. (2008) – Materials for hydrogen storage: current research trends and perspectives. *Chemical Communications*, 668–81.

van den Berg A.W.C., Bromley S.T., Flikkema E., Wojdel J., Maschmeyer T. & Jansen J.C. (2004) (a) – Molecular–dynamics analysis of the diffusion of molecular hydrogen in all–silica sodalite. *Journal of Chemical Physics*, 120, 10285–10289.

van den Berg A.W.C., Bromley S.T., Ramsahye N. & Maschmeyer T. (2004) (b) – Diffusion of molecular hydrogen through porous materials: the importance of framework flexibility. *Journal of Chemical Physics B*, 108, 5088–5094.

van den Berg A.W.C., Flikkema E., Jansen J.C. & Bromley S.T. (2005) – Self–diffusion of molecular hydrogen in clathrasils compared: dodecasil 3C versus sodalite. *Journal of Chemical Physics*, 122, 204710.

van den Berg A.W.C., Pescarmona P.P., Schooman J. & Jansen J.C. (2007) – High–density storage of H_2 in microporous crystalline silica at ambient conditions. *Chemistry*, 13, 3590–3595.

van den Bergh J., Zhu W., Kapteijn F., Moulijn J.A., Yajima K., Nakayama K., Tomita T. & Yoshida S. (2008) – Separation of CO_2 and CH_4 by a DDR membrane. *Research on Chemical Intermediates*, 34, 467–474.

van der Donk G., Serra J.M., Marler B., Meulenberg W.A. & Gies H. (2008) – Formation of clathrasils layers by secondary growth of DOH–type nuclei for gas separation applications. *Microporous and Mesoporous Materials*, 115, 3–10.

van Koningsveld H. & Gies H. (2004) – Similarities between the clathrasils DOH, DDR, MEP and MTN. *Zeitschrift für Kristallographie*, 219, 637–643.

Vitillo J.G., Ricchiardi G., Spoto G. & Zecchina A. (2005) – Theoretical maximal storage of hydrogen in zeolitic frameworks. *Physical Chemistry Chemical Physics*, 7, 3948–3954.

Von Lasaulx A. (1876) – Mineralogisch–kristallographische Notizen. VII. Melanophlogit, ein neues Mineral. *Neues Jahrbuch für Mineralogie, Geologie und Paläontologie*, 250–257.

Weiler J. (1935) – Die intensitätsverteilung in den rayleighlinien kompromierter gase I. Experimenteller Teil. CO_2. *Annalen der Physik*, 23, 493–506.

Wu Y.H., Sasaki S. & Shimizu H. (1995) – High–pressure Raman study of dense methane: CH_4 and CD_4. *Journal of Raman Spectroscopy*, 26, 963–967.

Xu H., Zhang J., Zhao Y., Guthrie G.D., Hickmott D.D. & Navrotsky A. (1997) – Compressibility and pressure–induced amorphization of guest–free melanophlogite: An in–situ synchrotron X–ray diffraction study. *American Mineralogist*, 92, 166–173.

Xu H., Zhang J., Zhao Y., Guthrie G.D., Hickmott D.D. & Navrotsky A. (2007) – Compressibility and pressure–induced amorphization of guest–free melanophlogite: an in situ synchrotron x–ray diffraction study. *American Mineralogist*, 92, 166–173.

Yagi T., Iida E., Hirai H., Miyajima N., Kikegawa T. & Bunno M. (2007) – High–pressure behavior of a SiO_2 clathrate observed by using various pressure media. *Physical Review B*, 75, 174115.

Yang Z., Xia Y. & Mokaya R. (2007) – Enhanced hydrogen storage capacity of high surface area zeolite–like carbon materials. *Journal of the American Chemical Society*, 129, 1673–1679.

Žák L. (1967) – Find of pyrophanite and melanophlogite in Chvaletice (E. Bohemia). *Časopis pro mineralogii a geologii*, 12, 451–452.

Žák L. (1972) – A contribution to the crystal chemistry of melanophlogite. *American Mineralogist*, 57, 779–796.

Zheng Z., Hall A.S. & Guliants V.V. (2008) – Synthesis, characterization and modification of DDR membranes grown on α–alumina supports. *Journal of Materials Science*, 43, 2499–2502.

ACKNOWLEDGMENTS

A special thanks to Prof. Mario Tribaudino, my supervisor, and to Prof. Mauro Riccò and Prof. Daniele Pontiroli, my co–tutors.

I would like to thank all those who have helped me to carry out the experimental analyses and procedures essential for this Ph.D. project:

Dott.ssa Luciana Mantovani and Dott. Francesco Mezzadri (Department of Chemistry, Life Sciences and Environmental Sustainability, University of Parma); Prof. Danilo Bersani and Dott. Giacomo Magnani (Department of Mathematical, Physics and Computer Sciences, University of Parma); Prof.ssa Chiara Milanese (Pavia H_2 Lab, Physical Chemistry Section of Department of Chemistry, University of Pavia); Dott. Mattia Gaboardi (Elettra Synchrotron); Dr. Stéphane Rols (ILL Institut Laue–Langevin); Dott.ssa Jasmine Rita Petriglieri.

Thanks to Prof. Emilio Acerbi and Dott. Marco E. Ciriotti, which have kindly donated their samples of melanophlogite, from Fortullino and Racalmuto respectively.

Samples of melanophlogite from Varano Marchesi have been kindly donated by Prof. Mario Tribaudino and Prof. Danilo Bersani.

I would like to thank my mum Adriana and my dad Ernesto.

My partner Marco.